COMPUTATIONAL FLUID DYNAMICS ANALYSIS ON HEAT AND FLUID FLOW OF SQUARE WAVE PROFILE TRANSVERSE RIB ROUGHENED SOLAR AIR HEATER DUCT

Thesis

Submitted to the Punjab Agricultural University
in partial fulfillment of the requirements
for the degree of

MASTER OF TECHNOLOGY
in
MECHANICAL ENGINEERING
(Minor Subject: Computer Science and Engineering)

By

Inderjeet Singh
(L-2015-AE-195-M)

Department of Mechanical Engineering
College of Agricultural Engineering & Technology

LUDHIANA-141004

2017

CERTIFICATE I

This is to certify that the thesis entitled, "**Computational Fluid Dynamics Analysis on Heat and Fluid Flow of Square Wave Profile Transverse Rib Roughened Solar Air Heater Duct**" submitted for the degree of **M. Tech.**, in the subject of **Mechanical Engineering** (Minor subject: Computer Science and Engineering) of the Punjab Agricultural University, Ludhiana, is a bonafide research work carried out by **Inderjeet Singh** under my supervision and that no part of this thesis has been submitted for any other degree.

The assistance and help received during the course of investigation have been fully acknowledged.

_____

Major Advisor

Dr. Sukhmeet Singh
Research Engineer
School of Renewable Energy Engineering
Punjab Agricultural University
Ludhiana -141004

CERTIFICATE II

This is to certify that the thesis report entitled, "**Computational Fluid Dynamics Analysis on Heat and Fluid Flow of Square Wave Profile Transverse Rib Roughened Solar Air Heater Duct**" submitted by **Inderjeet Singh (Admn No.: L-2015-AE-195-M)** to the Punjab Agricultural University, Ludhiana, in partial fulfillment of the requirements for the degree of **Master of Technology**, in the subject of **Mechanical Engineering** (Minor subject: Computer Science and Engineering) has been approved by the Student's Advisory Committee after an oral examination on the same.

_____

Dr. Sukhmeet Singh
(Major Advisor)

_____

Dr. Gurpreet Singh Sidhu
Principal
Lala Lajpat Rai Institute of Engineering and Technology, Moga
(External Examiner)

_____

Dr. VP Sethi
Head of Department

_____

Dr. (Mrs.) Neelam Grewal
Dean Postgraduate Studies

ACKNOWLEDGEMENT

I feel privileged to express my thanks and sense of profound gratitude to my Major Advisor **Dr. Sukhmeet Singh**, Research Engineer, School of Renewable Energy Engineering, Punjab Agricultural University, Ludhiana, for his expert guidance, ever-willing help, encouragement, inspiration and advice throughout my research work. It is my privilege to be guided by a person of calibre, whose blessings bring best in every one of my endeavours. It would have not been possible for me to bring out this thesis without his help and constant encouragement. I wish that he will keep in touch with me in future and will continue to give his valuable advice.

I would like to express my deepest thanks and sincere appreciation to the respected members of my advisory committee, **Dr. V.S. Hans**, Professor and Director, School of Renewable Energy Engineering, **Dr. Derminder Singh**, Associate Professor, School of Electrical Engineering and Information Technology, **Dr. V P Sethi**, Professor and Head, Department of Mechanical Engineering for their valuable guidance, constructive suggestions and continuous support.

I express insufficiency to trace out appropriate words to express my heartfelt gratitude and indebtedness my respected parents for their deep affection, constant encouragement, and heartful blessings that enabled me to this stage of career.

I also extend thanks to my colleagues **Daljit Singh**, **Manpreet Singh** and **Komalpreet Singh** who are always a moral support which is extremely important when one is feeling low. Special thanks are due for my senior **Amritpal Singh** for his untiring help during this period. I wholeheartedly thank them for being a wonderful company during my stay at PAU.

It is a nice and memorable association with all the staff of my department. I wish to give them my heartfelt thanks for their constant help.

I feel proud to be a part of PAU, Ludhiana where I learnt a lot and spent some unforgettable moments of my life.

Last but not least, I thank my God for everything.

Inderjeet Singh

Title of the thesis	:	Computational Fluid Dynamics Analysis on Heat and Fluid Flow of Square Wave Profile Transverse Rib Roughened Solar Air Heater Duct
Name of the Student and Admission No.	:	Inderjeet Singh (L-2015-AE-195-M)
Major Subject	:	Mechanical Engineering
Minor Subject	:	Computer Science and Engineering
Name and Designation of Major Advisor		Dr. Sukhmeet Singh Research Engineer
Degree to be awarded	:	Master of Technology (Mechanical Engineering)
Year of award of degree	:	2017
Total pages in thesis	:	71 + VITA
Name of the University	:	Punjab Agricultural University, Ludhiana-141004, Punjab, India

ABSTRACT

In this investigation, the thermal and hydraulic performance of solar air heater duct roughened with non-uniform cross-section square wave profiled transverse rib is carried out using Computational Fluid Dynamics software ANSYS Academic Research CFD 15.0. The 3-D investigation considered parameters as relative roughness pitch from 4-30, relative roughness width from 10-310, relative roughness height from 0.015-0.043 and Reynolds number from 3000-15000. The turbulence model RNG k-ε with enhanced wall treatment and one periodic length was selected for analysis. The CFD methodology has been validated with the experimental results available in literature. The maximum enhancement in Nusselt number and friction factor over smooth duct was found to be 2.22 times and 3.40 times respectively at relative roughness pitch of 10, relative roughness width of 85, relative roughness height of 0.043 and Reynolds number of 15000. The maximum thermohydraulic performance parameter was found to be 1.49 at relative roughness pitch of 10, relative roughness width from 85, relative roughness height from 0.043 and Reynolds number of 12000.

Keywords: Heat transfer, Reynolds number, Thermohydraulic, Nusselt number, Friction factor, Streamlines, Static temperature, Static pressure.

Signature of Major Advisor **Signature of the Student**

Kj gQ dw isrlK	:	kipatSnl PleIf fwienwimks nwl vrgwkwr lihr tWsvrs irb nwl Krdrl klql srjl hvw hltr nwll dw grml q qrl vihx ivSlSx
ividAwrQl dw nwm Aq dwKlw nbr	:	iedrjlq isG (A-l-2015-e.el.-195-A-m)
pmK ivSw	:	mknlkl iejlinAirg
sihXgl ivSw	:	kipatr swies Aq iejlinAirg
pmK slwhkwr dw nwm Aq Ahdw	:	fw. sKmlq isG irsrc iejlnlAr
ifgrl	:	Am. t-k
ifgrl nwl snmwinq krn dw swl	:	2017
Kj pqr ivc kl pn	:	71 + vltw
XnlvristI dw nwm	:	pjwb KqlbwVl XnlvristI, liDAwxw–141 004, pjwb, Bwrq

swr-AS

ies qPqlS ivc vrgwkwr lihr tWsvrs irb nwl bnwvtl qrlk nwl Krdrl klql gel srjl hvw hitr nwll d nsl nbr Aq rgV Pktr d AiDAn klq ge hn[ieh qPqlS 3-AwXwm rwhl Alniss swPtvAr Akfimk irsrc sl.AP.fl. 15.0 ivc klql gel h[ies ivc rlitv Krdrl ipc, rlitv Krdrl cVwel, rlitv Krdrl acwel Aq rnlf nbr d vK-vK nmn lwe ge hn j ik kmvwr 4-30, 10-310, 0.015-0.043 Aq 3000-15000 hn[ies ivc q&wnl mwfl d rlnrmlwelzSn smh k-Apswelln n Krdrl nwll a-pr vrqx lel cixAw igAw[ies sl.AP.fl. ivDl n swihq d ipCl nqlijAW nwl pmwixq klqw igAw h[pDrl nwll d mkwbl nsl nbr q rgV Pktr ivc 2.22 Aq 3.40 gxw AiDkqm vwDw rlitv Krdrl ipc 10, rlitv Krdrl cVwel 85, rlitv Krdrl acwel 0.043 Aq rnlf nbr 15000 q pwieAw igAw[rlitv Krdrl ipc 10, rlitv Krdrl cVwel 85, rlitv Krdrl acwel 0.043 Aq rnlf nbr 12000 a-pr 1.49 rkm dl Qrmhwelfilk kwrgzwrl dl imkdwr sB q vDlAw pwel gel[

mK Sbd : tWsvrs irb, Qrmhwelfilk, rnlf nbr, q&wnl mwfl, nsl nbr, rgV Pktr, siQr dbwv, siQr qwpmwn

_____ _____

ਮੁੱਖ ਸਲਾਹਕਾਰ ਦੇ ਹਸਤਾਖ਼ਰ **ਵਿਦਿਆਰਥੀ ਦੇ ਹਸਤਾਖ਼ਰ**

CONTENTS

LIST OF TABLES

LIST OF FIGURES

LIST OF ABBREVIATIONS

D	-	Hydraulic diameter of duct, m
e	-	Rib height, m
h	-	Heat transfer coefficient, W/m^2k
k	-	Thermal conductivity of air, W/m K
L	-	Length of duct, m
ΔP	-	Pressure drop, Pa
p	-	Rib pitch, m
v	-	Velocity of air in duct, m/s
W	-	Width of duct, m
Re	-	Reynolds number
e/D	-	Relative roughness height
P/e	-	Relative roughness pitch
g/e	-	Relative gap width
w/W	-	Relative roughness width ratio
e^+	-	Roughness Reynolds number
S/e	-	Relative short way length of mesh
L/e	-	Relative long way length of mesh
f	-	Friction factor of roughened duct
f_s	-	Friction factor of smooth duct
Nu	-	Nusselt number of roughened duct
Nu_s	-	Nusselt number of smooth duct
W/H	-	Duct aspect ratio
μ	-	Dynamic viscosity, Ns/m^2
ρ	-	Density of air, kg/m^3
α	-	Angle of attack, degree
G_d/L_v	-	Relative gap distance
G_d	-	Gap distance, m

CHAPTER-I

INTRODUCTION

Renewable energy is becoming an increasingly significant concern in today's world. Industrial evolution and population expansion have led to a hike in the global demand of energy in recent years. Fossil fuels are becoming too expensive and are environmentally damaging and additionally they rely on finite natural resources that will eventually fade out. Therefore, alternative forms of energy like solar energy, wind energy, biomass energy, hydro energy, geothermal energy etc. have got attention. However, none of these is sufficiently developed or abundant enough to completely substitute for fossil fuels use. Each one of these energy sources has low environmental costs, and have the potential to be important in avoiding a massive crisis when there is scarcity of fossil fuel reserves.

Solar energy is the most promising source of renewable energy as it is abundantly available almost everywhere. Future energy demands as well as high cost of energy have resulted in increased efforts of designing more efficient equipment for conversion of solar energy. Solar energy can be used directly for generating electricity, space heating, drying of agricultural products, water heating, solar cooling, and a variety of commercial and industrial uses (Kumar and Kim 2015). There is a wide range of equipment available for the utilization of solar energy such as solar water heater, solar air heater, solar crop dryer, solar photovoltaic systems, etc. (Tiwari 2013).

Solar air heater is one of the widely-used equipment through which the solar energy is converted into thermal energy which is absorbed by the working medium i.e. air. A conventional solar air heater consists of glass cover(s), absorber plate, ducts or channels of fluid flow, glazing, air blower, etc. The solar air heaters are often employed for space heating, crop drying and other industrial uses (Sukhatme and Nayak 2011).

The conventional solar air heater is thermally inefficient due to the low value of convective heat transfer coefficient between the smooth absorber plate and flowing air (Alam and Kim 2017). When turbulent air flows through the smooth duct, a laminar sub-layer is formed near to plate surface which decreases the convective heat transfer coefficient (Hans *et al* 2009).

Different techniques for boosting the thermal performance of conventional solar air heaters has been explored such as packed bed (Kumar and Kim 2017), double pass (Ravi and Saini 2016), baffles and obstacles (Karwa *et al* 2005), artificial rib roughness (Yadav and

Thapak 2014), corrugated absorber (Hwang *et al* 2006), etc. All the methods significantly increase the heat transfer with the parallel increase in frictional losses.

Among all these methods, implementation of artificial rib roughness on the absorber plate efficiently increases the heat transfer rate with lesser increase in pumping power requirement as compared to other enhancement methods (Hans *et al* 2017). The artificial roughness is used on the underside of the absorber plate. Only the flow at the near wall region is disturbed by the small roughness elements which breaks the laminar sub-layer adjacent to absorber plate and the core flow is not affected (Singh *et al* 2015). Artificial roughness in different geometries has been explored by numerous investigators for improving the thermo-hydraulic performance of the conventional solar air heaters (Alam and Kim 2017).

A number of experimental as well as Computational Fluid Dynamics (CFD) studies on artificial roughness have been conducted for different shapes to evaluate the performance of artificially roughened solar air heater (Yadav and Bhagoria 2013). Nearly all of the investigations employed the rib of uniform circular or square cross-section except in a study by Singh *et al* (2015) that used non-uniform rib cross-section in his CFD analysis and reported better thermal and hydraulic performance. The CFD modelling involves numerical solutions of the conservation equations for mass, momentum and energy that describe fluid flow for predefined geometries and boundary conditions. While the experimental studies on artificial roughness are time consuming, expensive and only provide knowledge of the overall heat transfer coefficient, CFD approach provides fast and less costly solutions for the optimization of the roughened solar air heaters and provides in depth analysis of the fluid flow. This research is expected to optimize the roughness and flow parameters of this rib roughness for increasing the thermo-hydraulic performance and will be a step towards enhancing the knowledge of rib roughness geometries employed in solar air heater duct.

Keeping above in mind a study on non-uniform cross-section rib roughness titled "**Computational fluid dynamics analysis of heat and fluid flow of square wave profile transverse rib roughened solar air heater duct**" has been proposed with the following specific objectives:

i. To study the effect of roughness and flow parameters on Nusselt number and friction factor in non-uniform cross-section square wave profile transverse rib roughened solar air heater duct.

ii. To determine optimum roughness and flow parameters based on thermo-hydraulic performance.

CHAPTER-II

REVIEW OF LITERATURE

Numerous shapes of artificial rib roughness have been investigated by different authors to evaluate the performance of artificially roughened solar air heater. Most of these geometries have uniform cross section. A few rib roughness geometries employing non-uniform cross section have also been reported. The review of various rib roughness geometries available in the literature is given below.

Prasad and Mullick (1983) introduced the concept of fixing small diameter wires on the underside of the absorber plate for heat transfer augmentation. The relative roughness height of 0.019 and relative roughness pitch of 12.7 were taken as the roughness parameters in this investigation. The outcome of this study reported the enhancement in the efficiency from 62 % to 72 % at Reynolds number of 40000.

Prasad and Saini (1988) experimentally investigated the influence of small diameter protrusion wires applied as roughness elements on the absorber plate to study their effect on heat transfer coefficient and friction factor in fully developed region. The study was carried out for relative roughness pitch from 10-20, relative roughness height from 0.020-0.033 and Reynolds number from 5000-50000. The application of rib roughness reported the Nusselt number enhancement of 2.38 times and friction factor enhancement of 4.35 times evaluated over a smooth duct. The optimum values of relative roughness pitch and relative roughness height were found to be 10 and 0.027 respectively. The study also suggests that the height of the roughness elements should be nearly equal to the laminar sub-layer thickness.

Gupta *et al* (1997) conducted an experimental study on the application of the inclined circular transverse ribs to investigate the heat and fluid flow characteristics of a roughened solar air heater duct. The investigation encompassed the relative roughness height from 0.018-0.052, Reynolds number from 3000-18000, duct aspect ratio from 6.8-11.5, and fixed relative roughness pitch of 10. The study reported the maximum augmentation in Nusselt number and friction factor of 1.8 and 2.7 times that of a smooth duct at relative roughness height of 0.033 and angle of attack of 60°. Further the best thermohydraulic performance of roughened duct was obtained at relative roughness height of 0.033 corresponding to Reynolds number of 14000. The variation of Stanton number in transitional and fully developed flow was also studied. Stanton number was observed as increasing with the increment in Reynolds number up to 12000 and thereafter it decreased.

Saini and Saini (1997) determined the heat transfer characteristics and friction factor of a solar air heater duct roughened with expanded metal mesh geometry. As an alternative to transverse ribs, authors suggested the use of commercially available metal matrix which can

be easy to fix on absorber plate. The investigation considered relative long-way mesh length from 25-71.87, relative short-way mesh length from 15.62-46.87, relative roughness height from 0.12-0.039 and Reynolds number from 1900-13000. The maximum enhancement in Nusselt number of 4 times was observed at long-way mesh length of 46.87 and relative short-way mesh length of 25. The maximum friction factor enhancement of 5 times was reported at the relative long-way mesh length of 71.87 and relative short-way mesh length of 15.62.

Karwa (1999) carried out an experimental study to determine the effect of chamfered ribs applied in transverse direction as artificial roughness for predicting the thermo-hydraulic performance of the roughened solar air heater duct. One wall was roughened and subjected to uniform heat flux while other walls were kept insulated. The parameters range were taken as duct aspect ratio from 4.8-12, relative roughness height from 0.0141-0.0328, relative roughness pitch from 4.5-8.5, rib chamfer angle from -15° to 18° and Reynolds number from 3000-20000. The maximum enhancement in Stanton number and friction factor was found to be 2 and 3 times at relative roughness height of 0.0265, relative roughness pitch of 7.5 and rib chamfer angle of 15°.

Verma and Prasad (2000) made use of transverse wire roughness and investigated the thermo-hydraulic performance in actual outdoor conditions. The parameters range were taken as relative roughness pitch from 10-40, roughness Reynolds number (e^+) from 8-42 and relative roughness height from 0.01-0.03. Maximum thermo-hydraulic performance of 71% has been obtained at roughness Reynolds number (e^+) of 24, relative roughness pitch of 10 and relative roughness height of 0.0228.

Momin *et al* (2002) performed an experimental investigation on thermo-hydraulic performance due to application of V-shape rib roughness on the absorber plate. The parameters were taken as Reynolds number from 2500-18000, angle of attack from 30°-90°, relative roughness height from 0.02-0.034 and fixed relative roughness pitch of 10. The obtained values of Nusselt number and friction factor were substantially higher than the smooth duct and maximum value of Nusselt number enhancement and friction factor enhancement were reported as 2.20 and 2.83 times respectively. Angle of attack of 60° and relative roughness height of 0.034 reported the maximum Nusselt number, friction factor and thermo-hydraulic performance parameter. Further, V-shape rib roughness was found to 1.14 times better than inclined ribs under similar conditions.

Karwa (2003) performed an experimental investigated solar air heater duct roughened using different rib geometries viz. transverse, inclined, V-up continuous, V-down continuous, V-up discrete and V-down discrete ribs. The parameters were considered as Reynolds number from 2800-15000, relative roughness height from 0.0467-0.050 and relative roughness pitch of 10. The Stanton number improvement was reported as 65-90%, 87-112%, 102-137%, 110-

147%, 93-134%, 102-142% respectively and concluded that V-down discrete rib resulted in maximum thermal performance.

Sahu and Bhagoria (2005) experimentally studied the thermal performance of the broken transverse rib roughened solar air heater duct. Experiments were conducted for Reynolds number from 3000-12000, roughness pitch (P) from 10-30 mm and rib height of 1.5 mm. Nusselt number attains maximum value at roughness pitch (P) of 20 mm and thereafter it decreases. The heat transfer coefficient of the roughened absorber plate is increased by 1.25-1.4 times than the smooth plate operating under similar conditions.

Jaurker *et al* (2006) performed an experimentation on the combination of rib and groove geometry as artificial roughness elements. The parameters in this experimentation were taken as Reynolds number from 3000-21000, relative roughness pitch from 4.5-10, relative roughness height from 0.0181-0.0363 and relative groove position ratio from 0.3-0.7. The application of rib-grooved roughness enhanced the Nusselt number by 2.7 times and friction factor by 3.6 times over the smooth duct. The best thermal and hydraulic performance was reported at relative roughness pitch of 6, relative groove position of 0.4 and relative roughness height of 0.0363.

Karmare and Tikekar (2007) explored the fluid flow and heat transfer characteristics of rectangular duct which is made rough by using metal grit roughness on the underside of the absorber surface. The effect of metal grit geometry was investigated for the parameter range as Reynolds number from 4000-17000, relative roughness pitch from 12.5-36, relative roughness height from 0.035-0.044, relative length of grit from 1.72-1. It was observed that the roughened plate with relative roughness pitch of 17.5, relative roughness height of 0.044 and relative length of grit of 1.72 reported maximum heat transfer coefficient. The maximum friction factor was reported for relative roughness pitch of 12.5, relative roughness height of 0.044 and relative length of grit of 1.72. Also it was shown that at lower Reynolds number, smooth plate was better than roughened plate.

Aharwal *et al* (2008) conducted an experimentation on heat and fluid flow characteristics in a rectangular solar air heater duct roughened with periodic inclined ribs of square cross-section with a gap. The investigation considered relative roughness pitch of 10, relative roughness height of 0.0377, and angle of attack of 60°. The relative gap width, relative gap position and Reynolds number were varied from 0.5–2, 0.1667–0.667 and 3000-18000 respectively. The maximum enhancement observed in Nusselt number and friction factor was 2.59 and 2.87 times respectively obtained at rib parameters viz. relative gap width of 1.0 and the relative gap position of 0.25 at Reynolds number of 12000.

Saini and Saini (2008) experimentally studied the performance of solar air heater duct roughened with arc shaped parallel wires as roughness elements. Study on the heat transfer

coefficient and friction factor was conducted for the rib parameters range of relative roughness height from 0.0213-0.0422 and relative arc angle (α/90) from 0.3333- 0.6666 and studied for the Reynolds number from 2000-17000. The application of arc shaped roughness geometry resulted in the maximum enhancement in Nusselt number and friction factor of 3.80 and 1.75 times obtained at relative arc angle (α/90) of 0.3333 and relative roughness height of 0.0422.

Saini and Verma (2008) introduced the new concept of dimple shaped artificial roughness provided onto the underside of absorber plate of the duct. Investigation range of Reynolds number from 2000-12000, relative roughness height from 0.018-0.037, relative roughness pitch from 8-12 was considered. The maximum Nusselt number was obtained corresponding to relative roughness pitch of 10 and relative roughness height of 0.0379. Whereas friction factor was found to be lowest at relative roughness height of 0.0289 and relative roughness pitch of 10.

Varun *et al* (2008) studied the roughness combination of transverse and inclined ribs for the parameters as Reynolds number from 2000-14000, relative roughness pitch from 3-8, relative roughness height of 0.030 and duct aspect ratio of 10. Results show that the relative roughness pitch of 8 gave the best thermal performance.

Bopche and Tandale (2009) carried out an experimentation to predict the thermo-hydraulic performance of solar air heater duct artificially roughened with inverted U-shaped turbulator. The investigation considered the parameters as Reynolds number from 3800-18000, relative roughness height from 0.0186-0.03986, relative roughness pitch from 6.67-57.14 and angle of attack of 90°. The enhancement obtained in Nusselt number and friction factor using U-shaped turbulators was 2.82 and 3.72 times as compared to the smooth duct.

Hans *et al* (2010) presented a study of the heat transfer and friction factor for multiple V-ribs roughness selecting the parameters range as relative roughness height from 0.019-0.043, relative roughness pitch from 6-12, angle of attack from 30-75° and relative roughness width from 1-10 and Reynolds number from 2000-20000. The investigation revealed that Nusselt number peaks at relative roughness width of 6 and is lower on both sides. The enhancement in Nusselt number and friction factor due to application of multi V-rib roughness was reported to be 6 and 5 times respectively that of smooth duct.

Lanjewar *et al* (2011) conducted an experimental study on the thermo-hydraulic performance of the W-shaped rib roughened solar air heater duct. The parameters were taken as Reynolds number from 2300-14000, relative roughness height from 0.018-0.03375, angle of attack from 30-75° and fixed relative roughness pitch of 10. The Nusselt number and friction factor were enhanced by 2.36 and 2.01 times respectively that of a smooth duct under similar conditions.

Singh *et al* (2011) carried out experimentation on the heat and fluid flow characteristics of a solar air heater duct roughened with periodic discrete v-down ribs. The studies covered the parameter range as relative roughness pitch from 4-12, relative gap width from 0.5-2.0, relative gap position (d/w) from 0.20-0.80, angle of attack from 30-75°, relative roughness height from 0.015-0.043 and investigated for Reynolds number from 3000-15000. The maximum enhancement in Nusselt number and friction factor as a result of providing this rib roughness was reported as 3.04 and 3.11 times respectively. This enhancement is attributed to the increased flow mixing and turbulence resulted from flow through the gap.

Kumar *et al* (2012) presented an experimental study on solar air heater duct roughened by multiple v-shaped rib with gap. The investigation incorporated the parameter range of Reynolds number from 2000-20000, relative gap distance from 0.24-0.80 and relative gap width from 0.5-1.5. Other geometrical parameters were kept fixed as relative roughness height of 0.043, relative roughness pitch of 10, angle of attack of 60° and relative width ratio of 6. The maximum augmentation in Nusselt number and friction factor over the smooth duct was reported to be 6.32 and 6.12 times respectively.

Yadav *et al* (2013) employed arc shaped dimple roughness for the parameter range of Reynolds number from 3600-18100, relative roughness pitch from 12-24, relative roughness height from 0.015-0.03 and angle of the protrusion arrangement from 45-75°. They found that the maximum enhancement in Nusselt number and friction factor was 2.89 and 2.93 times respectively as compared to smooth duct for the relative roughness height of 0.03, relative roughness pitch of 12, and arc angle value of 60°.

Yadav and Bhagoria (2014a) investigated heat and fluid flow characteristics of rectangular solar air heater duct comprising periodic transverse rib roughness of square cross-section. Simulations were carried out in 2-D using CFD code ANSYS FLUENT 12.1. Twelve different rib configurations of square section were evaluated in the parameter range of relative roughness pitch from 7.14-35.71, relative roughness height from 0.021-0.042 and Reynolds number from 3800-18000. Best thermohydraulic performance parameter with square cross-section transverse rib has been found to be 1.88 at the parameters; relative roughness pitch of 10.71, relative roughness height of 0.042 and Reynolds number of 12000.

Yadav and Bhagoria (2014b) conducted a 2-D numerical investigation on equilateral triangular sectioned transverse rib roughness by use of CFD code ANSYS FLUENT 12.1. Parameters range were taken as relative roughness pitch from 7.14-35.71, relative roughness height from 0.021-0.042 and Reynolds number from 3800-18000. Maximum enhancement in Nusselt number of 3 times and friction factor enhancement of 3.56 times over that of smooth duct was observed corresponding to the relative roughness pitch of 7.14, Reynolds number of 15000 and relative roughness height of 0.042.

Jin *et al* (2015) presented a 3-D numerical investigation of heat and fluid flow characteristics of a solar air heater duct having multiple V-shaped ribs. Computations were performed using the CFD Code ANSYS Fluent 14.0 and RNG k-ε turbulence model. The investigation covered spanwise V-rib number from 3-10, relative rib pitch from 3-20, relative rib height from 0.03-0.11, angle of attack from 30˚-75˚, and for Reynolds number from 8000-20000. The maximum thermo-hydraulic performance parameter was obtained at relative roughness pitch of 5, Reynolds number of 8000, spanwise rib number (W/w) of 5 and relative roughness height of 0.03.

Alam and Kim (2016) conducted a numerical study on thermohydraulic performance improvement of solar air heater duct employing semi ellipse shaped obstacles. 3-D simulations have been performed in ANSYS Fluent 16.0 using Renormalization-group (RNG) k-ε turbulence model. Two different forms namely; inline and staggered arrangements were examined. The staggered rib arrangement was found resulting in maximum Nusselt number enhancement of 2.05 times and friction factor enhancement of 6.93 times respectively, at an angle of attack of 75˚ while the corresponding improvement obtained in the inline arrangement was 1.73 and 6.12 times that of smooth duct.

Deo *et al* (2016) experimentally studied the heat transfer, friction factor and thermohydraulic performance characteristics of rectangular solar air heater duct employing artificial roughness in the form of multi-gap V-down ribs combined with staggered ribs. The duct had aspect ratio of 12 and the Reynolds number range from 4000 to 12000 was investigated. The range of rib parameters was incorporated as relative roughness pitch from 4-14, angle of attack from 40°-80°and relative roughness height from 0.026-0.057. The fixed parameters were gap width to rib height ratio of 1, staggered rib length to rib height ratio of 4.5, relative staggered rib pitch of 0.65. The maximum values of Nusselt number enhancement and thermohydraulic performance parameter were 3.34 and 2.45 times respectively.

Gawande *et al* (2016) carried out experimental and 2-D CFD investigation of solar air heater with reverse L-shaped ribs using the CFD code ANSYS FLUENT with design variables such as relative roughness pitch from 7.14-17.86, Reynolds number from 3800-18000. Whereas the relative roughness height was kept fixed as 0.042. The maximum enhancement in Nusselt number over the smooth duct of 2.827 times was achieved at the relative roughness pitch of 7.14, relative roughness height of 0.042 at Reynolds number 15000 and the enhancement in friction factor has been found to be 3.424 times over the smooth duct at Reynolds number of 3800 for the same rib parameters.

Kumar and Kim (2016) carried out 3-D CFD analysis of various V-pattern ribs namely, V- rib, protrusion rib in V-pattern, dimpled rib in V-pattern, and V- rib combined with groove in the Reynolds number range 5000-20000. The fixed parameters were relative roughness height of 0.040, relative roughness pitch of 10 and angle of attack of 60°. They concluded that V-pattern rib with a combination of groove results in maximum

thermohydraulic performance as compared to other investigated shapes of V-pattern rib in this study.

Hans *et al* (2017) experimentally evaluated the heat transfer and fluid flow characteristics of broken arc rib roughened solar air heater duct. The investigation considered rib parameters as relative roughness pitch from 4 to 12, relative gap width from 0.5-2.5, relative gap position from 0.2-0.8, relative roughness height from 0.022-0.043 and arc angle from 15˚-75˚ for Reynolds number range of 2000–16000. The enhancement obtained in Nusselt number and friction factor values were 2.63 and 2.44 times respectively corresponding to geometrical parameters as relative roughness pitch of 10, relative gap width of 1.0, arc angle of 30˚, relative gap position of 0.65 and relative roughness height of 0.043.

Kumar *et al* (2017) studied the influence of the arc shape wire ribs arranged in 'S' shape on the heat transfer and friction factor characteristics of solar air heater. The experimentation considered Reynolds number from 2400-20000 and rib parameters as relative roughness pitch from 4–16, relative roughness height from 0.022–0.054, relative roughness width from 1–4 and arc angle from 30–75˚. Experimentation shows the maximum enhancement in Nusselt number and friction factor of 4.64 and 2.71 times over the smooth duct at relative roughness width of 3, relative roughness pitch of 8 and arc angle of 60˚.

Singh *et al* (2015a) introduced the concept of non-uniform cross-section ribs as roughness elements and presented a 3-D CFD investigation using CFD code ANSYS FLUENT 15.0. A non-uniform saw toothed cross-sectioned transverse rib was compared with uniform cross sectioned circular, square and trapezoidal transverse ribs. Reynolds number was varied from 3000-15000. The maximum enhancement in Nusselt number for saw-tooth rib and trapezoidal rib was 1.78 and 1.50 respectively. The corresponding enhancement in friction factor was found to be 2.49 and 3.74 respectively.

Singh and Singh (2017) numerically evaluated the solar air heater duct roughened with non-uniform cross-section saw tooth rib. The 3-D CFD investigation encompassed the parameter range as Reynolds number from 3000-15000 and relative roughness pitch from 4-30. The relative roughness height and saw-tooth angle were taken as 0.043 and 45° respectively. Both the Nusselt number and friction factor were maximum at relative roughness pitch of 16 for the investigated Reynolds number range. The maximum Nusselt number and friction factor enhancement over smooth duct was 2.18 and 3.34 respectively at Reynolds number of 15000 and relative roughness pitch of 16.

The above literature review has been summarized in Table 2.1. It has been observed from the literature that as compared to uniform cross-section ribs, the enhancement in Nusselt number was more in non-uniform cross-section rib roughness, and pumping power penalty was also less. So, it was decided to investigate in detail the transverse rib with non-uniform cross-section of another profile in the form of square wave for which detailed study is not available.

Table 2.1 Summary of previous investigations on artificially roughened solar air heater ducts.

Investigators	Geometrical Illustration	Parameter range	Optimum values
Prasad and Saini (1988)	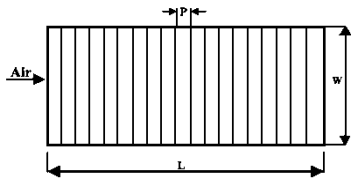 Transverse wire rib	P/e: 10-20 e/D: 0.20-0.33 Re: 5000-50000	P/e: 10 e/D: 0.027 Re: 12000
Gupta *et al* (1997)	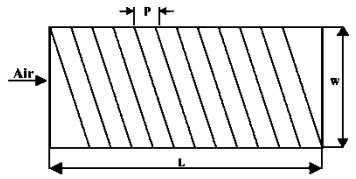 Inclined continuous rib	e/D: 0.02-0.05 α: 60°-70° P/e: 10 Re: 4000-18000	e/D: 0.033 α: 60° Re: 14000
Saini and Saini (1997)	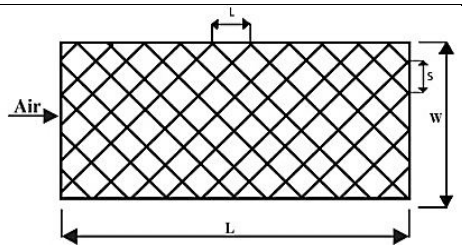 Expanded metal mesh rib	e/D: 0.012-0.039 S/e: 15.62-46.87 L/e: 25-71.87 Re: 1900-13000	e/D: 0.039 S/e: 15.62 L/e: 71.87 Re: 9500
Karwa *et al* (1999)	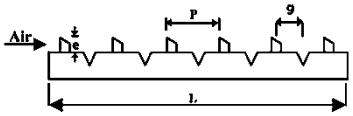 Chamfered rib	e/D: 0.14-0.32 □: 15°-18° P/e: 4.5-8.5 Re: 3000-20000	e/D: 0.0265 P/e: 7.25 □:15° Re: 8000
Verma and Prasad (2000)	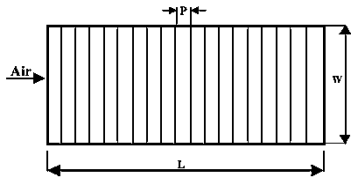 Transverse wire rib	e/D: 0.01-0.03 P/e: 10-40 e^+: 8-42 Re: 5000-20000	e/D: 0.022 P/e: 10 e^+: 24 Re: 15000
Momin *et al* (2002)	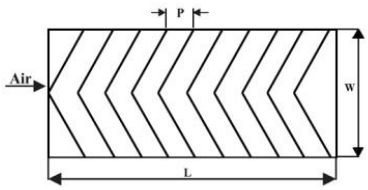 V-shaped rib	e/D: 0.020-0.034 P/e: 10 α: 30°-90° Re: 2500-18000	e/D: 0.034 α: 60° Re: 12000

Karwa *et al* (2003)	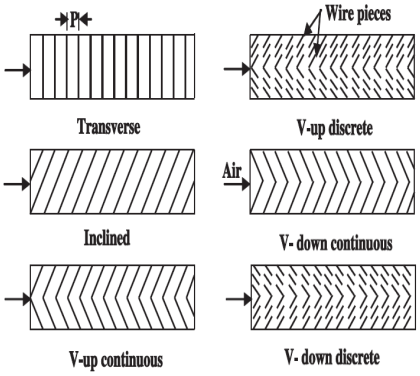 Various V- Shapes	e/D: 0.0467-0.050 W/H: 7.19-7.79 P/e: 10 Re: 2800-15000	e/D: 0.050 W/H:7.42 Re: 14000
Sahu and Bhagoria (2005)	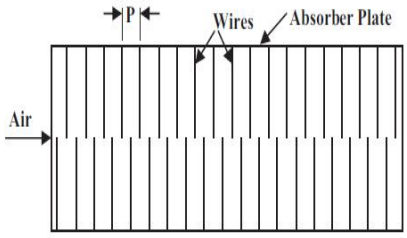 90° broken transverse rib	P: 10-30 mm W/H: 8 Re: 3000-12000 e: 1.5 mm	P: 20 mm Re: 9000
Jaurker *et al* (2006)	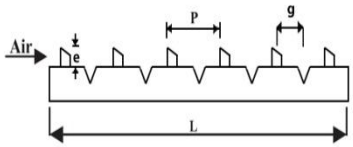 Grooved rib	e/D: 0.018-0.0363 P/e: 4.5-10 g/p: 0.3-0.7 Re: 3000-21000	e/D: 0.0363 P/e: 6 g/p: 0.4 Re: 18000
Karmare and Tikekar (2007)	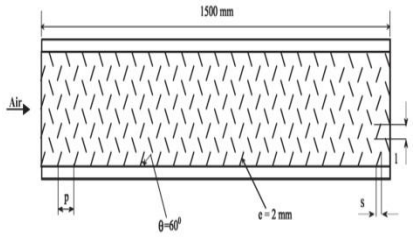 Metal grit rib	e/D: 0.030-0.044 P/e: 12.5-36 l/s: 1-1.72 Re: 4000-17000	e/D: 0.044 P/e: 17.5 l/s: 1.72 Re: 15000
Aharwal *et al* (2008)	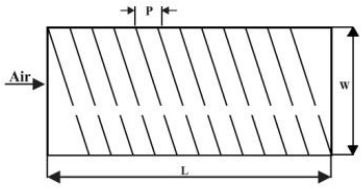 Inclined continuous rib with gap	P/e: 10 e/D: 0.0377 W/H: 5.87 α: 60°-90° g/e: 0.5-2.0 Re: 3000-18000	α: 60° g/e: 1.0 Re: 17000

Saini and Saini (2008)	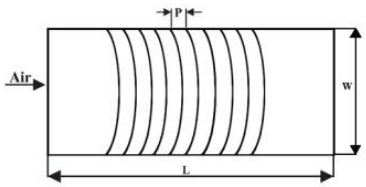 Arc shaped rib	e/D: 0.0213-0.0422 P/e: 10 α/90: 0.333-0.666 W/H: 12 Re: 2000-17000	e/D: 0.0422 α/90: 0.333 Re: 16000
Saini and Verma (2008)	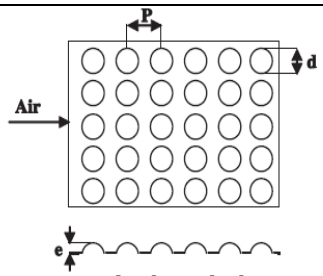 Dimple shaped rib	e/D: 0.18-0.37 P/e: 8-12 Re: 2000-12000	e/D: 0.026 P/e: 10 Re: 12000
Varun *et al* (2008)	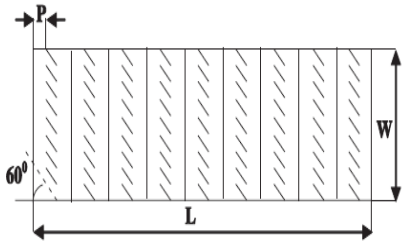 Combination of inclined and transverse rib	e/D: 1-6 P/e: 3-8 W/H: 10 Re: 2000-14000	e/D: 6 P/e: 8 Re: 12000
Bopche and Tandale (2009)	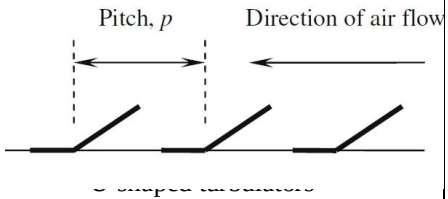	e/D: 0.018-0.0398 P/e: 6.67-57.14 α: 90° Re: 3800-18000	e/D:0.0398 P/e: 6.67 Re: 12000
Hans *et al* (2010)	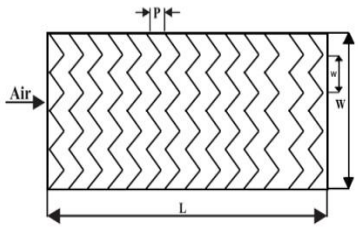 Multi v-shaped rib	P/e: 6-12 e/D: 0.019-0.043 W/w: 1-10 α: 30°-75° Re: 2000-20000	P/e: 8 W/w: 6 α: 60° Re: 15000
Lanjewar *et al* (2011)	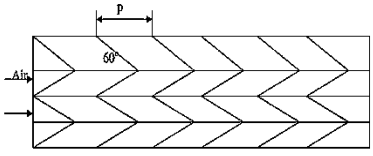 W-shaped ribs	P/e: 10 e/D: 0.018-0.0337 α: 30°-75° Re: 2300-14000	e/D: 0.0337 α: 60°

Singh *et al* (2011)	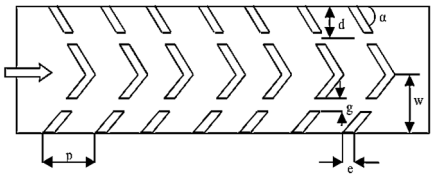 Discrete V-down ribs	P/e: 4-12 e/D: 0.015-0.043 α: 30°-75° g/e: 0.5-2.0 d/w: 0.20-0.80 Re: 3000-15000	P/e: 8 e/D: 0.043 α: 60° g/e: 1 d/w: 0.65
Kumar *et al* (2012)	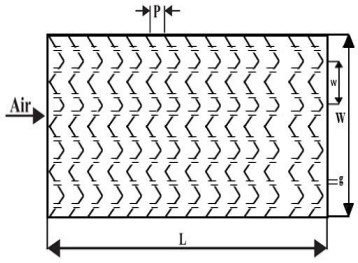 Multi v- shaped rib with gap	e/D: 0.043 P/e: 10 α: 60° W/w: 6 d/w: 0.24-0.80 g/e: 0.5-1.5 Re: 2000-20000	d/w: 0.69 g/e: 1 Re: 18000
Yadav and Bhagoria (2013)	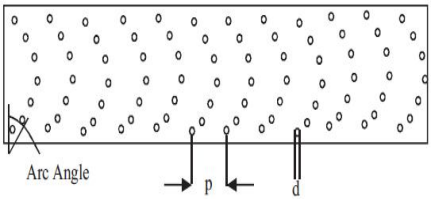	P/e: 12-24 e/D: 0.015-0.03 α: 45°-75° Re: 3600-18100	P/e: 12 e/D: 0.03 α: 60°
Yadav and Bhagoria (2014a)	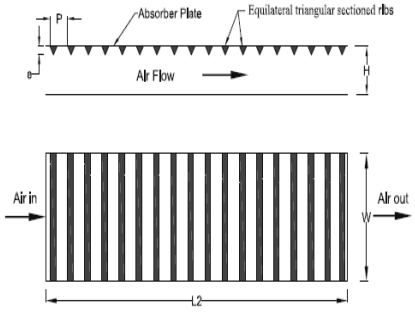 Triangular shaped rib	P/e: 7.14-35.71 e/D: 0.021-0.042 Re: 3800-18000	P/e: 7.14 e/D: 0.042 Re:15000
Yadav and Bhagoria (2014b)	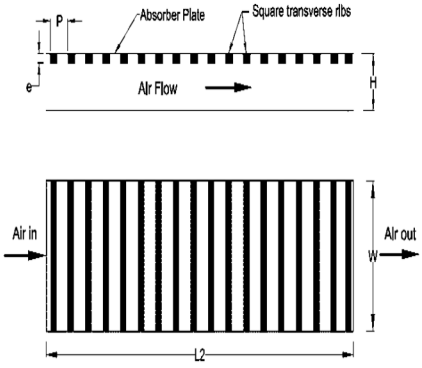 Square shaped rib	P/e: 7.14-35.71 e/D: 0.021-0.042 Re: 3000-18000	P/e: 10.71 e/D: 0.042 Re:12000

Jin *et al* (2015)	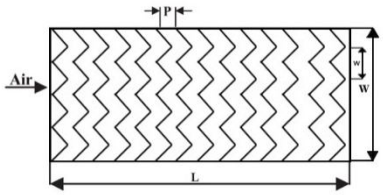 Multi V-shaped ribs	P/e: 3-20 e/D: 0.03-0.11 α: 30˚-75˚ Re: 8000-20000	P/e: 3 W/w: 6 α: 45˚
Singh *et al* (2015)	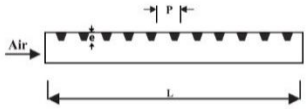 Trapezoidal rib  Non-uniform saw tooth shaped rib	P/e: 8 e/D = 0.043 Re: 3000-15000	Re:6000
Alam and Kim (2016)	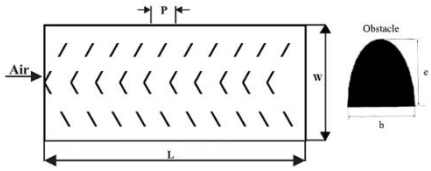 Semi ellipse shaped obstacles	P/e: 3.5 α: 30˚-90˚ Re: 6000-18000	α: 75˚
Deo *et al* (2016)	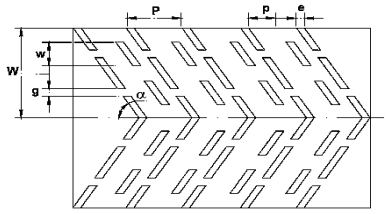 Multi-gap V-down with staggered ribs	P/e: 4-14 e/D: 0.026-0.057 α: 40˚-80˚ g/e: 1 w/e: 4.5 Re: 4000-12000	P/e: 12 e/D: 0.044 α: 60˚ Re: 12000
Gawande *et al* (2016)	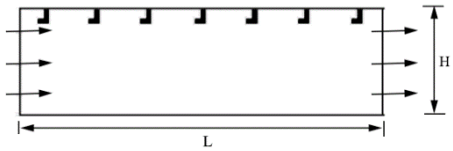 Reverse L-shaped ribs	P/e: 7.14-17.86 e/D: 0.042 Re: 3800-18000	P/e: 7.14 Re: 15000
Kumar and Kim (2016)	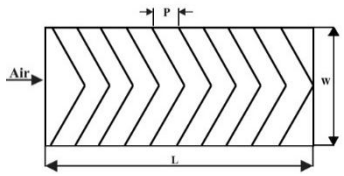 • V-rib • Dimpled in V-pattern • Protrusion in V-pattern • Grooves in V-pattern	P/e: 10 e/D: 0.040 α: 60˚ e/d_p: 0.5 g/p: 0.6 Re: 5000-20000	-

Hans *et al* (2017)	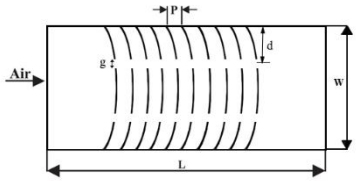 Broken arc ribs	P/e: 4-12 e/D: 0.022-0.043 α: 15˚-75˚ g/e: 0.5-2.5 d/w: 0.20-0.80 Re: 2000-16000	P/e: 10 e/D: 0.043 α: 30˚ g/e: 1 d/w: 0.65 Re: 12000
Kumar *et al* (2017)	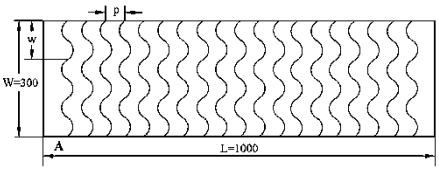 S shaped ribs	P/e: 4-16 e/D: 0.022-0.054 α: 30˚-75˚ W/w: 1-4 Re: 2400-20000	P/e: 8 e/D: 0.043 α: 60˚ W/w: 3
Singh and Singh (2017)	 Non-uniform saw tooth shaped rib	P/e: 4-30 e/D: 0.043 θ: 45˚ Re: 3000-15000	P/e: 16 Re: 9000

CHAPTER-III

MATERIALS AND METHODS

The research titled "Computational Fluid Dynamics Analysis on Heat and Fluid Flow of Square Wave Profile Transverse Rib Roughened Solar Air Heater Duct" was conducted at School of Renewable Energy Engineering, Punjab Agricultural University, Ludhiana, in the year 2016-17. The present study investigates the influence of repeated non-uniform cross-section transverse ribs of square wave profile on the Nusselt number and friction factor characteristics. The methodology adopted for the CFD analysis of the solar air heater duct is presented in the sections below:

COMPUTATIONAL DETAILS

The CFD analysis of solar air heater duct with square wave profiled transverse ribs has been carried out in 3-D using ANSYS Academic Research CFD 15.0. CFD employs the principle of resolving the problem under consideration in number of small cells and applying the continuity, momentum and energy equations on each cell and simulate the results for the pressure and temperature distribution in the roughened duct.

Fig. 3.1 illustrates the schematic view of the solar air heater duct employing roughness elements in the form of non-uniform cross-section transverse rib of square wave profile. The three-dimensional duct has a length, width and height as 1000 mm, 300 mm and 25 mm respectively and hydraulic diameter of 46.15 mm. The periodic ribs are applied underneath the absorber plate and the remaining walls were kept smooth and considered adiabatic. The roughened plate is subjected to heat flux of 1000 W/m^2.

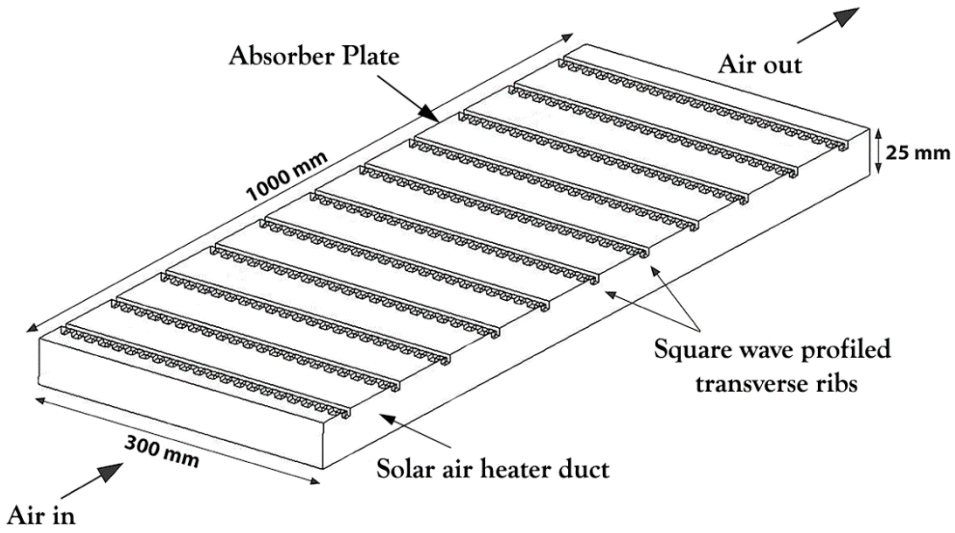

Fig. 3.1 Schematic view of solar air heater duct roughened with non-uniform cross-section square wave profiled transverse ribs.

ROUGHNESS GEOMETRY AND RANGE OF PARAMETERS

The present study is conducted on transverse rib of non-uniform cross-section of square wave profile as shown in Fig. 3.2. The investigation considered the parameters, relative roughness pitch from 4-30, relative roughness height from 0.015-0.043, relative roughness width from 10-310 and Reynolds number from 3000-15000. The investigated values of parameters considered in the present study are summarized in Table 3.1.

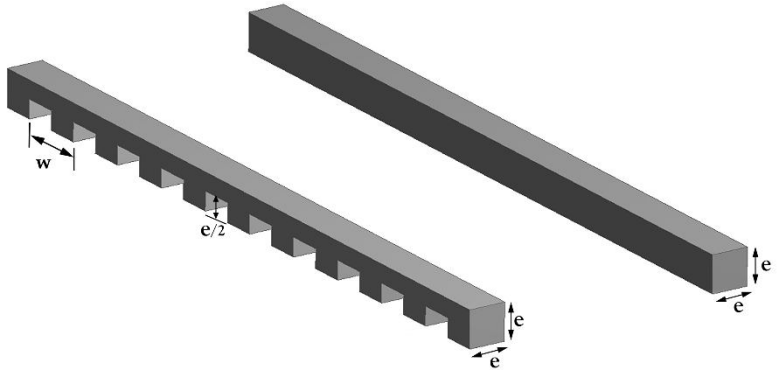

Fig. 3.2 Transverse ribs of square wave profile non-uniform cross-section and uniform square cross-section.

Table 3.1 Summary of the parameters covered in the present investigation.

Parameter	Values
Reynolds number (Re)	3000, 6000, 9000, 12000, 15000
Relative roughness pitch (P/e)	4, 10, 16, 24, 30
Relative roughness height (e/D)	0.015, 0.019, 0.029, 0.035, 0.043
Relative roughness width (W/w)	10, 85, 160, 235, 310

Table 3.2 Various combination of parameters investigated in the present study.

S. No.	Relative roughness pitch	Relative roughness width	Relative roughness height	Reynolds number
1	4	160	0.043	3000
2	4	160	0.043	6000
3	4	160	0.043	9000
4	4	160	0.043	12000
5	4	160	0.043	15000
6	10	160	0.043	3000
7	10	160	0.043	6000
8	10	160	0.043	9000
9	10	160	0.043	12000
10	10	160	0.043	15000
11	16	160	0.043	3000
12	16	160	0.043	6000
13	16	160	0.043	9000
14	16	160	0.043	12000
15	16	160	0.043	15000
16	24	160	0.043	3000

S. No.	Relative roughness pitch	Relative roughness width	Relative roughness height	Reynolds number
17	24	160	0.043	6000
18	24	160	0.043	9000
19	24	160	0.043	12000
20	24	160	0.043	15000
21	30	160	0.043	3000
22	30	160	0.043	6000
23	30	160	0.043	9000
24	30	160	0.043	12000
25	30	160	0.043	15000
26	10	10	0.043	3000
27	10	10	0.043	6000
28	10	10	0.043	9000
29	10	10	0.043	12000
30	10	10	0.043	15000
31	10	85	0.043	3000
32	10	85	0.043	6000
33	10	85	0.043	9000
34	10	85	0.043	12000
35	10	85	0.043	15000
36	10	160	0.043	3000
37	10	160	0.043	6000
38	10	160	0.043	9000
39	10	160	0.043	12000
40	10	160	0.043	15000
41	10	235	0.043	3000
42	10	235	0.043	6000
43	10	235	0.043	9000
44	10	235	0.043	12000
45	10	235	0.043	15000
46	10	310	0.043	3000
47	10	310	0.043	6000
48	10	310	0.043	9000
49	10	310	0.043	12000
50	10	310	0.043	15000
51	10	85	0.015	3000
52	10	85	0.015	6000
53	10	85	0.015	9000
54	10	85	0.015	12000
55	10	85	0.015	15000
56	10	85	0.019	3000
57	10	85	0.019	6000
58	10	85	0.019	9000
59	10	85	0.019	12000
60	10	85	0.019	15000
61	10	85	0.026	3000
62	10	85	0.026	6000
63	10	85	0.026	9000
64	10	85	0.026	12000
65	10	85	0.026	15000
66	10	85	0.035	3000
67	10	85	0.035	6000
68	10	85	0.035	9000
69	10	85	0.035	12000
70	10	85	0.035	15000

3.3 GOVERNING EQUATIONS

The turbulent air flow through the solar air heater duct is governed by 3-D equations of continuity, momentum and energy which are represented by following mathematical equations (Kumar and Kim 2016):

Continuity Equation:

$$\nabla.(\rho.\vec{v}) = 0 \tag{3.1}$$

Momentum Equation:

$$\nabla.(\rho.\vec{v}.\vec{v}) = -\nabla p + \nabla.\left(\mu\left[(\nabla\vec{v} + \nabla\vec{v}^{T}) - \frac{2}{3}\nabla.\vec{v}I\right]\right) \tag{3.2}$$

Energy Equation:

$$\nabla.\left(\vec{V}(\rho E + p)\right) = \nabla.(k_{eff}\nabla T - h\vec{J} + \left(\mu\left[(\nabla\vec{v} + \nabla\vec{v}^{T}) - \frac{2}{3}\nabla.\vec{v}I\right].\vec{v}\right) \tag{3.3}$$

3.4 SELECTION OF TURBULENCE MODEL AND FLOW DOMAIN

To ensure the accuracy of the numerical results in the CFD analysis, appropriate turbulence model must be selected. In a previous research conducted by Singh *et al* (2015), the Nusselt number was predicted for smooth duct by various turbulence models (Table 3.3). 3-D flow domain of smooth duct of full length of 1000 mm and a periodic duct length of 16 mm were considered. The predicted values were compared with Nusselt number determined using Gnielinski correlation (Eq. 3.4) and Dittus-Boelter correlation (Eq 3.5).

$$\mathrm{Nu} = \frac{\left(\frac{f}{8}\right)(\mathrm{Re}-1000)\mathrm{Pr}}{1+12.7\left(\frac{f}{8}\right)^{0.5}\left(\mathrm{Pr}^{2/3}-1\right)} \qquad \text{for } 3000 < \mathrm{Re} < 10000 \tag{3.4}$$

$$\mathrm{Nu} = 0.023\,\mathrm{Re}^{0.8}\mathrm{Pr}^{0.4} \qquad \text{for } \mathrm{Re} > 10000 \tag{3.5}$$

Table 3.3 Percentage of Average absolute deviation in Nusselt number from empirical correlations predicted under periodic and non-periodic conditions by different turbulence models.

Turbulence Model	Average absolute deviation (%)	
	Periodic condition	Non-periodic condition
Standard k-ε model	32.12	20.26
Standard k- ε with enhanced wall treatment	12.52	12.87
Standard RNG k- ε	39.39	20.21
RNG k- ε with enhanced wall treatment	10.28	13.06
Standard Realizable k-ε	19.25	21.02
Realizable k- ε with enhanced wall treatment	11.93	12.81
Standard k-ω	25.68	13.99
SST k-ω	19.07	13.17

It is clear from the Table 3.3 that RNG k-ε with enhanced wall treatment provides most accurate predictions with deviation of 10.28% from the values calculated from the above empirical correlations. The periodic flow field provides more accuracy as compared to full duct length of 1000 mm.

The turbulence model RNG k-ε with enhanced wall treatment has also been employed in other widely accepted numerical studies on rib roughened solar air heater duct reported by Yadav and Bhagoria (2013), Yadav and Bhagoria (2014a), Yadav and Bhagoria (2014b), Kumar and Kim (2016), Jin *et al* (2015), Karmare and Tikekar (2010) and Gawande *et al* (2016). The numerical results reported by the above authors for different rib geometries are in conformity with the experimental results. Therefore, to reduce the computational effort of the solution and more accurate predictions, periodic flow domain and turbulence model RNG k-ε with enhanced wall treatment has been selected for present CFD analysis.

3.5 CFD METHODOLOGY

3.5.1 Pre-processing

In the present study, 3-D rib roughened rectangular flow domain is prepared using ANSYS DesignModeler 15.0. Only one pitch length was modelled for the investigation (Fig. 3(a)) and symmetric boundary conditions are applied at the inlet. The duct has aspect ratio of 12 with dimensions of 300 mm x 25 mm. Rib parameters were varied accordingly and their individual effect on the performance was investigated by keeping the other two parameters fixed at a time.

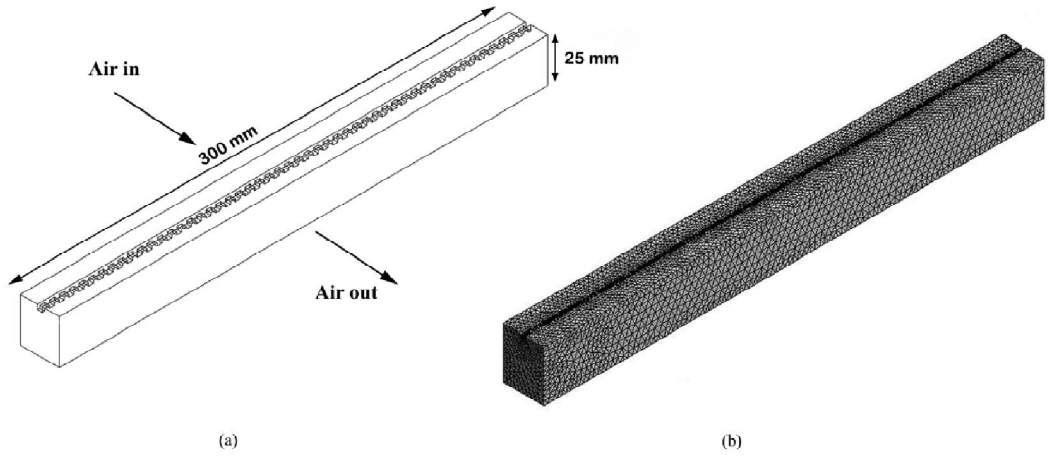

Fig. 3.3 (a) Schematic view of periodic computational domain of square wave rib roughened duct for CFD analysis (b) Grid generation on 3-D computational domain.

Grid generation for the computational domain was done in ANSYS Meshing component as shown in Fig. 3(b). Initially the flow domain is solved with coarse meshing and gradient adaption technique was sequentially used for refining the mesh in the areas where large variation occurs.

3.5.2 Grid independence test

For the solution refinement, grid independence test has been performed using gradient adaption technique. Mesh was made successively finer in the areas where large variation occurs. The gradient adaption was applied for maximum 10% variation in the parameters namely temperature, pressure, velocity, wall shear stress and turbulence intensity respectively (Singh and Singh 2017). The mesh after successive gradient adaptions for relative roughness pitch of 10, relative roughness width of 160, relative roughness height of 0.043 is shown in Fig. 3.4. The number of elements were increased from 49099 to 803226 in five steps. Table 3.2 shows the comparison for the resulting Nusselt number after successive gradient adaptions at relative roughness pitch of 10 and Reynolds number of 15000. It can be seen that after successive adaptions, the change in Nusselt number reduces and is small (<1%). So, the results after all the gradient adaptions can be considered as grid independent. Therefore, the gradient adaptions were done for all the combinations of rib and flow parameters as to make result grid independent.

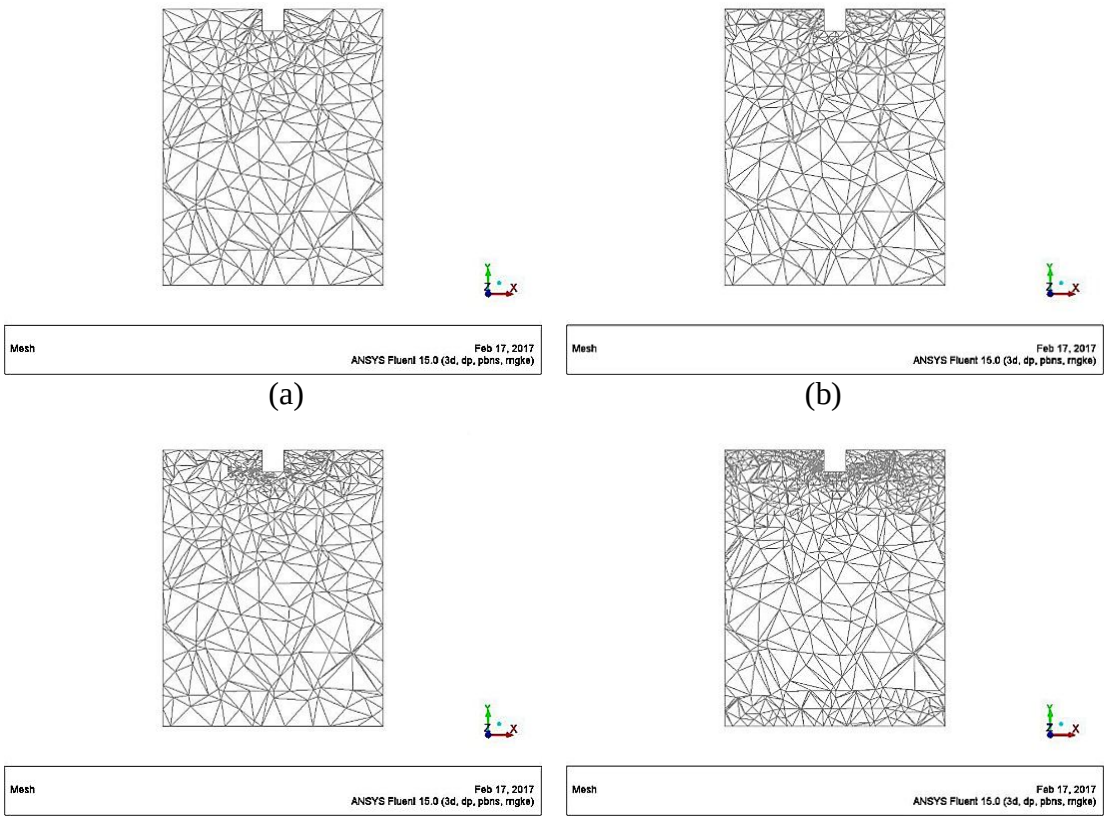

(a) (b)

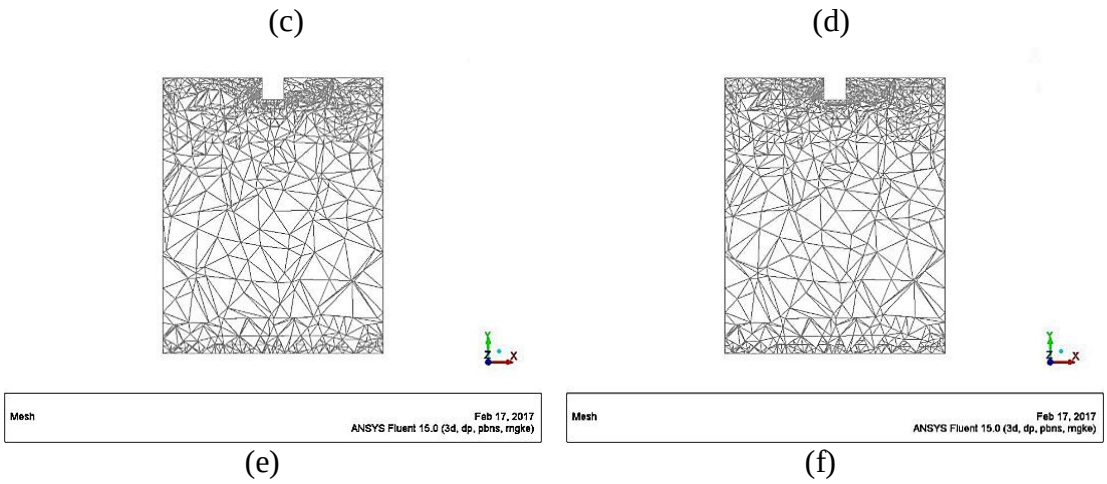

Fig. 3.4 Grid after successive gradient adaptions at relative roughness pitch (P/e) of 10 (a) Before adaptions (49099 cells) (b) Temperature gradient adaption (100584 cells) (c) Pressure gradient adaption (248515 cells) (d) Velocity gradient adaption (649663 cells) (e) Wall shear stress gradient adaption (684853) cells (f) Turbulence intensity gradient adaption (803226 cells).

Table 3.4 Nusselt number after successive gradient adaptions for relative roughness pitch of 10 and Reynolds number of 15000.

Adaptions	Number of Elements	Nusselt number	Variation in Nusselt number (%)
Before adaption	49099	76.28	-
Temperature	100854	72.29	5.23
Pressure	248515	72.44	0.20
Velocity	641663	72.53	0.12
Wall shear stress	684853	72.96	0.59
Turbulence intensity	803226	72.84	0.16

3.5.3 Solution calculation

Finite volume based numerical method is used to solve the governing equations. Fluid properties are specified and boundary conditions in terms of mass flow rate calculated using Reynolds number were applied at inlet. Uniform heat flux of 1000 W/m^2 was applied on the absorber plate. At the other walls, adiabatic boundary conditions were applied. Initially, air temperature in the duct is taken as 300K. Double precision pressure based solver and discretization upwind scheme of the second order is considered for the solution calculation. The residuals for the convergence of solution are selected as 10^{-10} for the energy equation and

10^{-5} each for the equations of continuity, velocity, turbulent kinetic energy and turbulent dissipation rate (Singh and Singh 2017).

3.6 VALIDATION OF THE CFD METHODOLOGY

For validation of the CFD methodology, the analysis on solar air heater duct with transverse rib roughness has been conducted using the CFD methodology and compared with the results from the experimental study by Gupta *et al* (1993). Fig. 3.5 illustrates the schematic of circular rib roughened solar air heater duct experimentally investigated by Gupta *et al* (1993) and the periodic rib roughness geometry investigated using CFD for the comparison purpose. The investigation parameters were taken same as in the experimental study conducted by Gupta *et al* (1993) viz., relative roughness pitch of 10, relative roughness height of 0.043, aspect ratio (W/H) of 11.5 and Reynolds number (Re) range of 3000-15000.

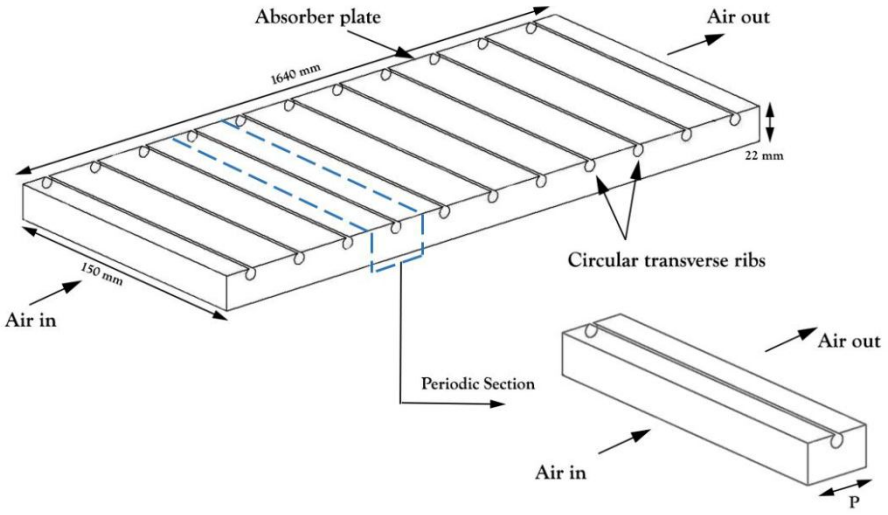

Fig. 3.5 Schematic of circular rib roughened solar air heater duct experimentally investigated by Gupta *et al* (1993) and periodic rib roughness geometry investigated using CFD.

Fig. 3.6 compares the Nusselt number predicted by the proposed CFD method with the experimental results. It can be seen that the trends of the CFD results are in good agreement with the experimental outcomes with average absolute deviation of 7.75% from the experimental values.

So, the proposed CFD methodology can be used to predict the experimental results within reasonable accuracy and therefore can be used for the analysis of the rib roughened solar air heater duct.

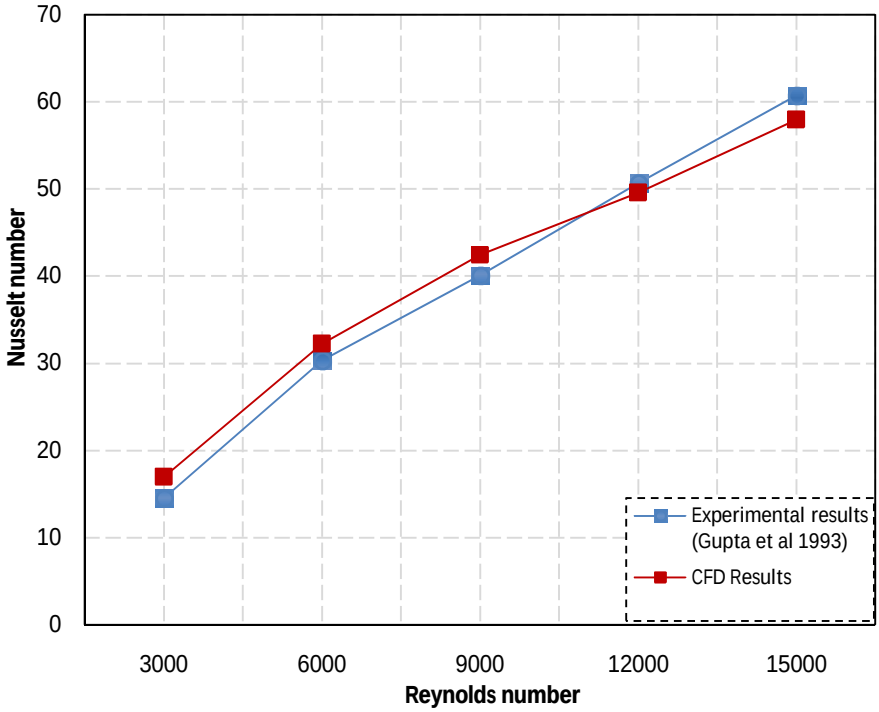

Fig. 3.6 Comparison of the CFD results with the results from experimental study conducted by Gupta *et al* (1993).

CHAPTER-IV

RESULTS AND DISCUSSION

The heat and fluid flow characteristics of the solar air heater duct employing non-uniform cross-section transverse rib of square wave profile are obtained using ANSYS Academic Research CFD 15.0. The investigation covered the rib parameters, relative roughness pitch (P/e) from 4-30, relative roughness height (e/D) from 0.015-0.043 and relative roughness width (W/w) from 10-310 and were investigated for Reynolds number (Re) from 3000-15000. The outcomes of the present study are discussed in detail below:

4.1 NUSSELT NUMBER CHARACTERISTICS

The application of non-uniform cross-section square wave profiled transverse rib as artificial roughness on the absorber plate causes obstruction to the flow breaking the laminar sub-layer adjacent to the absorber plate. This results in the augmentation in heat transfer coefficient between absorber plate and air as compared to smooth duct due to the separation and reattachment of the boundary layer. Consequently, higher Nusselt number is achieved as a result of providing roughness. The effect of different roughness and flow parameters on heat transfer enhancement of the roughened solar air heater duct are presented below:

4.1.1 Effect of Reynolds Number

Fig. 4.1 has been plotted to depict the Nusselt number variation with Reynolds number at relative roughness pitch values from 4-30 for non-uniform cross-section square wave profiled rib and compared with smooth duct. To study this effect, the relative roughness height and relative roughness width were kept fixed as 0.043 and 160 respectively. It has been noticed that the increase in Reynolds number leads to increase in Nusselt number for the investigated range of relative roughness pitch.

Fig. 4.2 illustrates the effect of Reynolds number on the flow pattern which clarifies the heat transfer characteristics at different Reynolds numbers. It can be evidently seen from Fig. 4.2 (a) that at lower Reynolds number of 3000, the reattachment distance is quite large and the flow reattachment length is very small. Thus, there exist a low heat transfer zone behind the rib due to flow recirculation which extends to a large distance downstream from the rib until reattachment starts happening. However, as the Reynolds number is increased to 9000, the reattachment point shifts closer to the rib on its upstream side.

As the reattachment distance decreases with the increase in Reynolds number, the reattachment length is increased (Fig. 4.2 (b)). More air comes in contact with the absorber plate and as result of this, Nusselt number increases at Reynolds number of 9000. Further increasing Reynolds number decreases the reattachment distance to a great extent and

reattachment of the flow occurs for more length (Fig. 4.2 (c)). Thus, more length resembles higher local Nusselt number and low heat transfer zone is significantly reduced. Thus, best extraction of heat is possible in this case and consequently Nusselt number is maximum at Reynolds number of 15000.

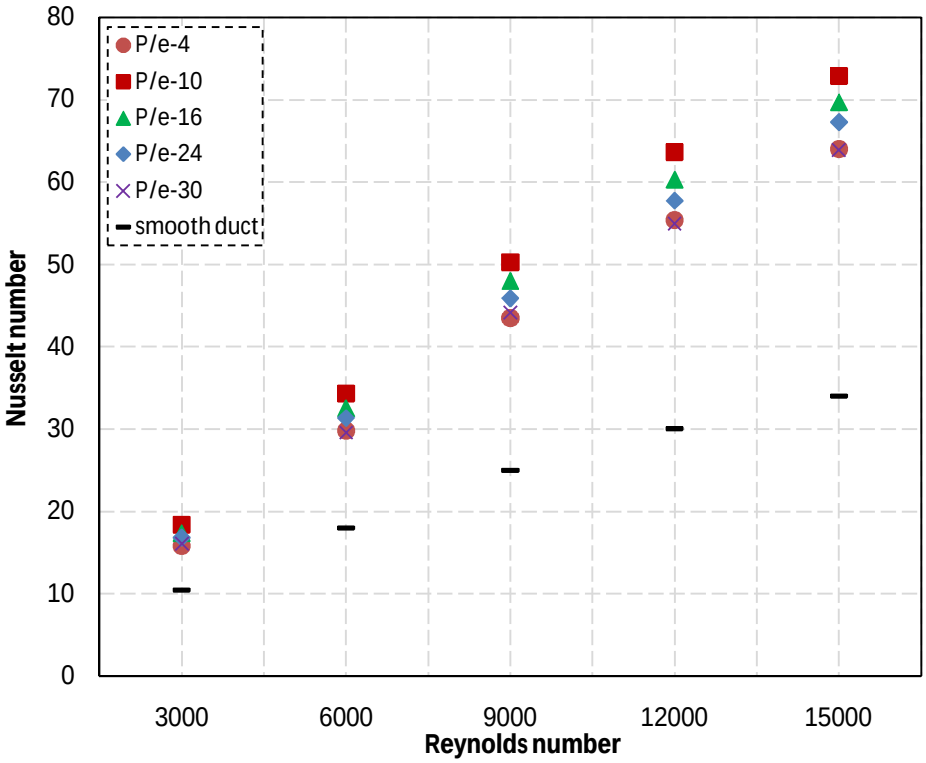

Fig. 4.1 Effect of Reynolds number on Nusselt number for different values of relative roughness pitch.

The contours of static temperature validate the above trend of Nusselt number variation with Reynolds number. It is clearly indicated in the Fig. 4.3 that the static temperature is higher behind the rib at lower Reynolds number and the area corresponding to the higher static temperature is also high (Fig. 4.3(a)). This is due to large flow reattachment distance on the downstream side of the rib. Fig. 4.3 (b) shows that at Reynolds number of 9000, the static temperature lowers at little distance behind the rib which indicates the reattachment of the flow. The area corresponding to higher static temperature reduces behind the rib which is due to the effect of reduction in flow reattachment distance as discussed earlier (Fig. 4.2 (b). At Reynolds number of 15000, there is further reduction in reattachment distance and hence reduction in low heat transfer area behind the rib which can be seen by lower static temperature from Fig. 4.3 (c).

As the lower static temperature implies better heat transfer rate, the Reynolds number of 15000 offers maximum value of Nusselt number. Also, slightly lower static temperature is

observed behind the rib where air flows through gaps as compared to area between two gaps where higher static temperature exists. This shows the improvement in the heat transfer characteristics at the gap positions behind the rib.

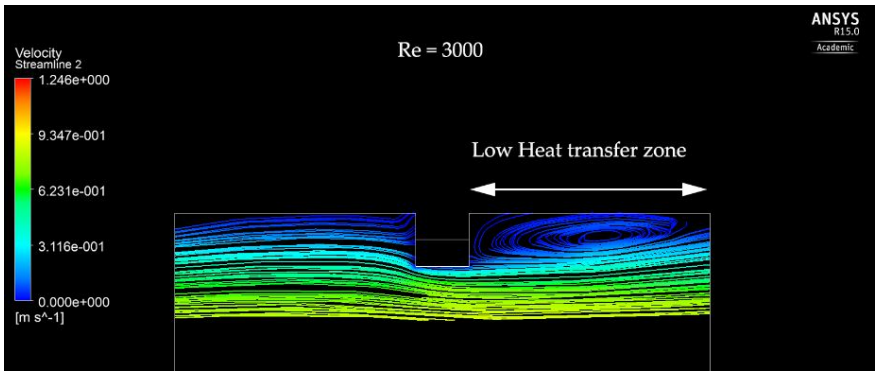

(a)

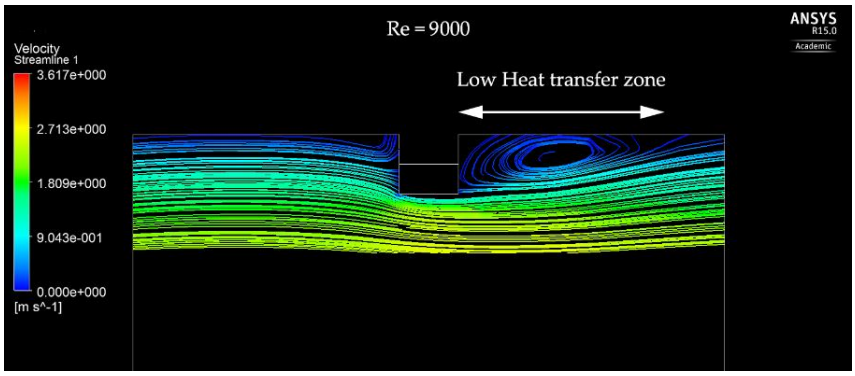

(b)

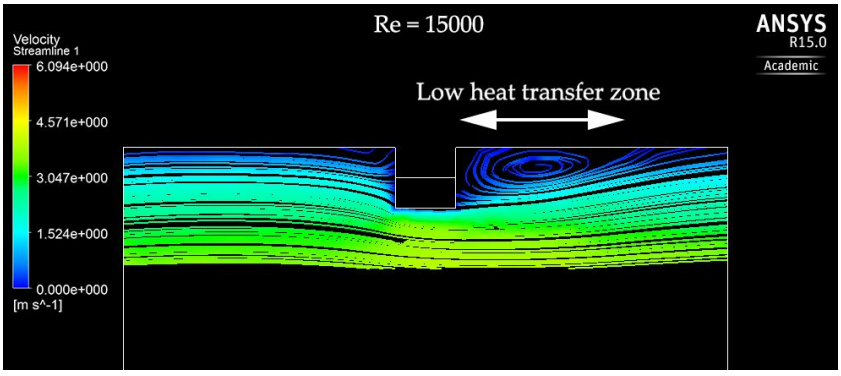

(c)

Fig. 4.2 Streamlines inside the duct on mid-plane normal to the absorber at P/e of 10 and Re values of (a) 3000 (b) 9000 and (c) 15000.

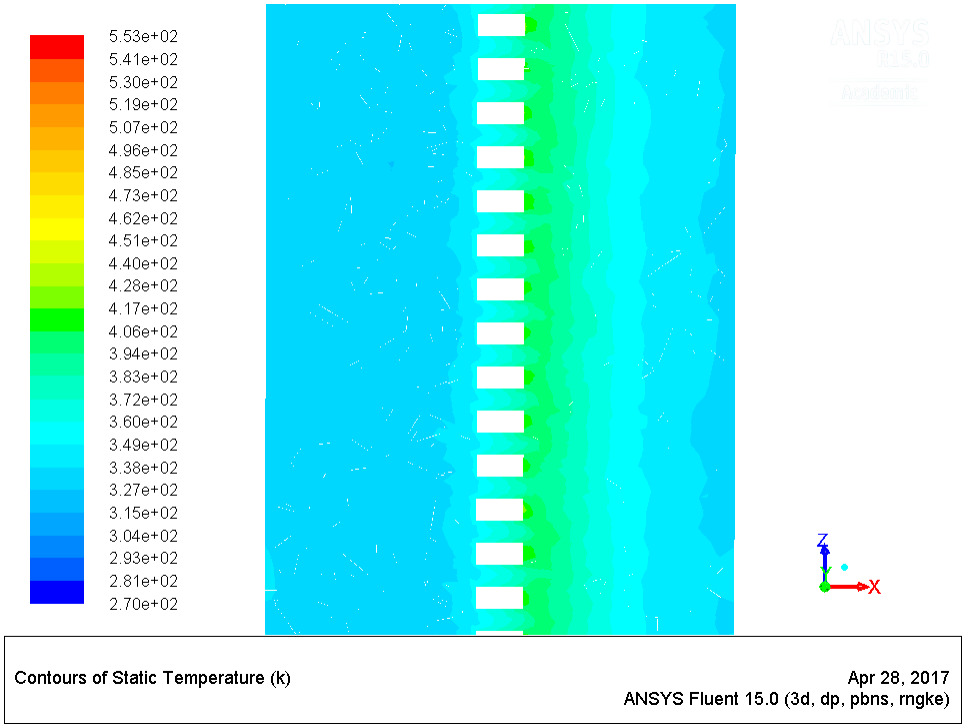
5.53e+02
5.41e+02
5.30e+02
5.19e+02
5.07e+02
4.96e+02
4.85e+02
4.73e+02
4.62e+02
4.51e+02
4.40e+02
4.28e+02
4.17e+02
4.06e+02
3.94e+02
3.83e+02
3.72e+02
3.60e+02
3.49e+02
3.38e+02
3.27e+02
3.15e+02
3.04e+02
2.93e+02
2.81e+02
2.70e+02
Z
X
Contours of Static Temperature (k)
Apr 28, 2017
ANSYS Fluent 15.0 (3d, dp, pbns, rngke)

(a)

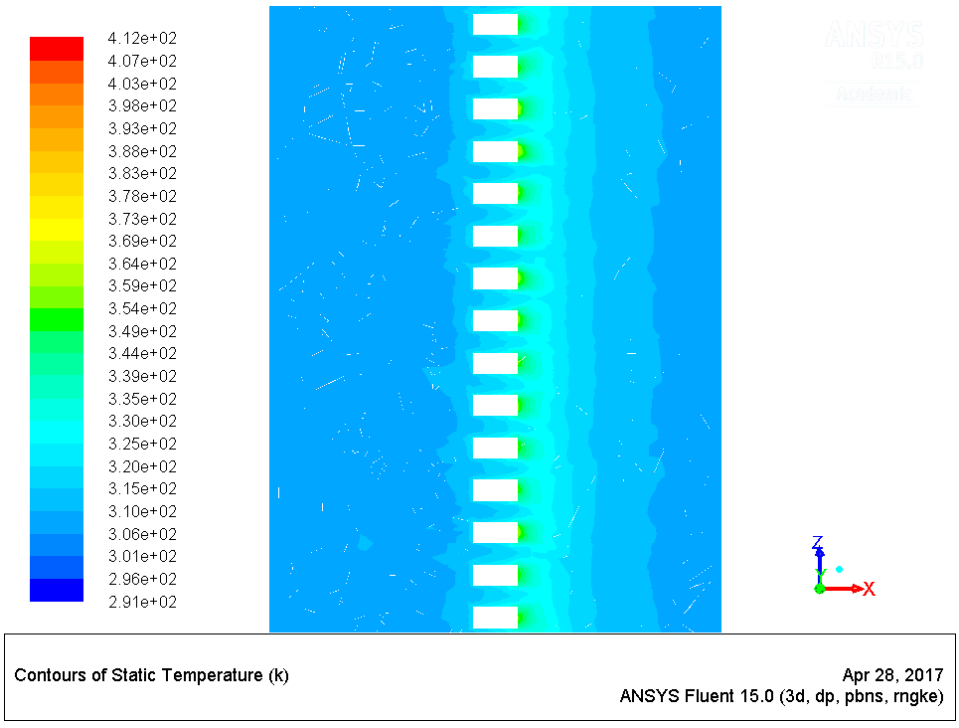
4.12e+02
4.07e+02
4.03e+02
3.98e+02
3.93e+02
3.88e+02
3.83e+02
3.78e+02
3.73e+02
3.69e+02
3.64e+02
3.59e+02
3.54e+02
3.49e+02
3.44e+02
3.39e+02
3.35e+02
3.30e+02
3.25e+02
3.20e+02
3.15e+02
3.10e+02
3.06e+02
3.01e+02
2.96e+02
2.91e+02
Z
X
Contours of Static Temperature (k)
Apr 28, 2017
ANSYS Fluent 15.0 (3d, dp, pbns, rngke)

(b)

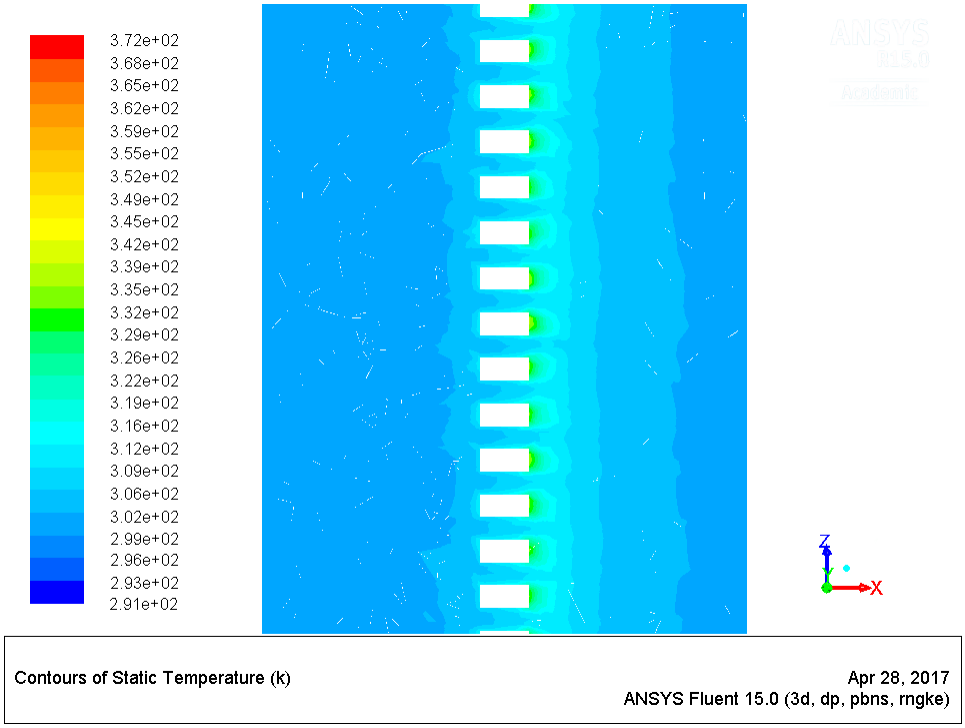

(c)

Fig. 4.3 Contours for static temperature on a parallel plane at distance of 1.5 mm from absorber at P/e of 10 and Re values of (a) 3000 (b) 9000 and (c) 15000.

4.1.2 Effect of relative roughness pitch

Fig 4.1 is redrawn as Fig. 4.4 for clearly understanding the influence of relative roughness pitch on Nusselt number. It has been observed that Nusselt number attains maximum value at relative rib pitch value of 10 and is lower on both sides of this value. The lowest Nusselt number corresponds to relative roughness pitch of 4. This is attributed to the phenomena of optimal length of the flow reattachment between the ribs which is accountable for the maximum enhancement in heat transfer rate.

The flow reattachment characteristics between two consecutive ribs is demonstrated in Fig. 4.5. It can be seen that the obstruction created by the ribs to the flow causes recirculation close to the rib area and reduction in the flow velocity. It is observed that flow reattachment is not possible for the relative roughness pitch of 4 (Fig. 4.5 (a)) which may be due to the fact that roughness elements are too close to allow the flow contact with the heat transfer surface. Hence major portion of the area between two successive ribs have low heat transfer rate due to the flow not coming in contact with the roughened absorber plate. But at relative rib pitch of 10, the reattachment of flow can be clearly seen (Fig. 4.5 (b)). The flow remains attached for an optimal length between the two ribs where local Nusselt number is

high and then the flow separation takes place at the next rib. With further increase in pitch of the roughness elements, the reattachment length of the flow becomes too large which can be seen from Fig. 4.5(c). The local Nusselt number starts reducing downstream as we move along the reattached flow. Laminar sub-layer starts developing as the distance between two consecutive ribs becomes large. Hence there is increase in lower heat transfer area between two ribs resulting in lower Nusselt number.

Thus, among the investigated values, relative pitch of 10 has more reattachment points per unit length. Higher local Nusselt number at the reattachment points results in higher overall Nusselt number. Consequently, the Nusselt number peaks at relative roughness pitch of 10 and decreases when increased beyond 10.

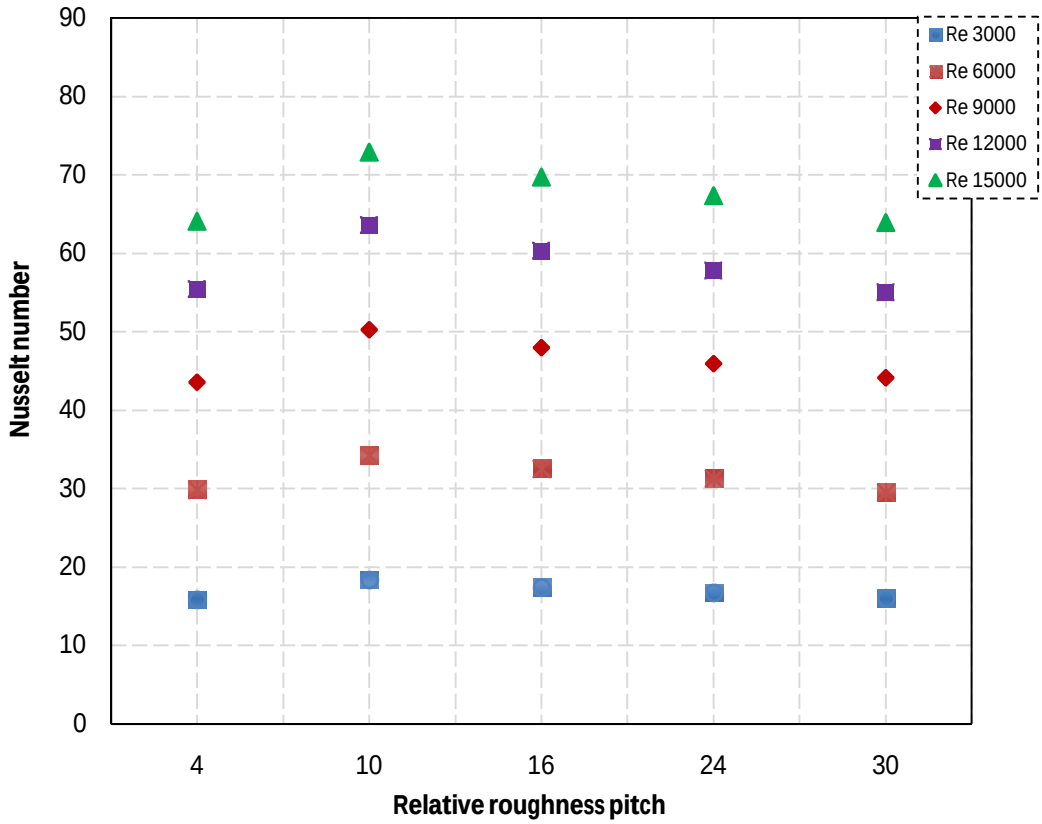

Fig. 4.4 Variation of Nusselt number with relative roughness pitch for different values of Reynolds number.

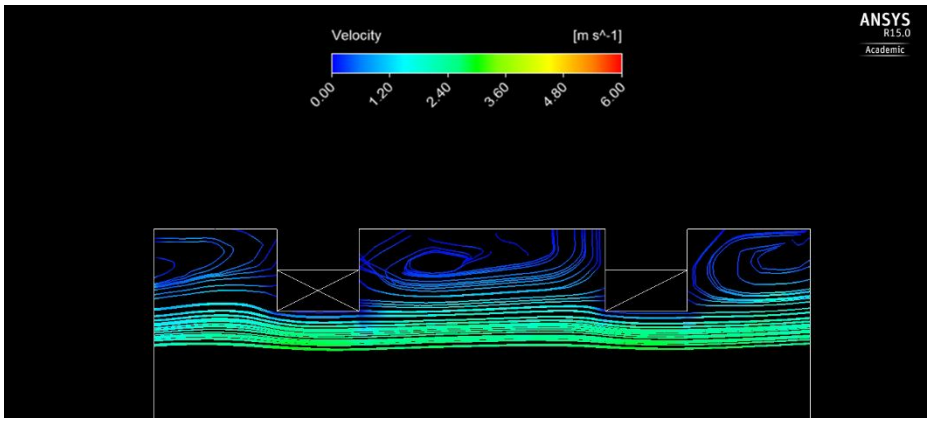

(a)

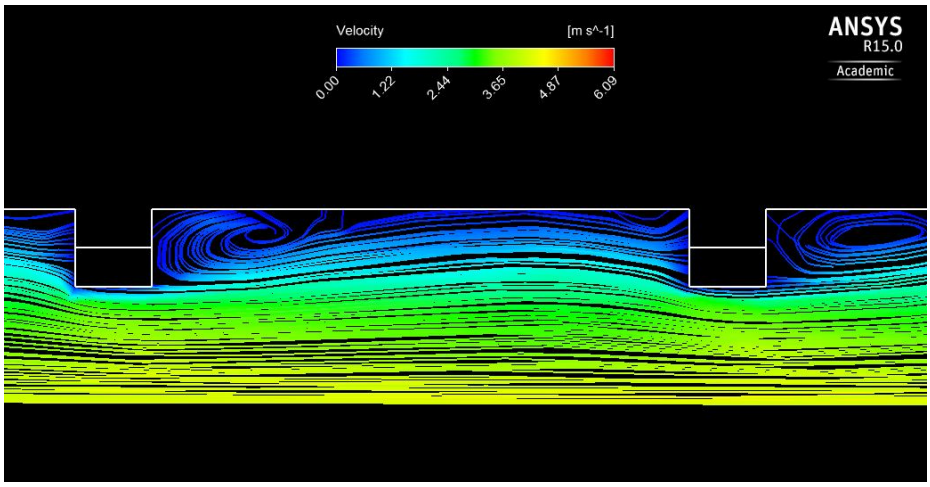

(b)

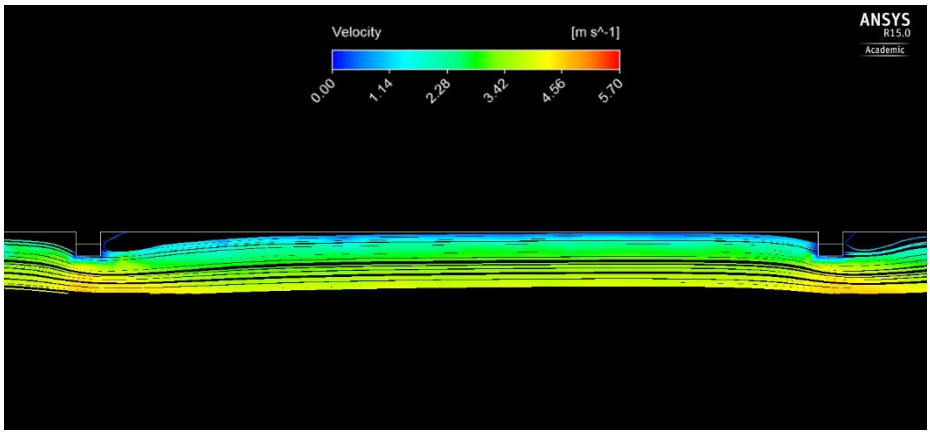

(c)

Fig. 4.5 Streamlines showing the flow characteristics and reattachment of the flow between two consecutive ribs on the mid-plane of the duct at Re of 15000 for P/e values of (a) 4 (b) 10 and (c) 30.

Fig. 4.6 presents the static temperature contours at different relative roughness pitch value for Reynolds number of 15000. It can be observed that the static temperature is high behind the rib because of the recirculation of the flow and lowers at a certain distance on both sides of the rib. Similar trend of static temperature is observed for other pitch values. Static temperature is lowest for relative roughness pitch of 10 which shows the conformity with the maximum heat transfer rate obtained at this value. Then it increases with further increase in relative pitch up to 30. This can be observed from the maximum scale values of contours of static temperature. At lower pitch, static temperature is higher downstream side of the rib as no re-attachment is happening in this case (Fig. 4.6 (a)). The laminar sub-layer formation at higher relative roughness pitch values results in higher scale value of static temperature throughout the duct length (Fig. 4.6 (c)) justifying comparatively lower Nusselt number at higher pitch values.

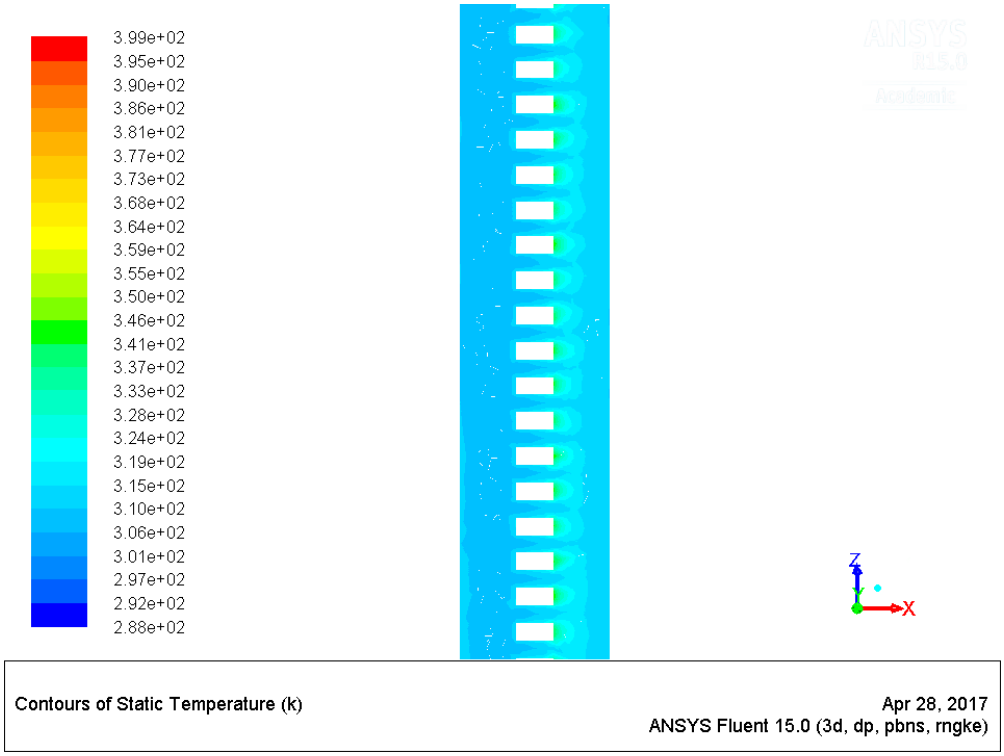

(a)

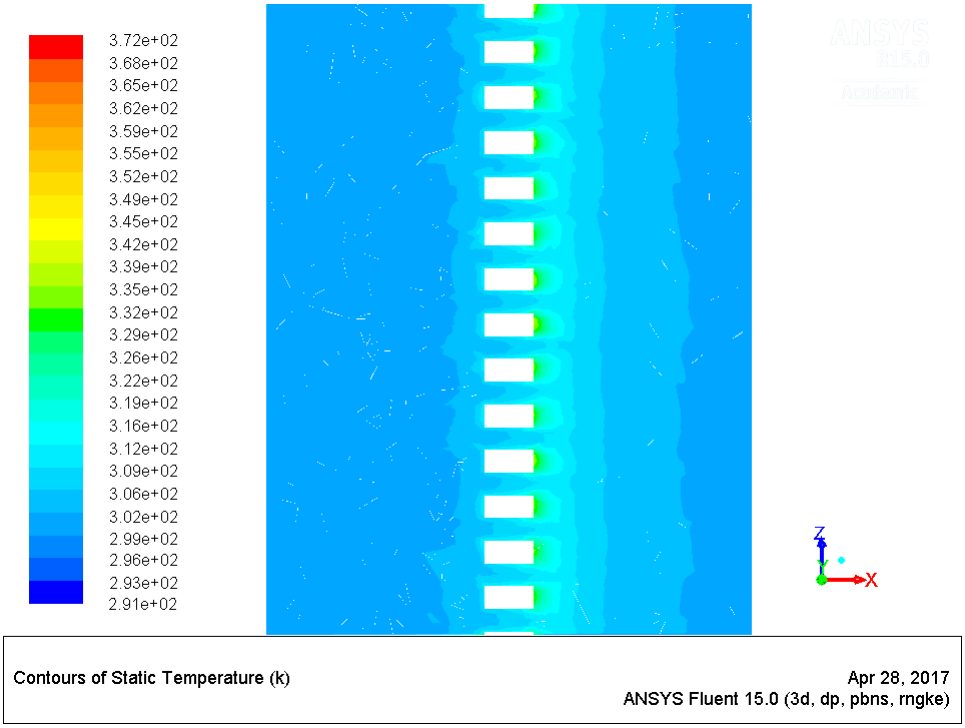

(b)

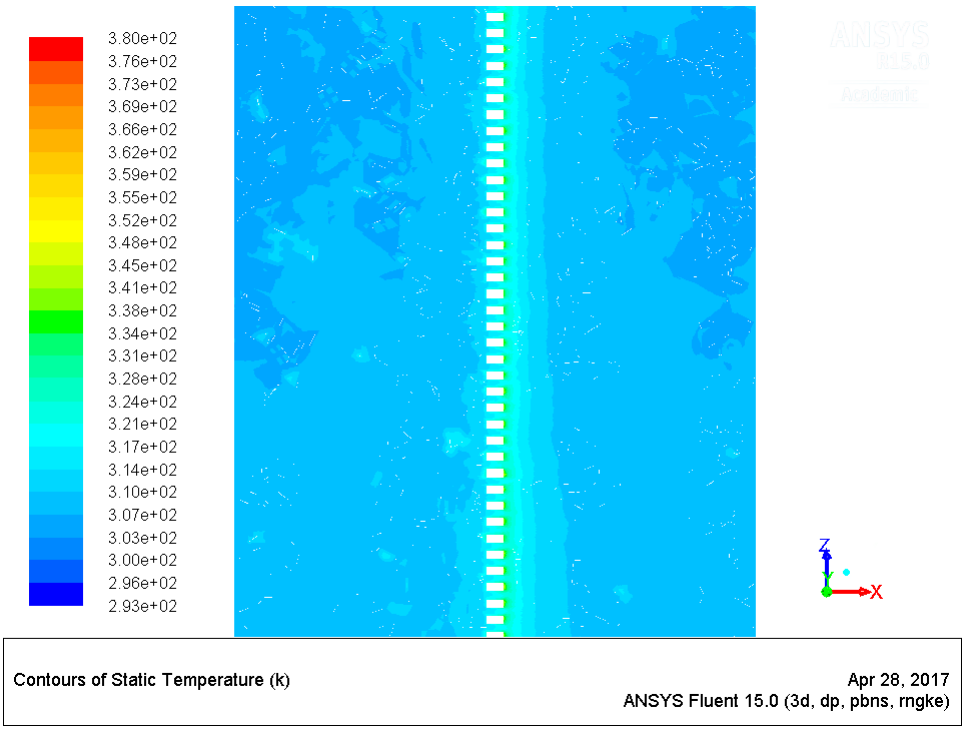

(c)

Fig. 4.6 Contours for Static temperature a parallel plane at distance of 1.5 mm from absorber for Re of 15000 and P/e values of (a) 4 (b) 10 (c) 30.

The variation of Nusselt number enhancement over that of smooth duct at different relative pitch values for Reynolds number range 3000-15000 can be seen in Fig. 4.7. The Nusselt number enhancement sharply increases up to relative roughness pitch of 10 and then decreases with further increase up to 30. The Nusselt number enhancement is maximum for the Reynolds number of 15000 for all the pitch values. The maximum enhancement of 2.14 times is achieved at relative roughness pitch of 10 and Reynolds number of 15000.

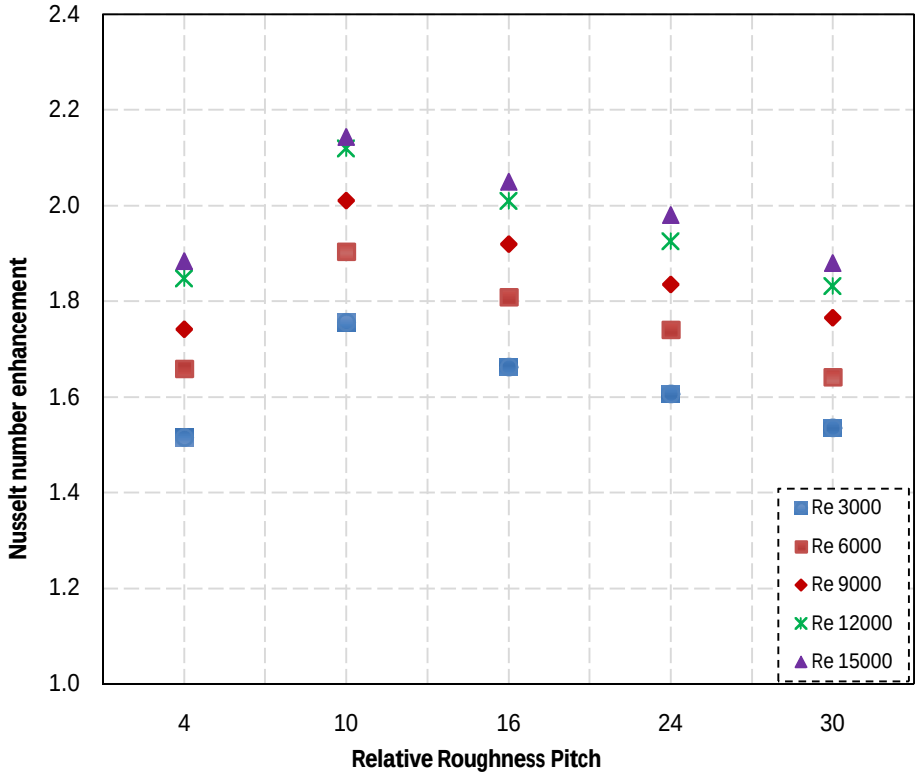

Fig. 4.7 Variation of Nusselt number enhancement with relative roughness pitch for different values of Reynolds number.

4.1.3 Effect of relative roughness width

To investigate the effect of relative roughness width on the performance of the rib roughened duct, relative roughness pitch was kept fixed as 10 as it accounts for maximum Nusselt number as obtained in earlier section. Relative height of the roughness elements was fixed as 0.043 and relative roughness width was varied as 10, 85, 160, 235, 310 and investigated for Reynolds number values of 3000, 6000, 9000, 12000 and 15000.

Fig. 4.8 shows the Nusselt number as a function of Reynolds number for different values of relative roughness width. As expected, there is increase in the Nusselt number with the increase in Reynolds number from 3000 to 15000 and the reason of this increase is same as discussed earlier in section 4.1.1 in reference to Fig. 4.2.

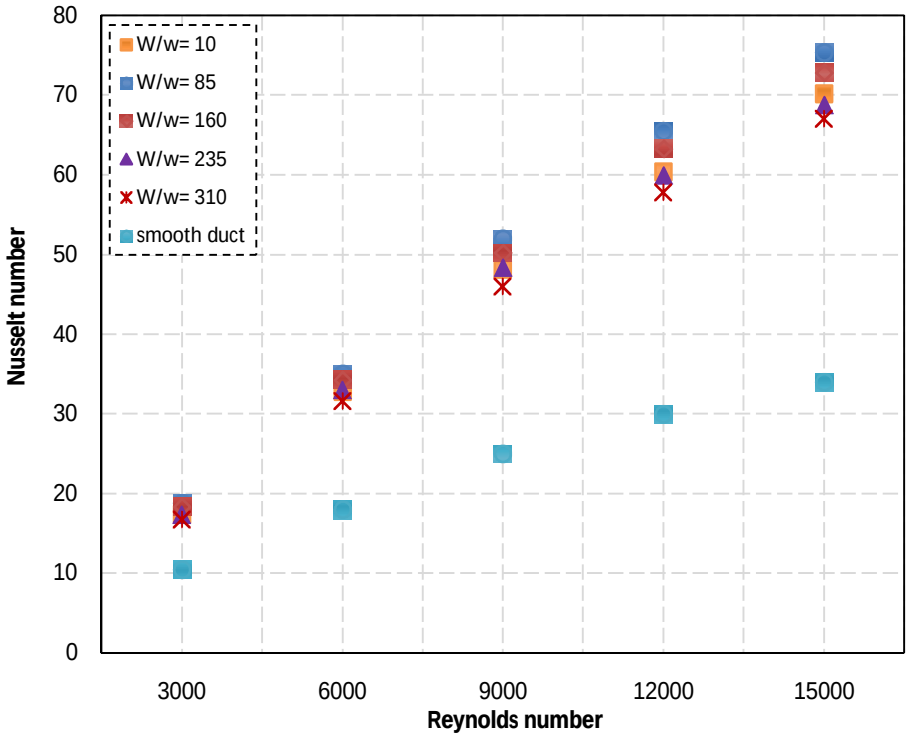

Fig. 4.8 Variation of Nusselt number with Reynolds number for different values of relative roughness width.

Fig. 4.8 is redrawn as Fig. 4.9 to determine the impact of relative roughness width on Nusselt number for the Reynolds number ranging 3000-15000. The Nusselt number has been observed maximum at the relative roughness width of 85 and is lower on both sides of this value. This might be for the reason that at lower relative roughness width of 10, the width of the gap is more and hence there is more area in between two consecutive gaps which resembles low heat transfer rate.

This phenomenon is illustrated by the velocity streamlines in Fig. 4.10 showing fluid flow characteristics at different relative width values. At relative roughness width of 10, the reattachment distance is large where the air flows over the full cross-section of the rib and this area along the whole duct width is more due to lower number of rib openings (Fig. 4.10 (a). Thus, the low heat transfer area in the whole duct is also higher due to more recirculation zone. Whereas the air flowing through the gaps lowers the reattachment distance. But due to higher gap width, more area on the backside of the full cross-section of the rib is unaffected as the flow goes straight across the gap (Fig. 4.11 (a)). The secondary flow through the gap affects only small area near the edges and flow velocity behind the rib reduces to great extent. Thus, local Nusselt number lowers at major portion of the area between two rib gaps and hence flow through the large gaps is not much effective. Consequently, average Nusselt number is less for relative roughness width of 10. However, at relative roughness width of 85,

the recirculation behind the ribs is substantially decreased due to the secondary flow through these gaps (Fig. 4.10 (b)). The reattachment distance for the relative width of 85 decreases and consequently reattachment length increases optimally. Further the flow through gaps expands past the gap and thus affects the flow between two consecutive gaps (Fig. 4.11 (b)). High flow velocity near the rib is maintained at the gap and the full cross-section region as compared to high velocity gradient for relative width value of 10. Thus, lower heat transfer area reduces as compared to relative roughness width of 10 and average Nusselt number value increases at the relative roughness width of 85. Further increasing the relative rib width reduces the gap size which causes reduction in the flow velocity and the strength of the secondary flow to break down the eddies Fig. 4.10 (c) and Fig. 4.11 (c). The reattachment points also shift farther through the full rib cross-section and rib openings, so reattachment length decreases. Consequently, the average Nusselt number decreases as relative roughness width is increased beyond 85.

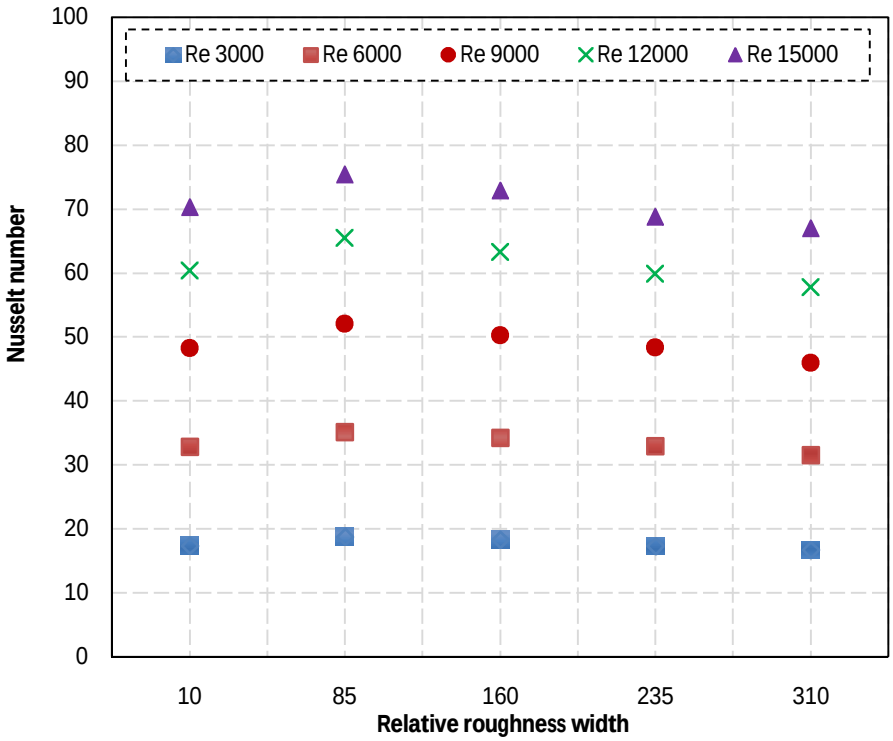

Fig. 4.9 Variation of Nusselt number with relative roughness width for different values of Reynolds number.

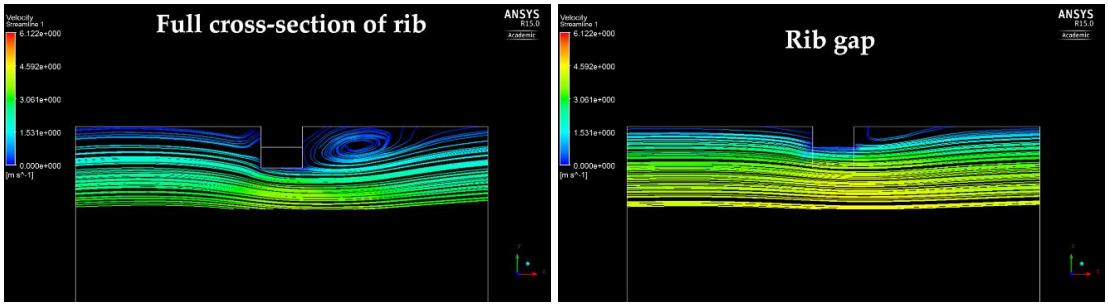

(a)

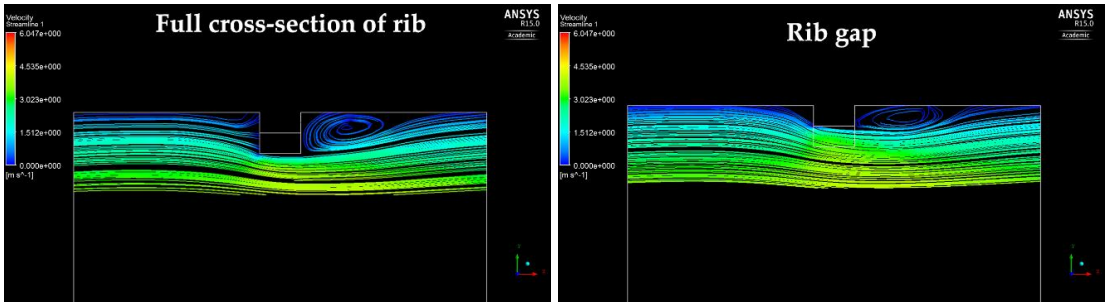

(b)

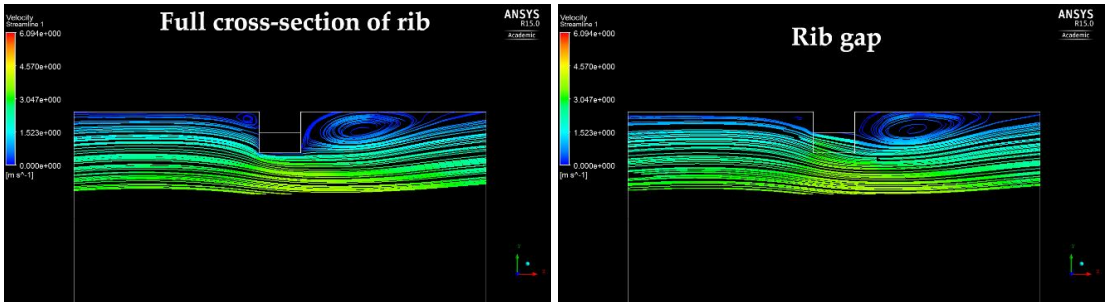

(c)

Fig. 4.10 Streamlines inside the duct near the mid-plane normal to absorber for Re of 15000 and W/w values of (a) 10 (b) 85 and (c) 310.

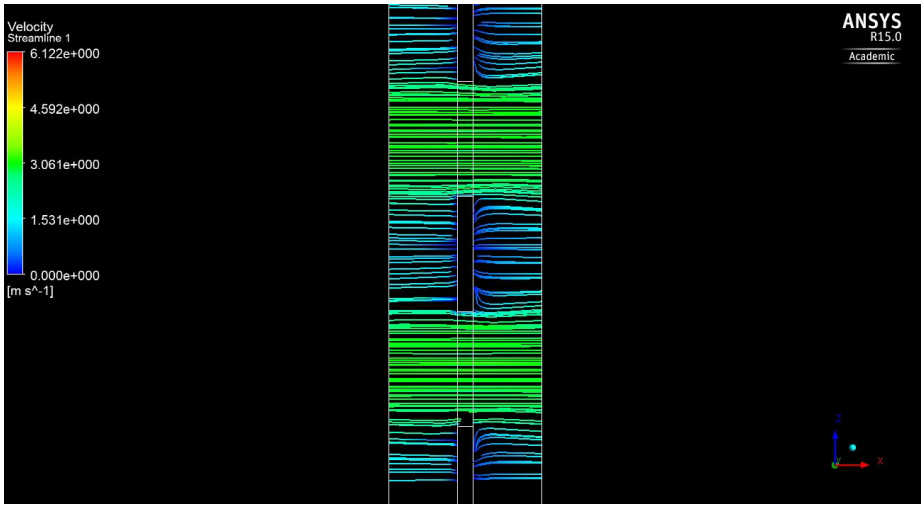

(a)

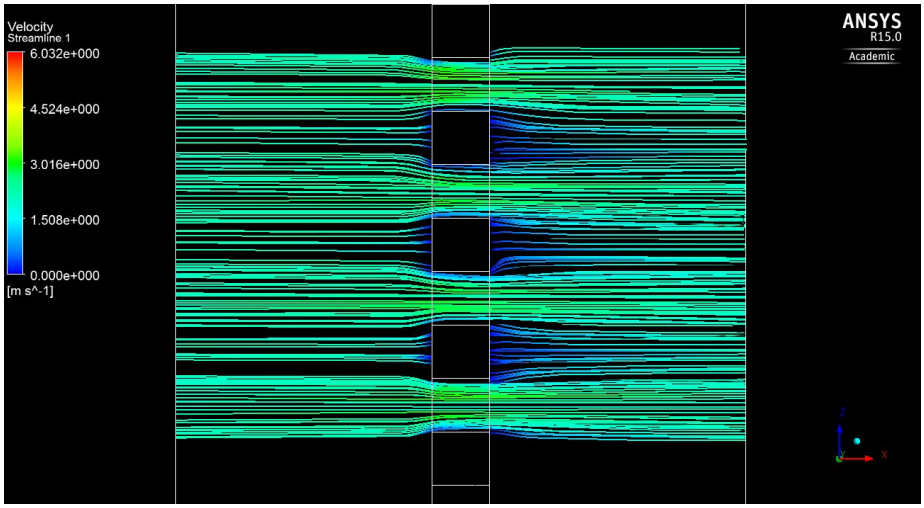

(b)

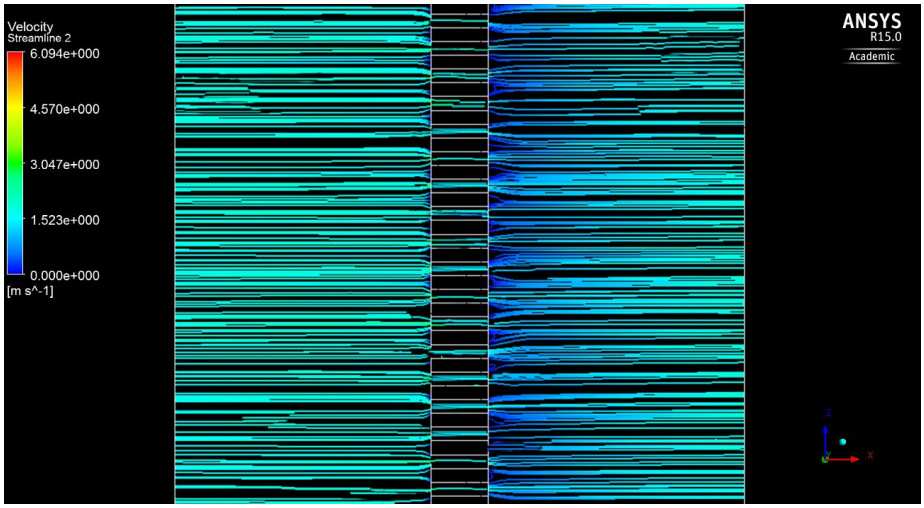

(c)

Fig. 4.11 Streamlines through the rib gaps on a parallel plane at distance of 1.5 mm from absorber at Re of 15000 and W/w values of (a) 10 (b) 85 and (c) 310.

Fig. 4.12 shows the variation in static temperature due to relative roughness width for relative roughness pitch of 10 and Reynolds number of 15000. The static temperature is higher behind the rib which indicates comparatively lower heat transfer zone. At relative width of 10, more area corresponds to the higher static temperature which signifies the lower heat transfer rate. This area is reduced at relative roughness width of 85 and again it develops with the increasing number of rib openings. The static temperature is lowest for the roughness width value of 85 which confirms the highest heat transfer rate. The maximum observed values of static temperature are 376 K, 369 K, 373 K, 381 K, 384 K for relative roughness width values of 10, 85, 160, 235, 310 respectively. As lower static temperature indicates higher rate of heat extraction, the relative roughness width of 85 offers maximum Nusselt number.

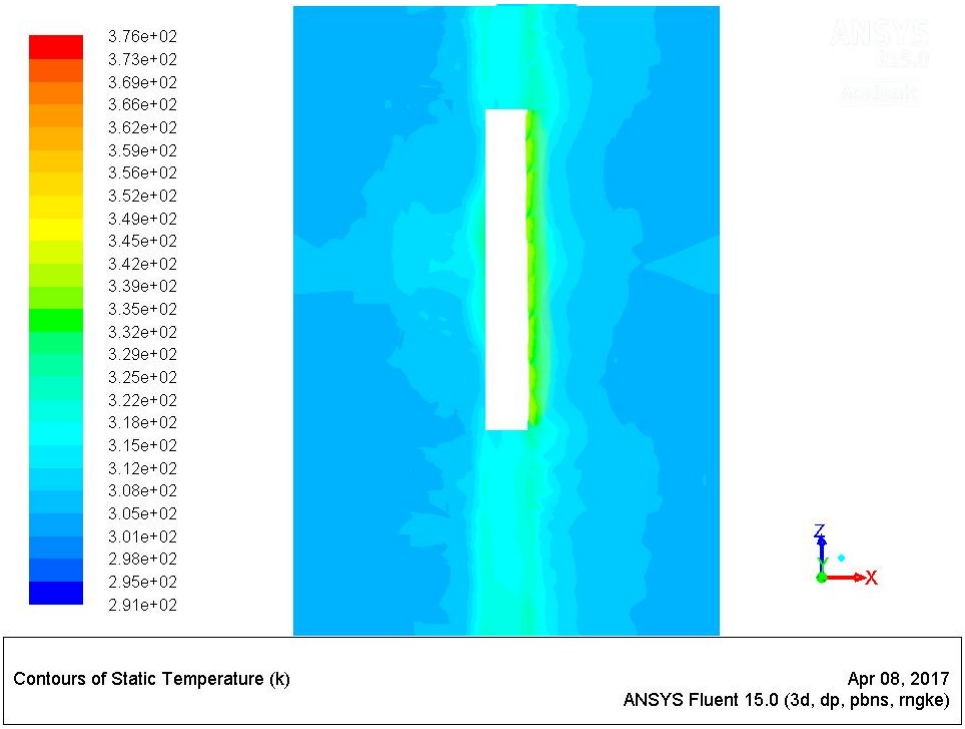

(a)

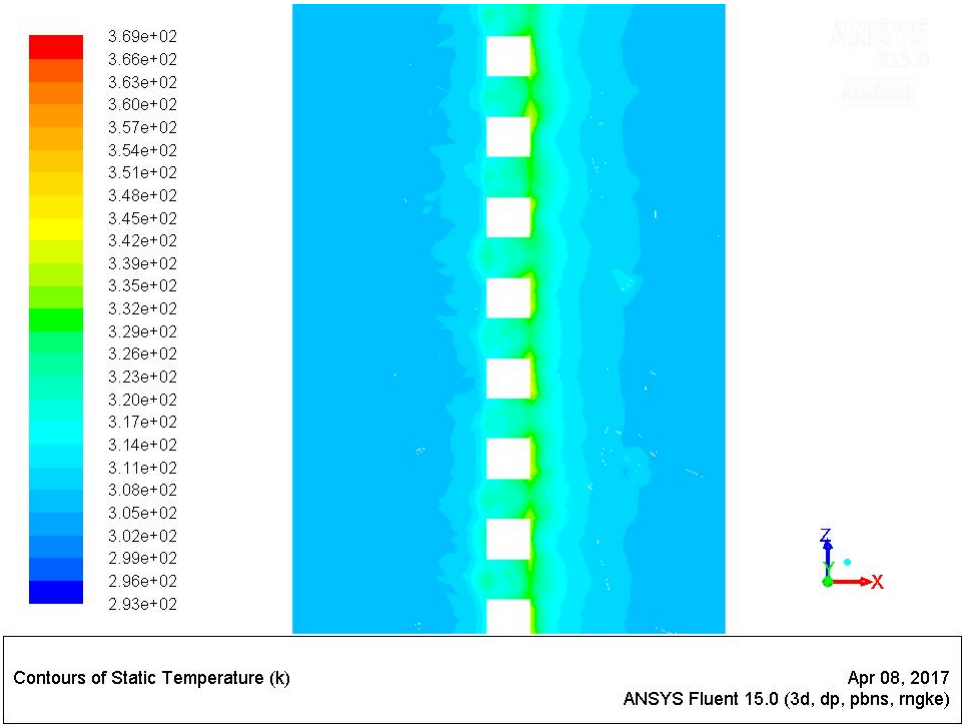

(b)

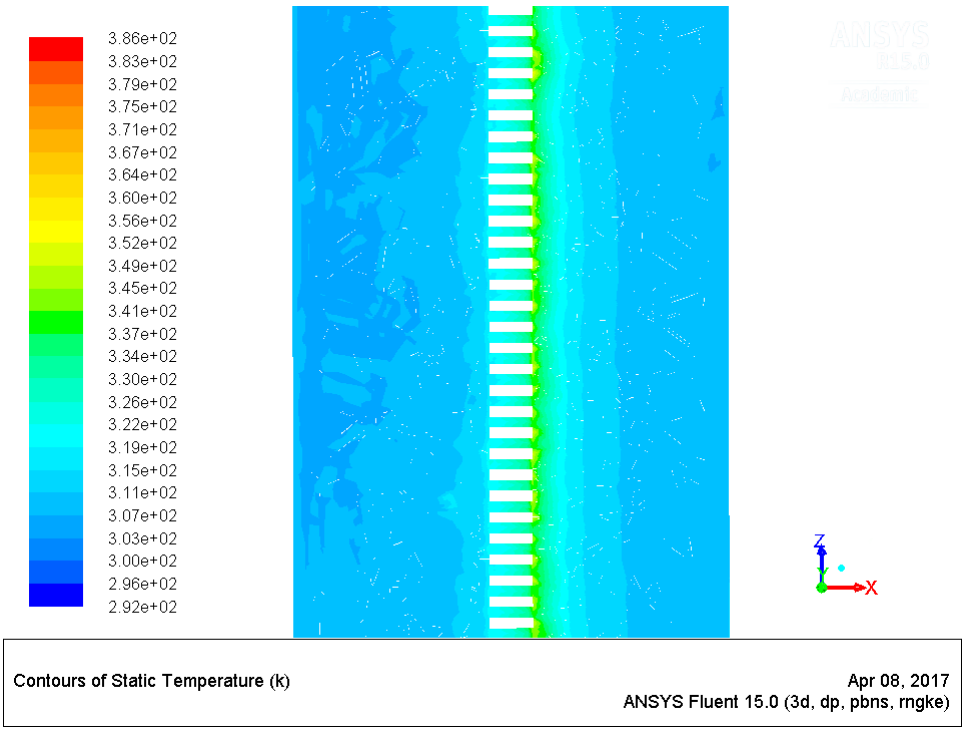

(c)

Fig. 4.12 Contours of static temperature on a parallel plane at distance of 1.5 mm from absorber for W/w values of (a) 10 (b) 85 and (c) 310.

Fig. 4.13 has been plotted to find out the impact of relative width of the roughness elements on the enhancement in Nusselt number. For the investigated Reynolds number range

of 3000-15000, Nusselt number enhancement improves up to relative roughness width of 85 and falls with further increase up to 310. The enhancement is maximum for Reynolds number of 15000 for all investigated values of relative width of the roughness elements. The maximum enhancement in Nusselt number is observed to be 2.22 times over the smooth duct at relative roughness width of 85 and Reynolds number of 15000.

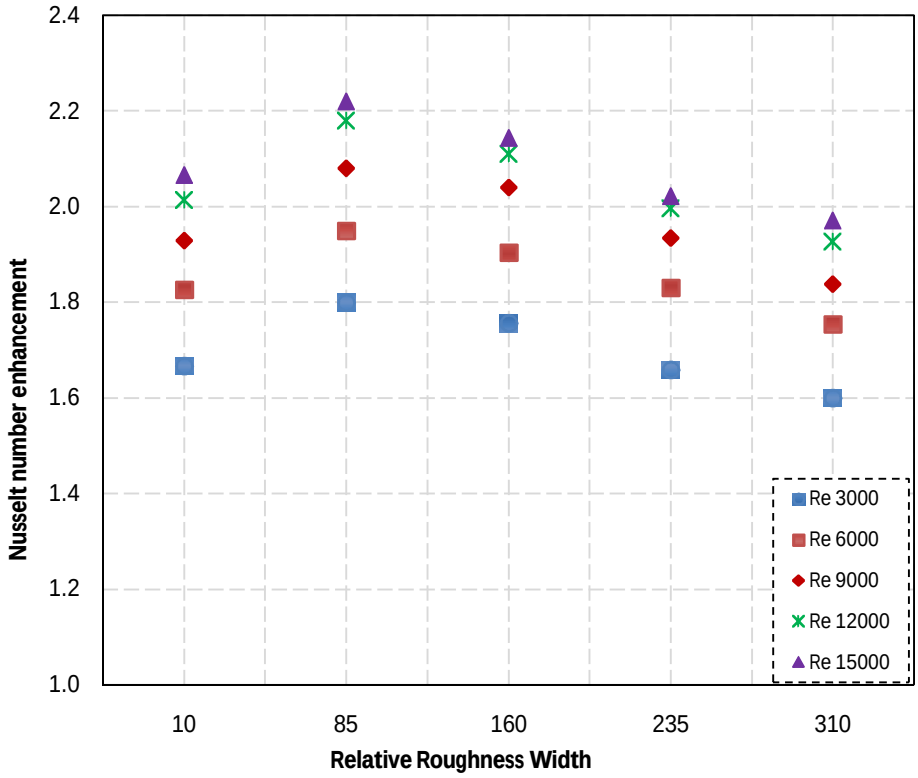

Fig. 4.13 Variation of Nusselt number enhancement with relative roughness width for different values of Reynolds number.

4.1.4 Effect of relative roughness height

To investigate the effect of the rib height on the Nusselt number characteristics of the rib roughened duct, relative roughness pitch and relative roughness width were kept fixed as 10 and 85 respectively as these parameters corresponds to maximum Nusselt number obtained above. Relative roughness height was varied as 0.015, 0.019, 0.026, 0.035, 0.043 and investigated for Reynolds number values of 3000, 6000, 9000, 12000 and 15000.

The effect of relative height of the rib on Nusselt number for Reynolds number 3000 - 15000 is presented in Fig. 4.14 and Fig. 4.15. In all the cases, Nusselt number tends to increase as the Reynolds number increases from 3000 to 15000 and this variation has been explained earlier in section 4.1.1. Nusselt number continuously enhances with the increment in relative rib height. For the entire Reynolds number range, Nusselt number is found to be highest for relative roughness height of 0.043.

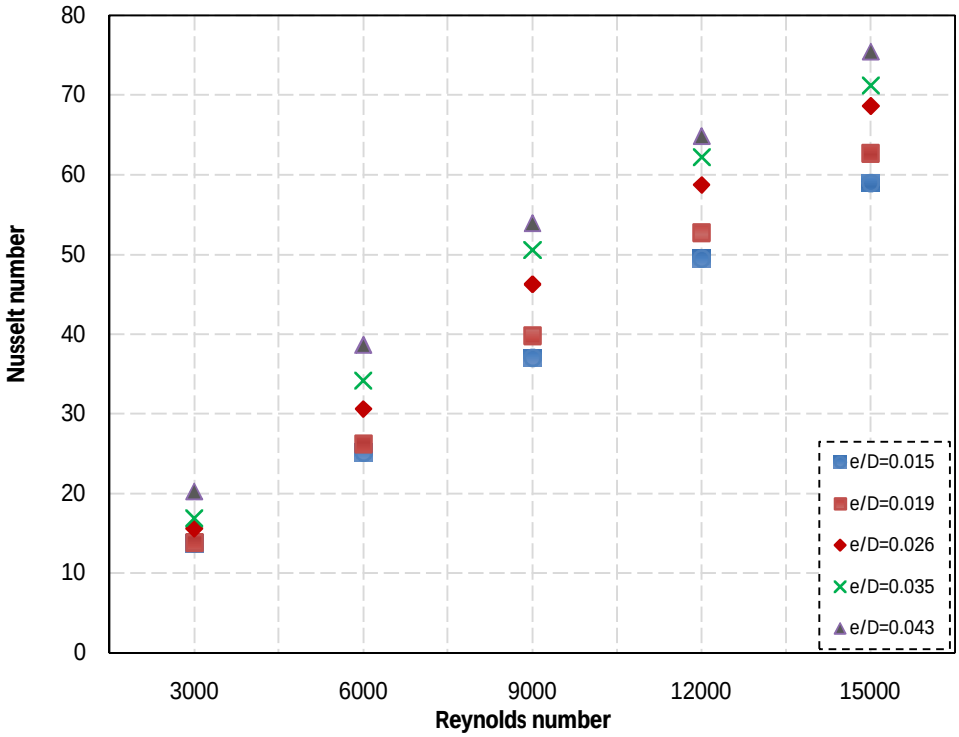

Fig. 4.14 Variation of Nusselt number with Reynolds number for different values of relative roughness height.

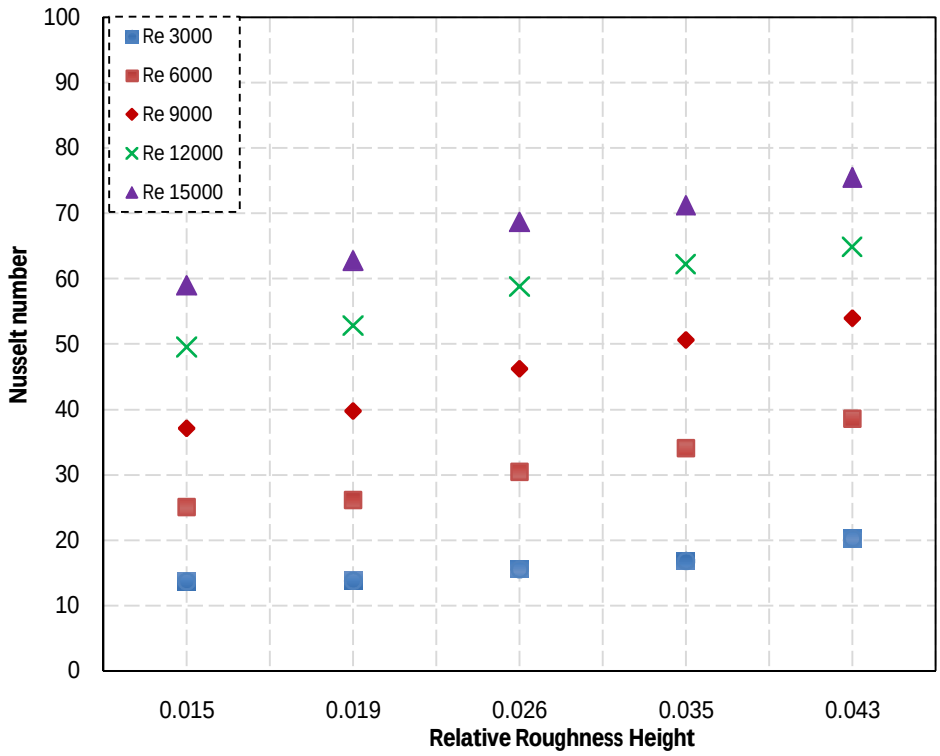

Fig. 4.15 Variation of Nusselt number with relative roughness height for different values of Reynolds number.

The Nusselt number characteristics with the variation in rib height can be clearly understood from streamlines inside the duct from Fig. 4.16. It can be seen that the application of rib roughness disrupts the viscous sub-layer and turbulence is generated close to the ribs. The turbulence intensifies with the increase in rib height as rib protrudes more into core flow. For all rib heights, relative roughness pitch was kept fixed as 10. So, with variation in rib height, the basic flow structure remains same. But as the relative roughness height is increased from 0.015 to 0.043, the reattachment distance is seen decreasing and consequently, the reattachment length is increased. It has been observed that for relative roughness height of 0.015, the reattachment starts nearly after 64% of the distance between the two ribs and approximately the reattachment length is just 21.4% of the inter-rib region (Fig. 4.16 (a)). The reattachment distance decreases with the increase in rib height and at relative roughness height of 0.026, the reattachment distance reduces to around 49% and reattachment length is increased to about 30% of the inter-rib region (Fig. 4.16 (b)). Further increase in relative roughness height shows more improvement in reattachment profile and reattachment distance reduces to around 40% and reattachment length is increased to 45% approximately. The reattachment length over the full duct length of 1000mm, increases from just approximately 171 mm at relative roughness height of 0.015 to 450 mm at relative roughness height of 0.043. This indicates the reduction in low heat transfer area with the increase in rib height. Consequently, Nusselt number is highest at relative roughness height of 0.043.

The contours of static temperature confirm the above trend of Nusselt number variation with rib height. It is clearly indicated in Fig. 4.17 that the static temperature is higher behind the rib at lower relative roughness height and the area corresponding to the higher static temperature is also high (Fig. 4.17(a)) This is due to large flow reattachment distance on the downstream side of the rib. Whereas Fig. 4.17 (b) shows that at relative roughness height of 0.026, the static temperature lowers at little distance behind the rib which indicates the reduction in flow reattachment distance as discussed earlier (Fig. 4.16 (b)). At relative roughness height of 0.043, there is further reduction in reattachment distance and hence reduction in low heat transfer area behind the rib which can be seen by lower static temperature from Fig. 4.17 (c). The maximum observed values of static temperature are 382 K, 380 K, 377 K, 373 K, 369 K for relative roughness height values of 0.015, 0.019, 0.026, 0.035 and 0.043 respectively. As the lower static temperature implies better heat transfer rate, the static temperature contours justify that relative roughness height of 0.043 offers maximum Nusselt number.

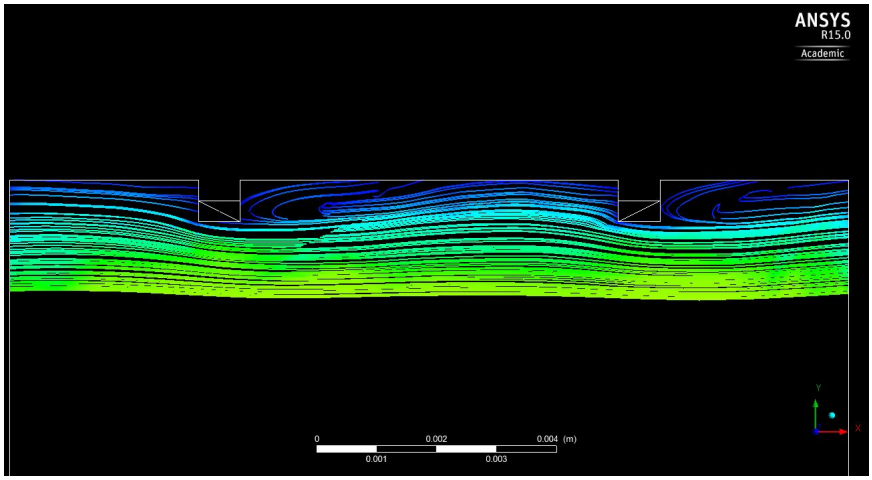
ANSYS
R15.0
Academic
0
0.002
0.004 (m)
0.001
0.003
Y
X

(a)

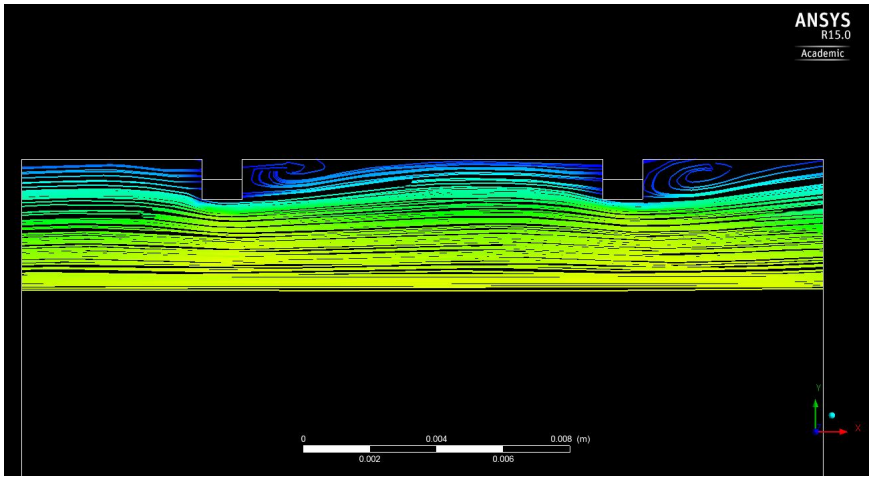
ANSYS
R15.0
Academic
0
0.004
0.008 (m)
0.002
0.006
Y
X

(b)

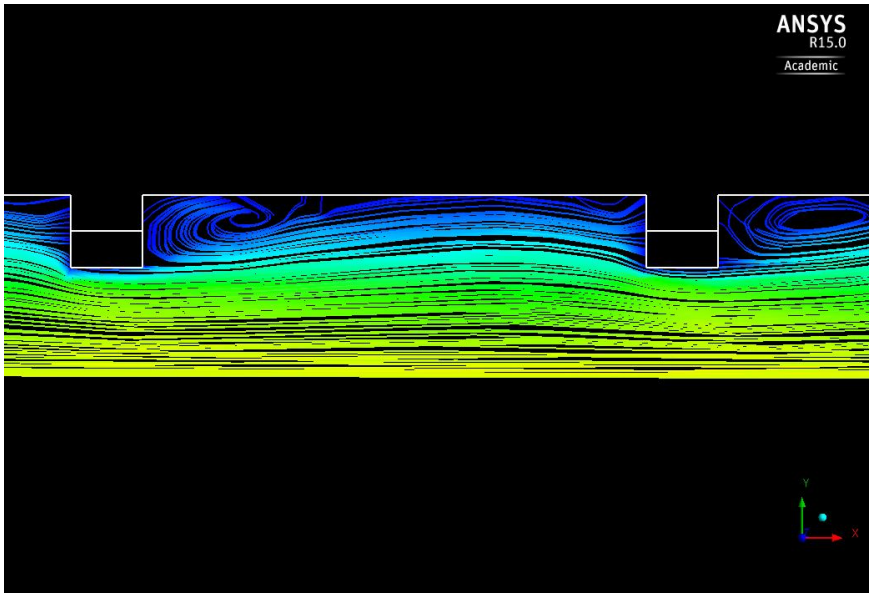
ANSYS
R15.0
Academic
Y
X

(c)

Fig. 4.16 Streamlines inside the duct at the mid-plane normal to absorber for e/D values of (a) 0.015 (b) 0.026 (c) 0.043.

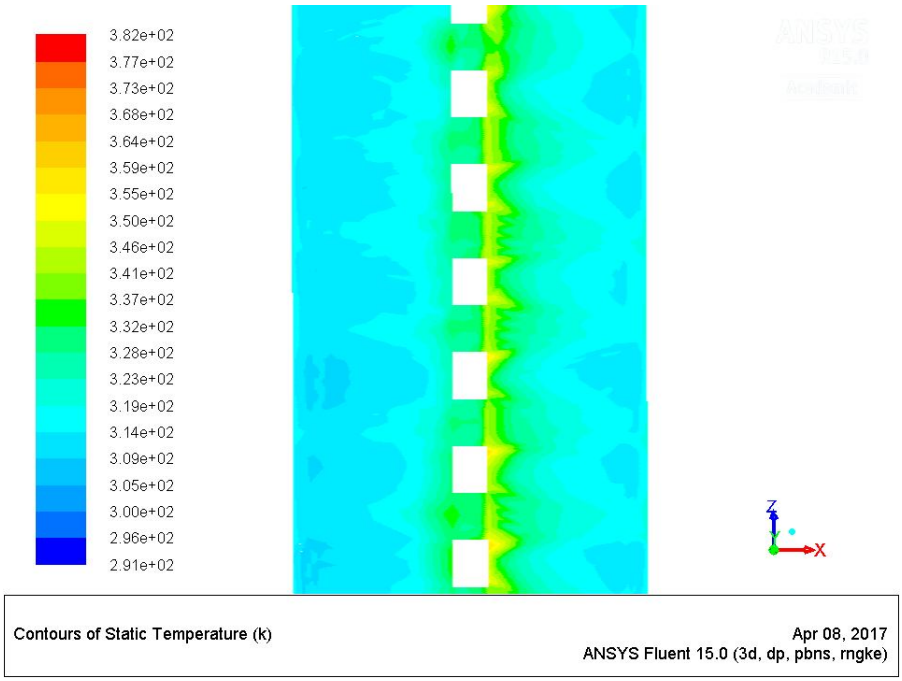

(a)

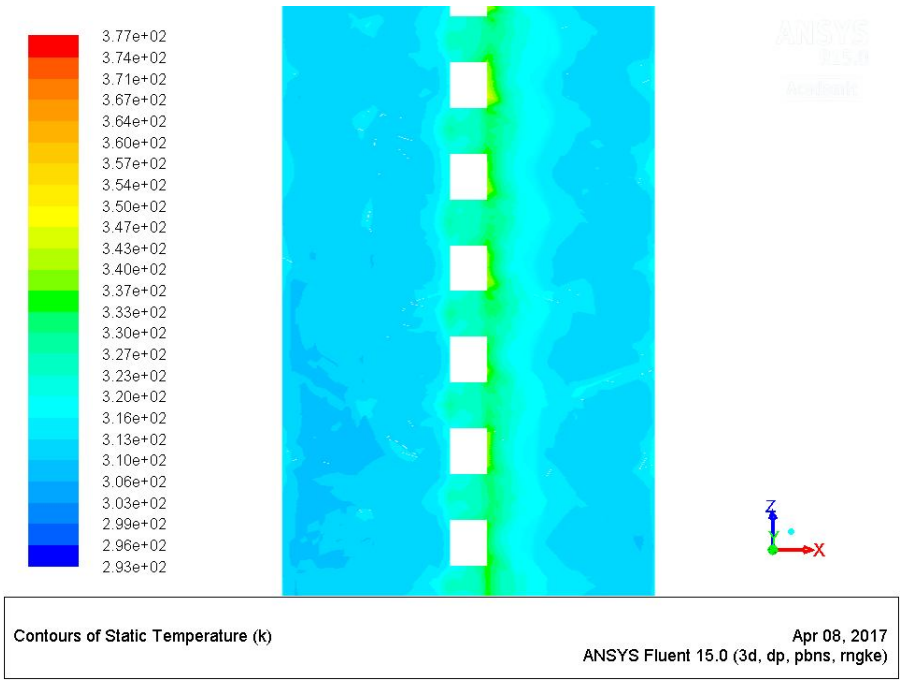

(b)

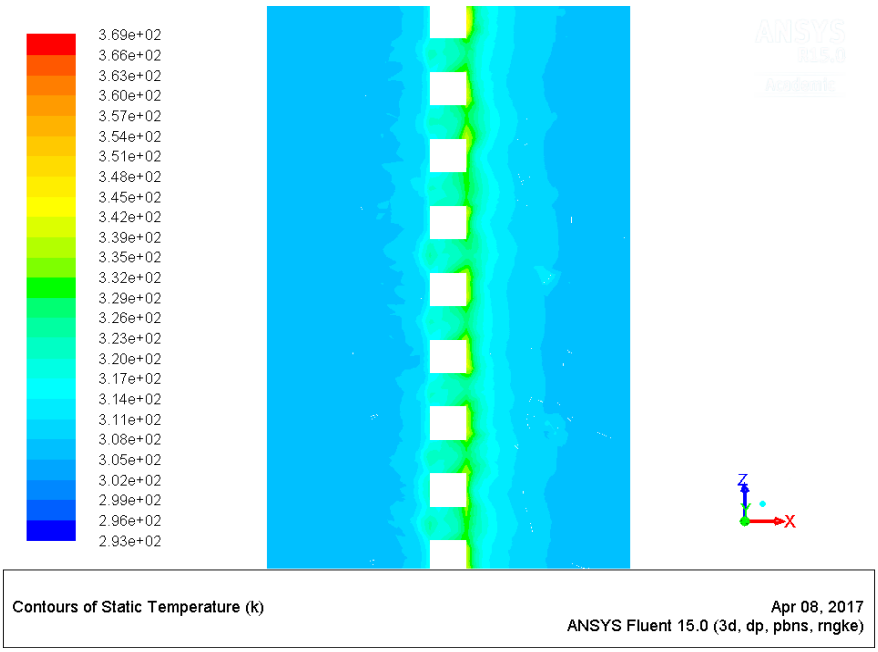

(c)

Fig. 4.17 Contours of static temperature on a parallel plane at distance of 1.5 mm from absorber for e/D values of (a) 0.015 (b) 0.026 (c) 0.043.

Fig. 4.18 shows the Nusselt number enhancement curve with respect to relative rib height over that of smooth duct for the Reynolds number range of 3000-15000. It can be seen that the heat transfer enhancement is always improving with the increase in the height of roughness elements. The relative roughness height of 0.043 features the maximum Nusselt number enhancement of 2.22 times over that of the smooth duct at Reynolds number of 15000.

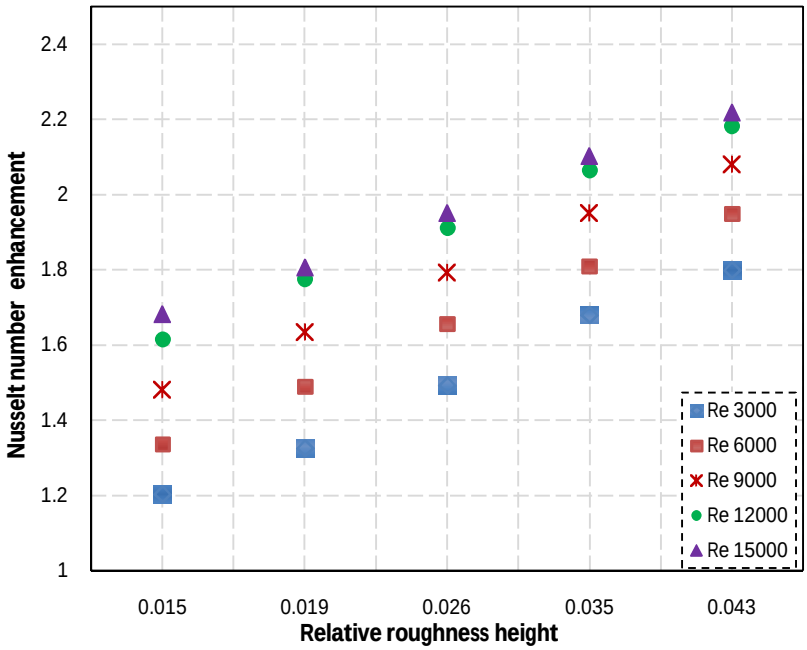

Fig. 4.18 Variation of Nusselt number enhancement with relative roughness height for different values of Reynolds number.

4.2 FRICTION FACTOR CHARACTERISTICS

The application of non-uniform cross-section square wave profiled transverse rib as artificial roughness on the absorber plate causes obstruction to the flow. This is reflected as higher pressure drop as compared to smooth duct due to the separation and reattachment of the boundary layer. This increase in pressure drop reflects in the enhancement of friction factor in roughened solar air heater duct as compared to smooth duct. The effect of the investigated range of roughness and flow parameters on friction factor characteristics are discussed in detail below:

4.2.1 Effect of Reynolds number

The impact of Reynolds number on friction factor is presented in Fig. 4.19. The friction factor tends to decrease with the increase in Reynolds number for all the investigated values of relative roughness pitch. This reduction is attributed to the decrease in the slope of pressure drop and much higher increase in "v^2" and consequently decrease in friction factor calculated from Eqn. (4.1) as:

$$f = \frac{2(\Delta P)_d D_h}{4\rho L v^2} \tag{4.1}$$

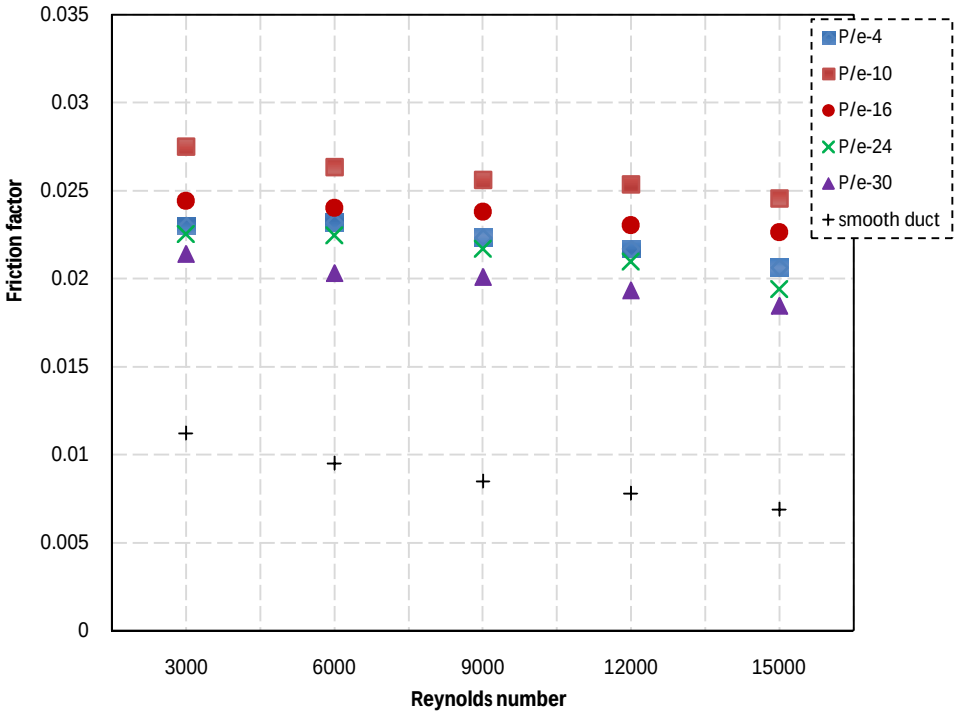

Fig. 4.19 Variation of friction factor with Reynolds number for different values of relative roughness pitch.

The pressure loss in the roughened duct is attributed to the cumulative effect of the flow around the obstacle and over the absorber plate. The pressure drag around the rib can be clearly seen from Static pressure contours (Fig. 4.20) which demonstrates that the air particles are more compressed on the upstream side and more spaced out behind the rib surface. High amount of pressure is lost in the recirculation zone behind the rib and the flow separation area at the surface of the rib. This pressure drag around the rib gives the backward pushing force to the flow causing higher pressure drop. In addition to pressure drag, frictional forces inside the duct also adds to the overall pressure drop. The frictional forces are higher on the rib surface and at the reattachment point. The frictional forces accelerate the flow in backward direction and hence there is increment in pressure drop.

It has been observed that pressure loss is higher at high flow velocity and vice-versa. At lower velocity, the reattachment distance is more and more recirculation area downstream can be seen (Fig. 4.2 (a)). Thus, low pressure zone is much higher behind the rib at lower Reynolds number (Fig. 4.20 (a)). However, increasing the flow velocity makes the low-pressure zone smaller as can be seen in Fig. 4.20 (a-c). This is due to the reduction of the reattachment distance i.e. flow recirculation zone at higher Reynolds number (Fig. 4.2). However, the reattachment length increases with the increase in Reynolds number, which increases the frictional forces. But the magnitude of this increase is not of much significance in cumulative effect of both pressure drag and frictional losses on overall pressure drop. Hence, the friction factor value falls with the increase in Reynolds number from 3000-15000.

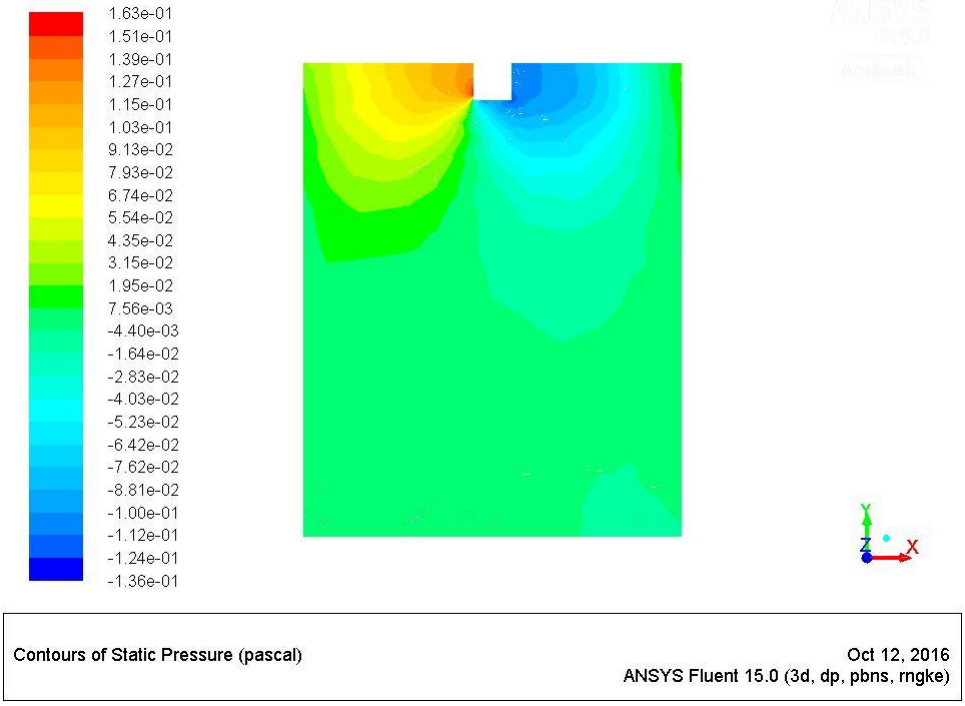

(a)

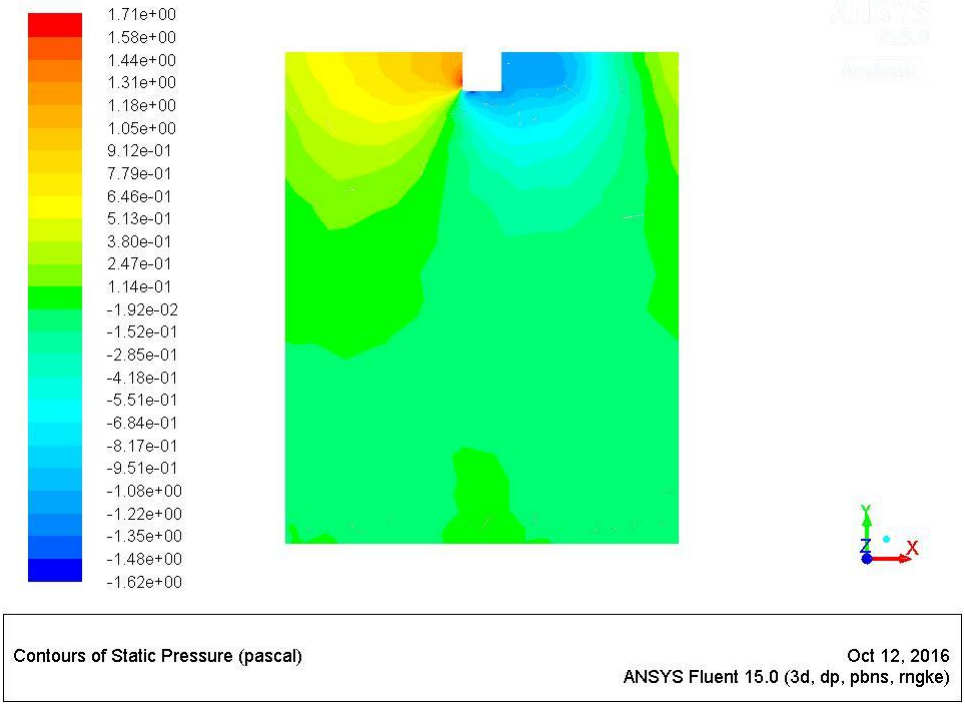

(b)

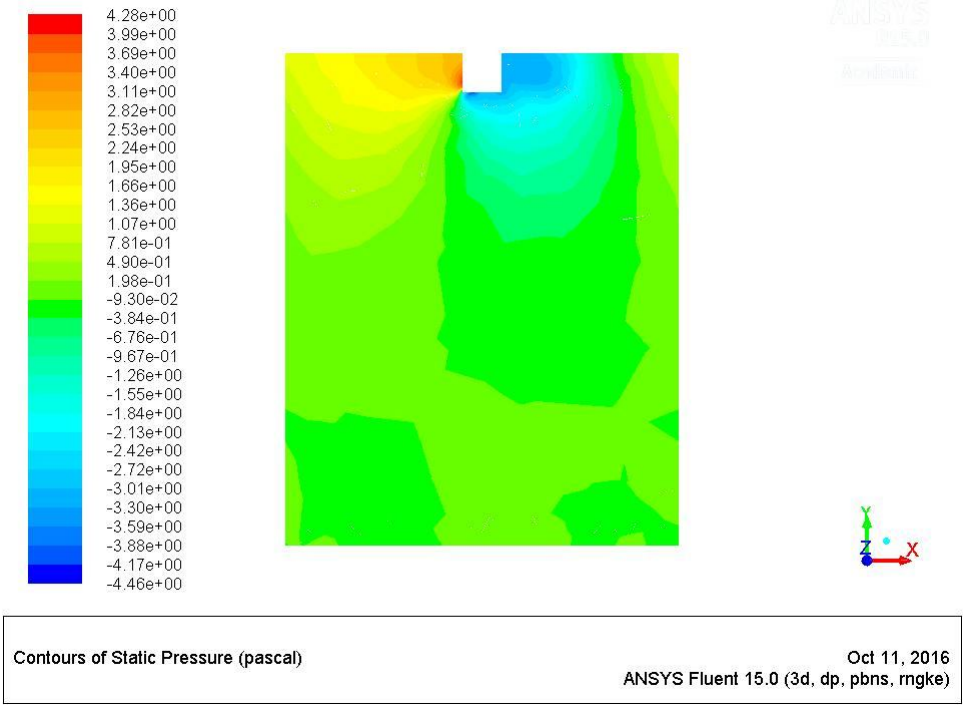

(c)

Fig. 4.20 Contours of static pressure at mid-plane normal to the absorber plate for P/e of 10 and Re values of (a) 3000 (b) 9000 and (c) 15000.

4.2.2 Effect of relative roughness pitch

To clearly depict the influence of relative rib pitch on friction factor, Fig. 4.19 is re-plotted as Fig. 4.21. It can be seen that the friction factor increases up to the relative roughness pitch of 10 and after that it decreases continuously up to the relative roughness pitch of 30. Similar trends are observed for all the Reynolds number values. This variation is may be attributed to the more reattachment points and the recirculation zones present behind the rib which causes higher pressure drop.

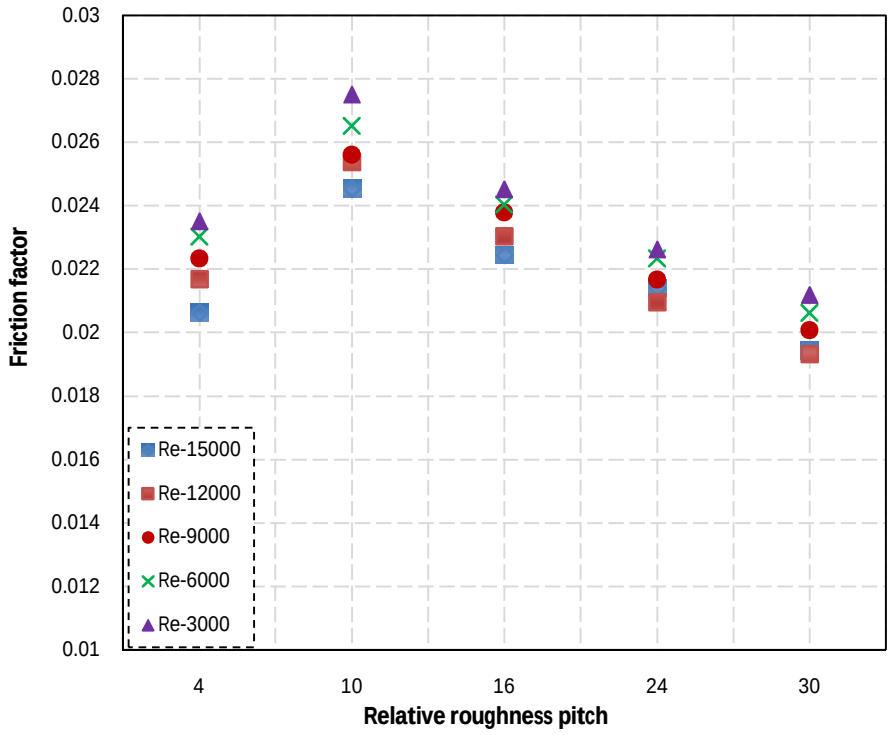

Fig. 4.21 Variation of friction factor with relative roughness pitch for different values of Reynolds number.

The static pressure contours are plotted for Reynolds number of 15000 and different relative roughness pitch values in Fig. 4.22 which confirm the trend of variation in friction factor. The maximum friction factor is seen for relative roughness pitch of 10. At relative roughness pitch of 4, no reattachment is happening as the flow is not coming in contact with the absorber plate (Fig. 4.5 (a)). Also, the recirculation zone behind the rib is also less and is reflected in Fig. 4.21 (a). So, the pressure gradient is less at this value. However, the relative roughness pitch of 10 offers most suitable reattachment characteristics i.e. highest reattachment points per unit length and optimal reattachment length between two ribs. Thus,

the pressure drop is maximum at this value. Further increasing the rib pitch decreases the number of interruptions inside the duct and the reattachment length also becomes much larger. Recirculation zones per unit length also decreases which results in reduced pressure drop. Hence, the friction factor reduces with increase in relative pitch of the roughness elements.

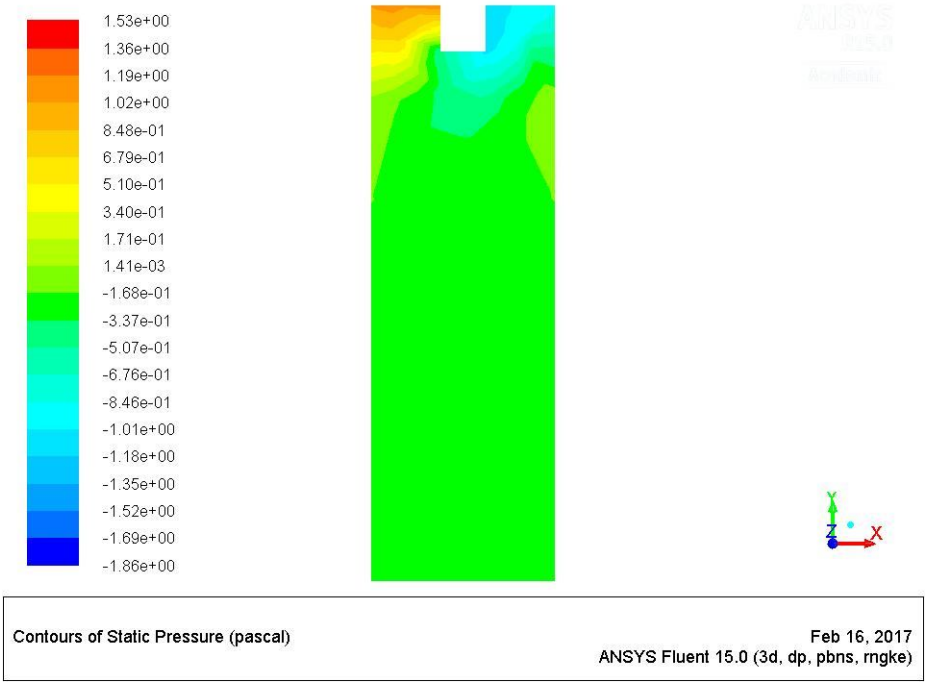

(a)

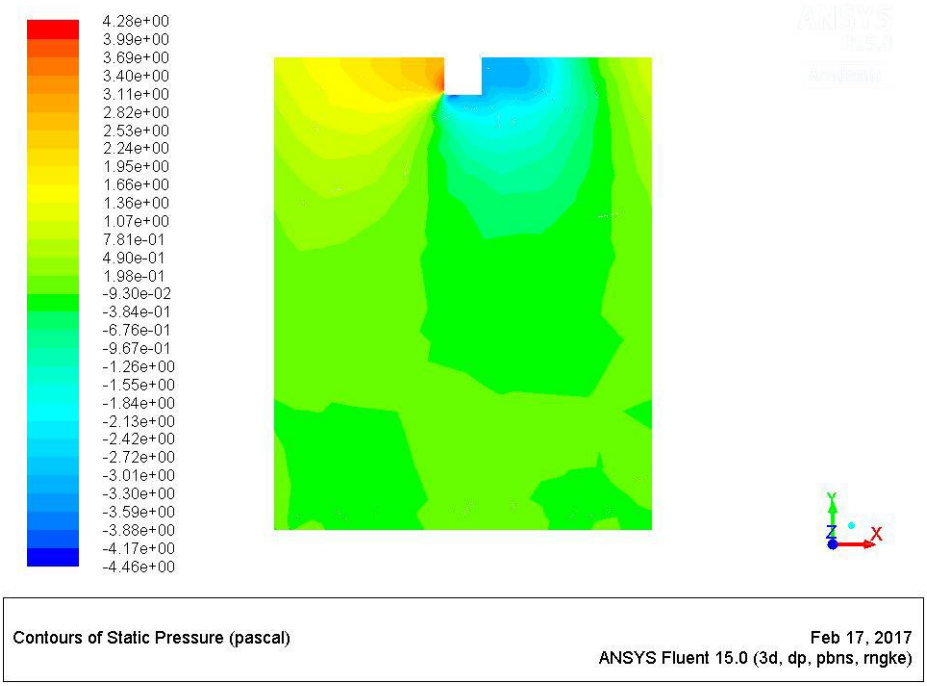

(b)

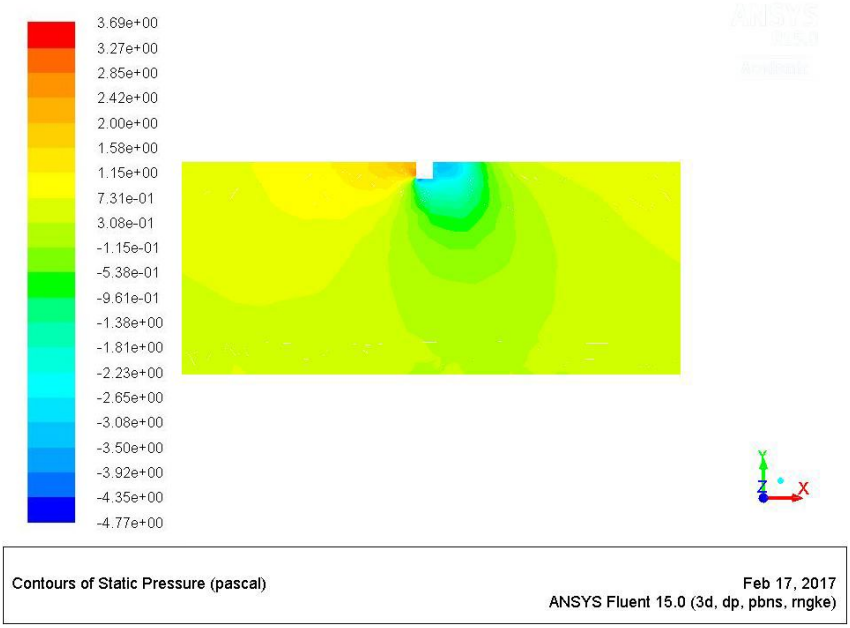

(c)

Fig. 4.22 Contours of static pressure at a mid-plane normal to the absorber at Re of 15000 and for pitch P/e values of (a) 4 (b) 10 c) 30.

Fig. 4.23 compares the friction factor enhancement at different relative roughness pitch values for Reynolds number ranging 3000-15000. The enhancement in friction factor increases sharply up to relative roughness pitch of 10 and then falls after that. The maximum enhancement is 3.55 times that of smooth duct for relative roughness pitch of 10 at Reynolds number of 15000.

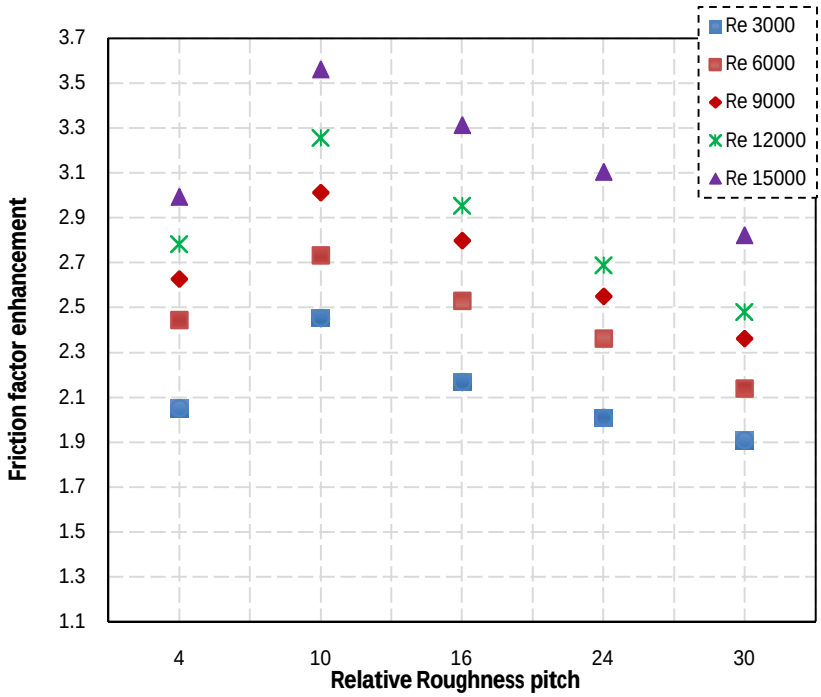

Fig. 4.23 Variation of friction factor enhancement with relative roughness pitch for different values of Reynolds number.

4.2.3 Effect of relative roughness width

To investigate the influence of relative roughness width on the friction factor characteristics of the roughened duct, relative roughness pitch and relative roughness height were kept fixed as 10 and 0.043 respectively. Relative roughness width was varied as 10, 85, 160, 235, 310 and investigated for Reynolds number values of 3000, 6000, 9000, 12000 and 15000.

The friction factor decreases with the increase in Reynolds number for all the investigated values of relative roughness width (Fig. 4.24). The cause of this reduction has already been discussed above in section 4.2.1. Fig. 4.24 has been re-plotted as Fig. 4.25 to study the variation in friction factor with roughness width. The increase in relative roughness width from 10 to 310 results in continuous increase in friction factor. This is because more number of gaps along the duct width causes higher flow disturbance that results in higher pressure drop.

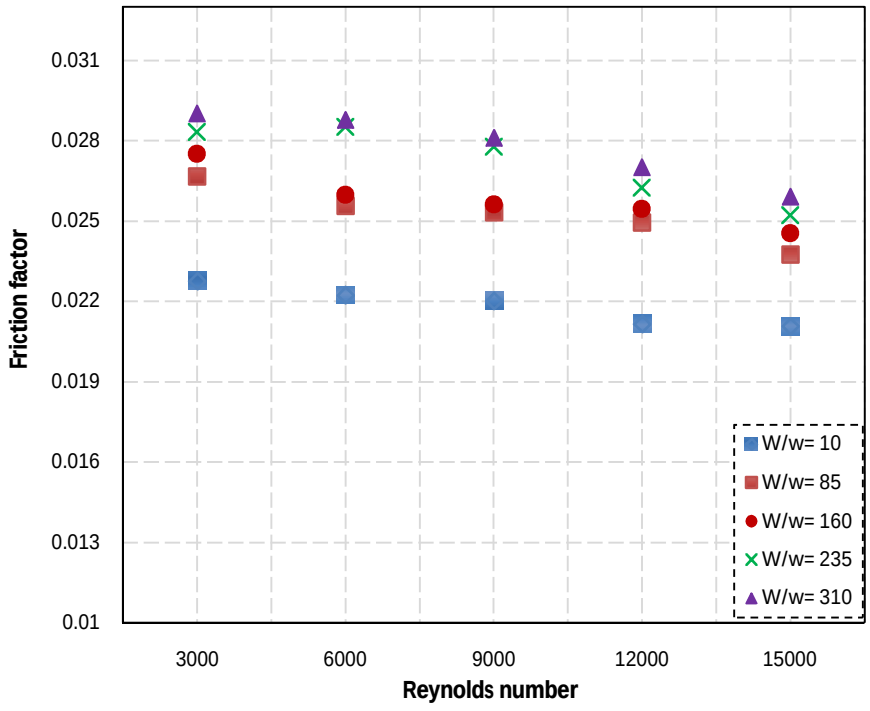

Fig. 4.24 Variation of friction factor with Reynolds number for different values of relative roughness width.

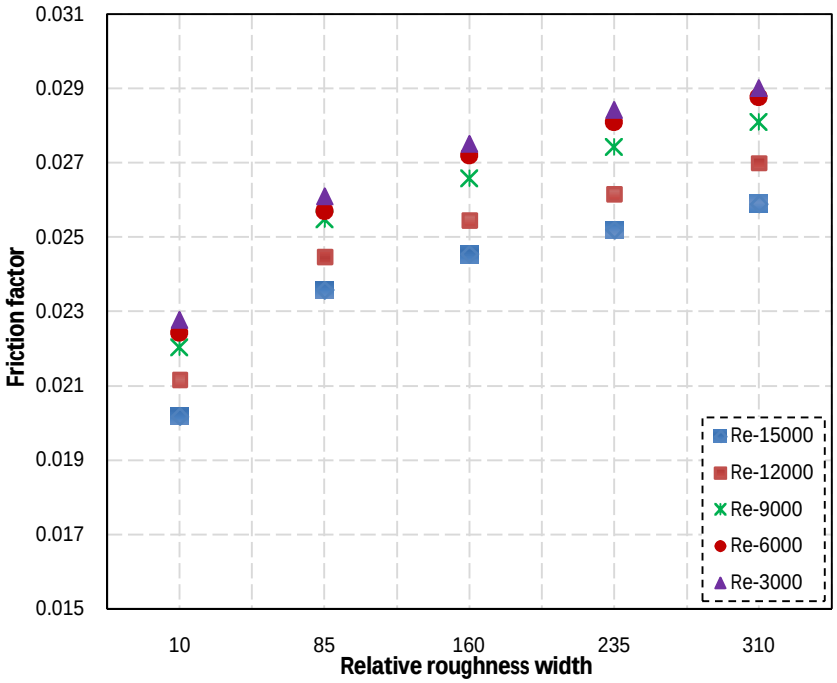

Fig. 4.25 Variation of friction factor with relative roughness width for different values of Reynolds number.

Fig. 4.26 presents the static pressure contours on the mid-plane of the duct normal to absorber at Reynolds number of 15000 and different relative roughness width values. The contours show the general conformity with the above results. At lower relative roughness width, the pressure gradient effects around the rib are less (Fig. 4.26 (a)). As the number of gaps are increased, the low-pressure zone behind the rib starts increasing. (Fig. 4.26 (b)) which adds to the pressure drop inside the duct. This area keeps on increasing continually up to relative roughness width of 310 and thus pressure drop is maximum at this value.

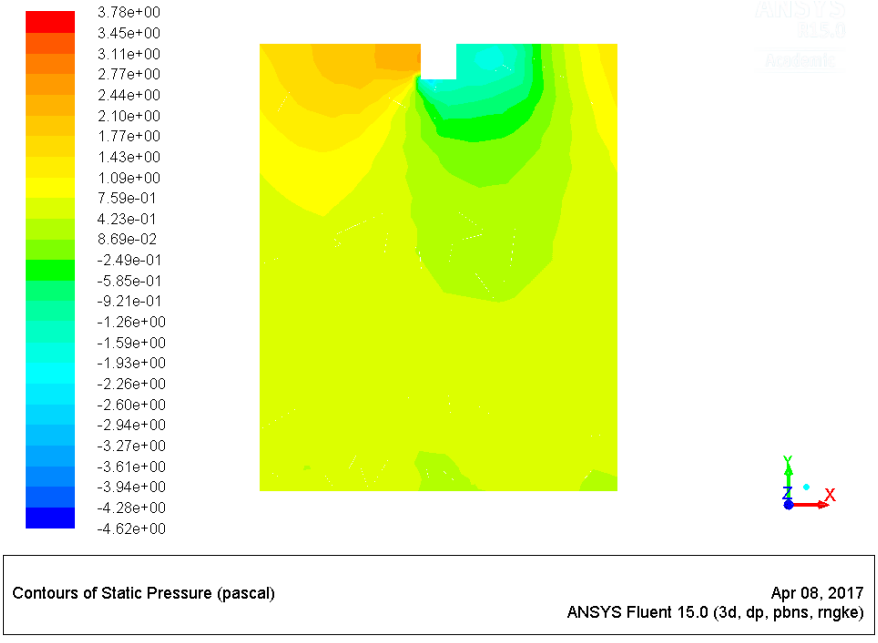

(a)

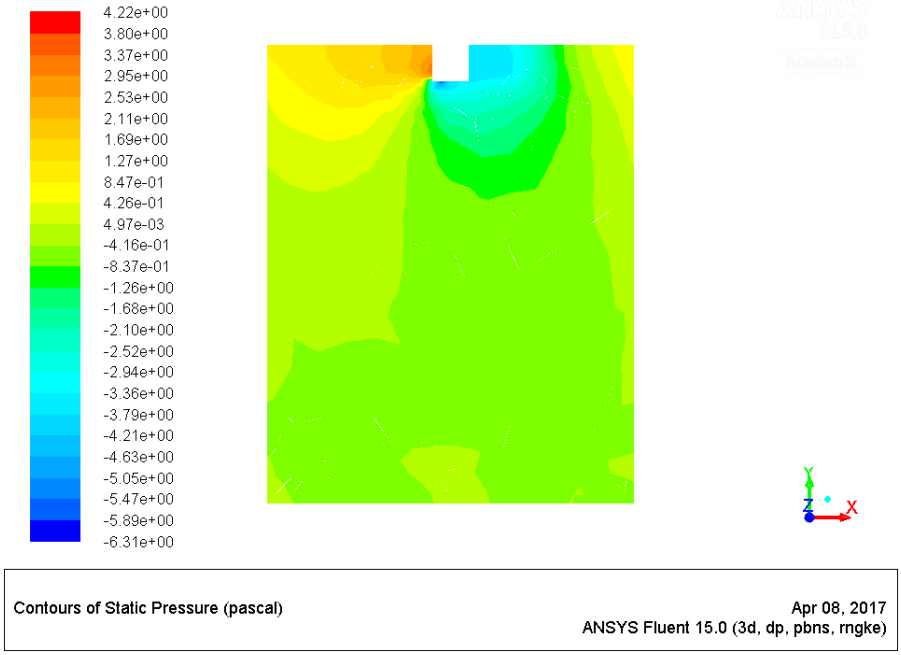

(b)

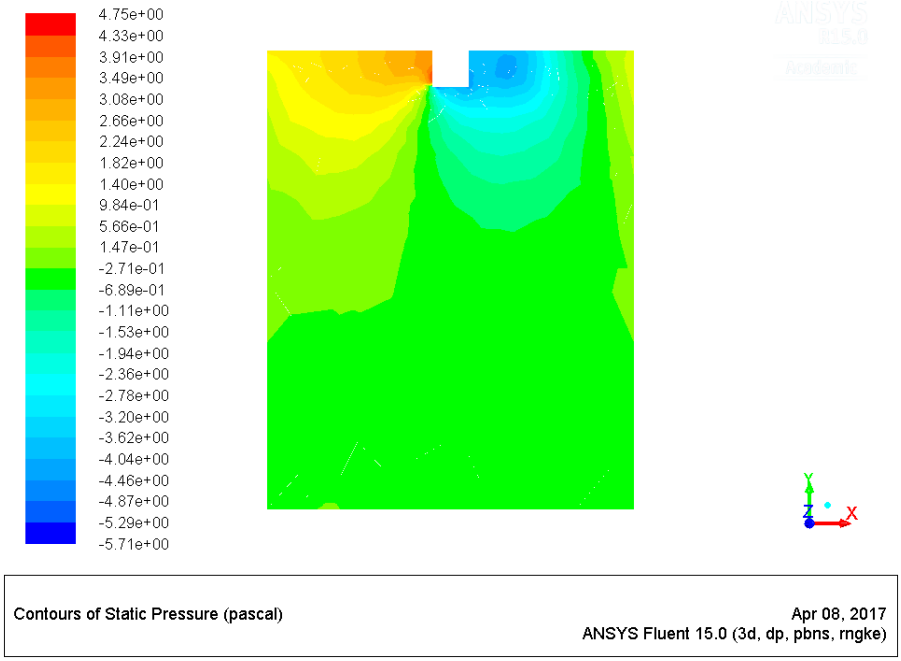

(c)

Fig. 4.26 Contours of static pressure at mid plane normal to the absorber plate at Re of 15000 and for W/w values of (a) 10 (b) 85 (c) 310.

Fig. 4.27 presents the friction factor enhancement versus relative roughness width curve for Reynolds number range from 3000-15000. It can be seen that the pumping power requirements amplifies as the relative roughness width is increased from 10 to 310. The peak enhancement value of 3.75 times corresponds to the relative roughness width of 310 and

Reynolds number of 15000 while the lowest enhancement in friction factor corresponds to relative roughness width of 10.

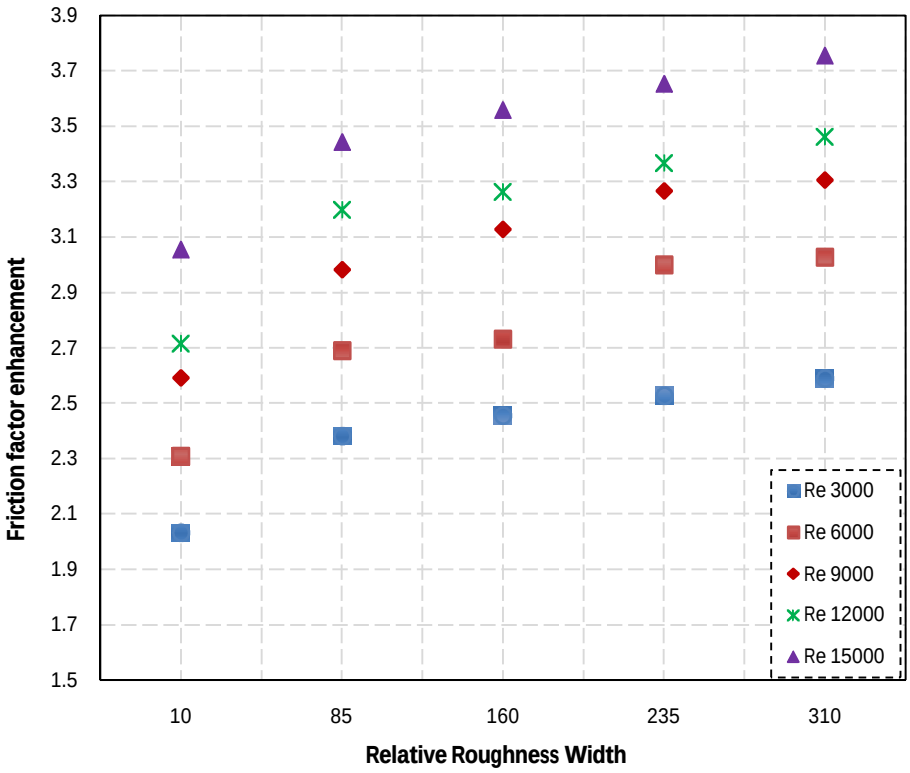

Fig. 4.27 Variation of friction factor enhancement with relative roughness width for different values of Reynolds number.

4.2.4 Effect of relative roughness height

To investigate the effect of relative roughness height on the fluid flow characteristics of the rib roughened duct, relative roughness pitch and relative roughness width were kept fixed as 10 and 85 respectively. Relative roughness height was varied as 0.015, 0.019, 0.026, 0.035, 0.043 and investigated for Reynolds number values of 3000, 6000, 9000, 12000 and 15000.

Fig. 4.28 presents the friction factor versus Reynolds number curve for different values of relative roughness height. As expected, the friction factor value declines as the Reynolds number is increased. To clearly show the influence of height of the rib on friction factor, Fig. 4.28 has been redrawn as Fig. 4.29. Sharp increase in friction factor has been found with the increase in relative roughness height from 0.015 to 0.043. The presence of rib in flow path causes drop in pressure due to obstruction in flow that leads to an ample rise in friction factor. This rise in friction factor is attributed to the amplification of the turbulence as the height of roughness elements is increased. It has been seen earlier in Fig. 4.16 that with the increase in rib height, the reattachment length and the height of the recirculation zone behind the rib increases. The rib protrudes further into the core turbulent flow creating more

obstruction and hence more pressure drop. Thus, friction factor is maximum at relative roughness height of 0.043.

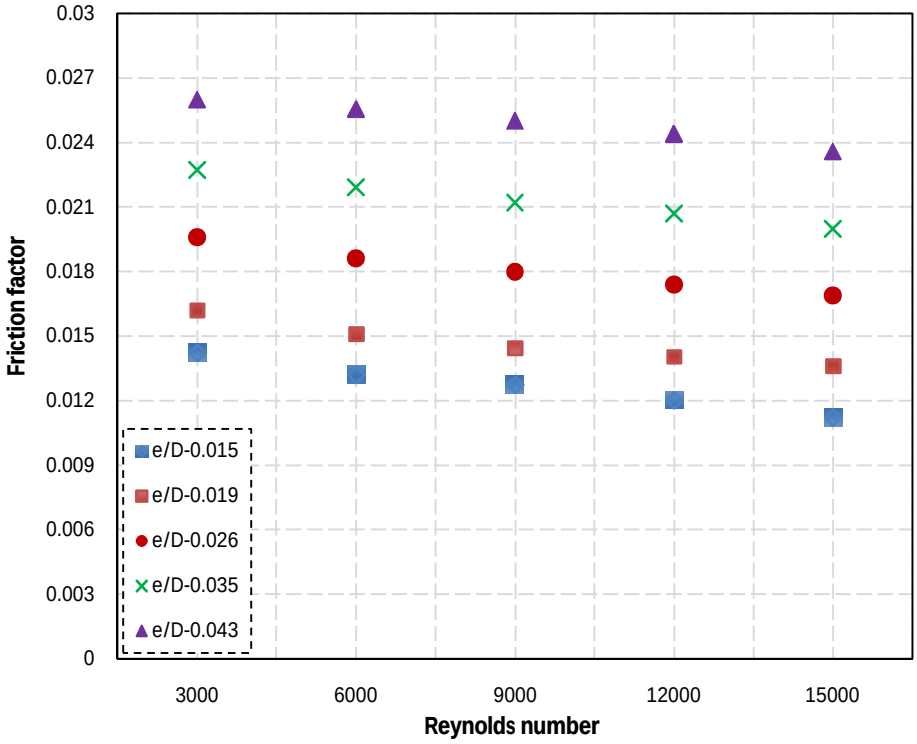

Fig. 4.28 Variation of friction factor with Reynolds number for different values of relative roughness height.

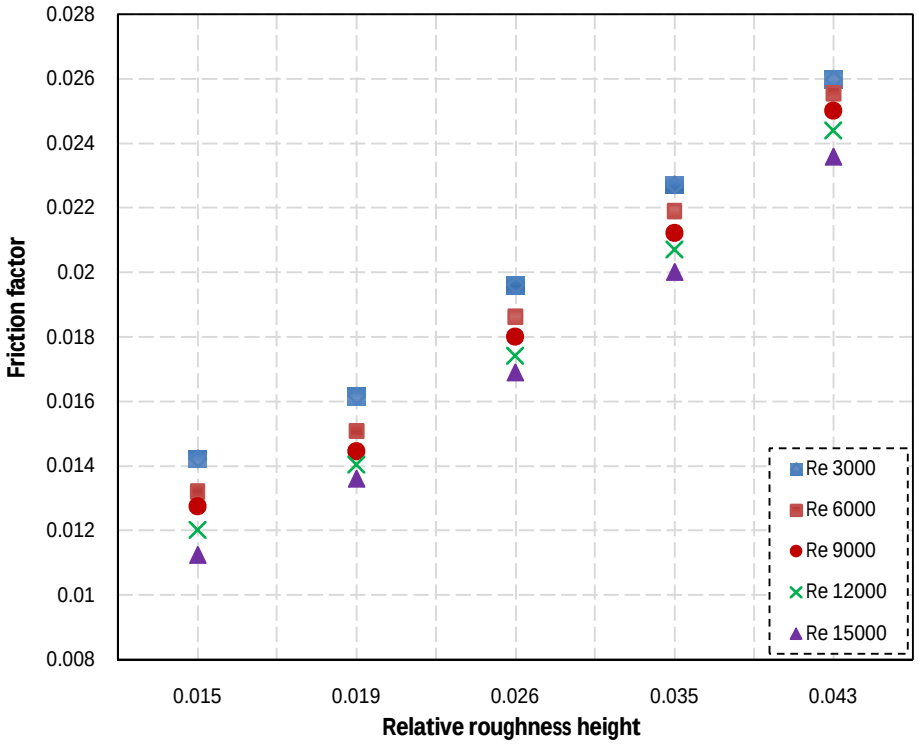

Fig. 4.29 Variation of friction factor with relative roughness height for different values of Reynolds number.

Fig. 4.30 shows the variation in static pressure contours at the mid-plane of the duct for investigated relative roughness height values. The pressure drag around the rib can be clearly seen (Fig. 4.30) which indicates that the air particles are more compressed before the rib and more spaced out behind the rib surface. Employing the rib of more height, there is increase in the intensity of frictional forces and pressure drag around the rib which causes the increase in friction factor. This has been reflected in the contours as the low-pressure zone behind the rib expands when the rib height is increased (Fig. 4.30 (a-c)). Thus, it is justified that with the increase in the rib height, friction factor continuously increases.

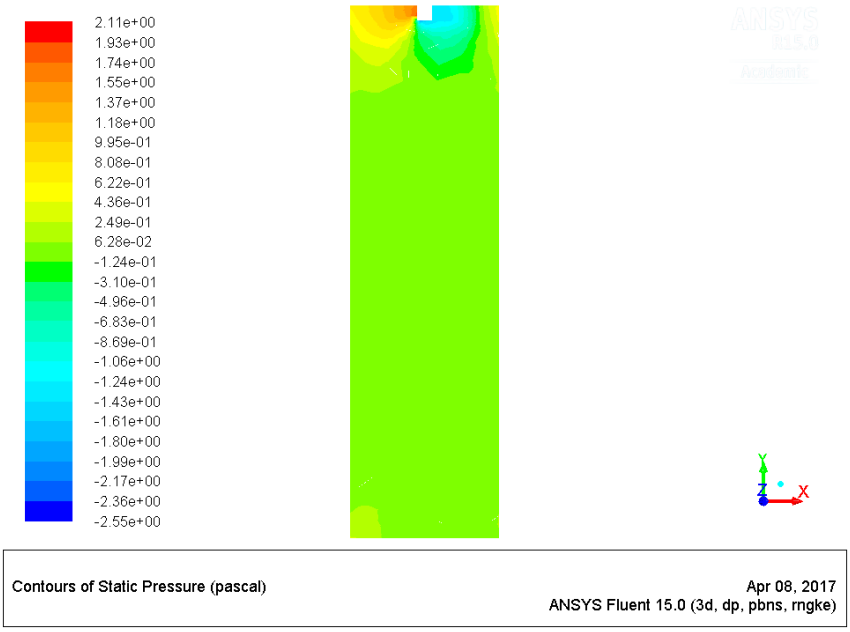

(a)

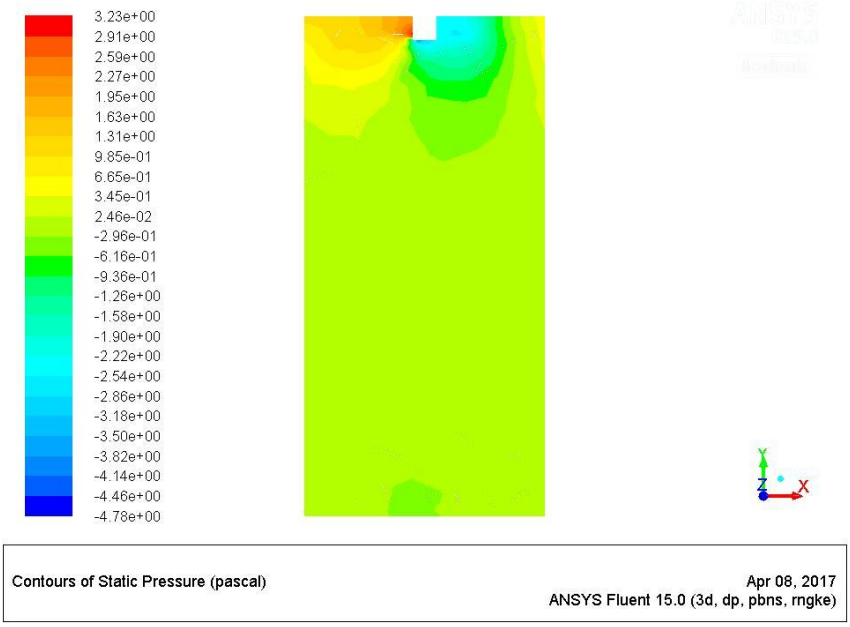

(b)

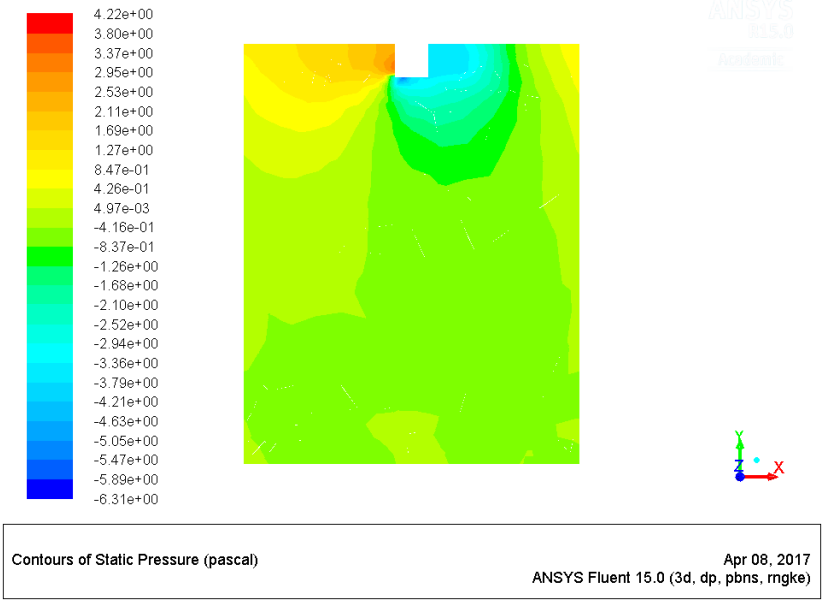

(c)

Fig. 4.30 Contour of static pressure at mid-plane of the duct normal to absorber for Re of 15000 and e/D values of (a) 0.015 (b) 0.026 (c) 0.043.

Fig. 4.31 represents the variation in friction factor enhancement over that of smooth duct with relative roughness height for different Reynolds number values. As expected, the friction factor enhancement is of the increasing order from relative roughness height of 0.015 to 0.043. The friction factor enhancement attains maximum value of 3.44 times at relative roughness height of 0.043 and Reynolds number of 15000.

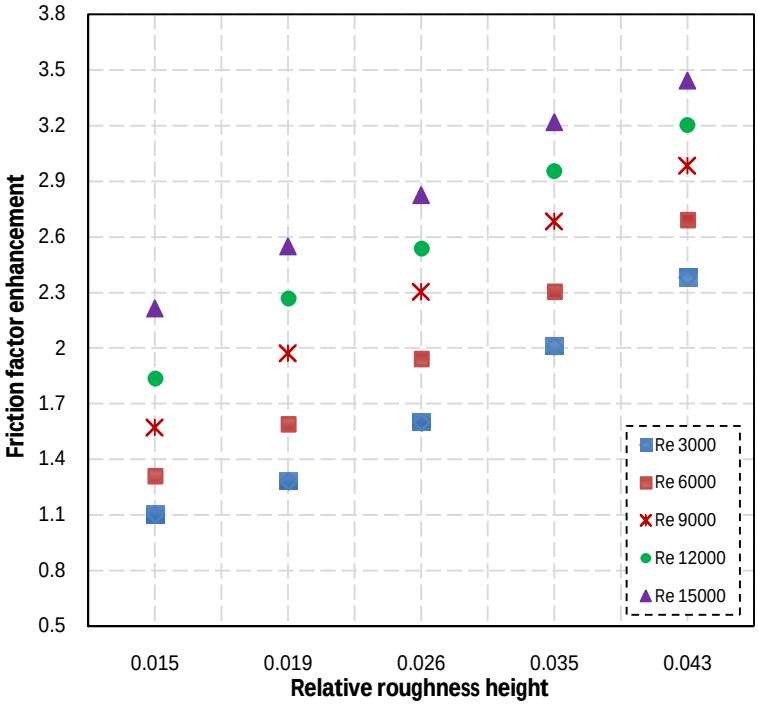

Fig. 4.31 Variation of friction factor enhancement with relative roughness height for different values of Reynolds number.

4.3 THERMO-HYDRAULIC PERFORMANCE

It is desirable to choose the roughness geometry which gives maximum heat transfer enhancement while keeping the pumping losses minimum. In the above section, Nusselt number and friction factor characteristics of the solar air heater duct with roughened absorber plates were evaluated for different parameters combination of relative roughness pitch, relative roughness width, relative roughness height and Reynolds number. It was observed that best thermal performance was obtained at relative roughness pitch of 10, relative roughness width of 85, relative roughness height of 0.043 and Reynolds number of 15000. The friction factor is also higher for the rib roughened duct. So, it is necessary to determine the optimum combination of roughness and flow parameters which could provide better heat transfer augmentation with lesser pumping power penalty.

So, the overall performance of a solar air heater duct is evaluated by the thermo-hydraulic performance parameter (THPP) given by Webb and Eckert (1972) i.e. considering both thermal and hydraulic performance simultaneously as given by Eqn (4.2):

$$\mathbf{THPP} = \frac{\mathbf{Nu_r/Nu_s}}{\mathbf{(f_r/f_s)^{1/3}}} \qquad (4.2)$$

4.3.1. Effect of relative roughness pitch

Fig. 4.32 and Fig. 4.33 presents the thermo-hydraulic performance of non-uniform cross-section square wave profiled transverse rib at different relative roughness pitch values for Reynolds number range of 3000-15000. The thermo-hydraulic performance parameter increases up to Reynolds number of 12000 and declines with further increase. The thermo-hydraulic performance parameter of non-uniform cross-section rib varies between 1.19 to 1.43 for the investigated range of relative roughness pitch and maximum value of thermo-hydraulic performance of 1.43 corresponds to the parameters as relative roughness pitch of 10 and Reynolds number of 12000.

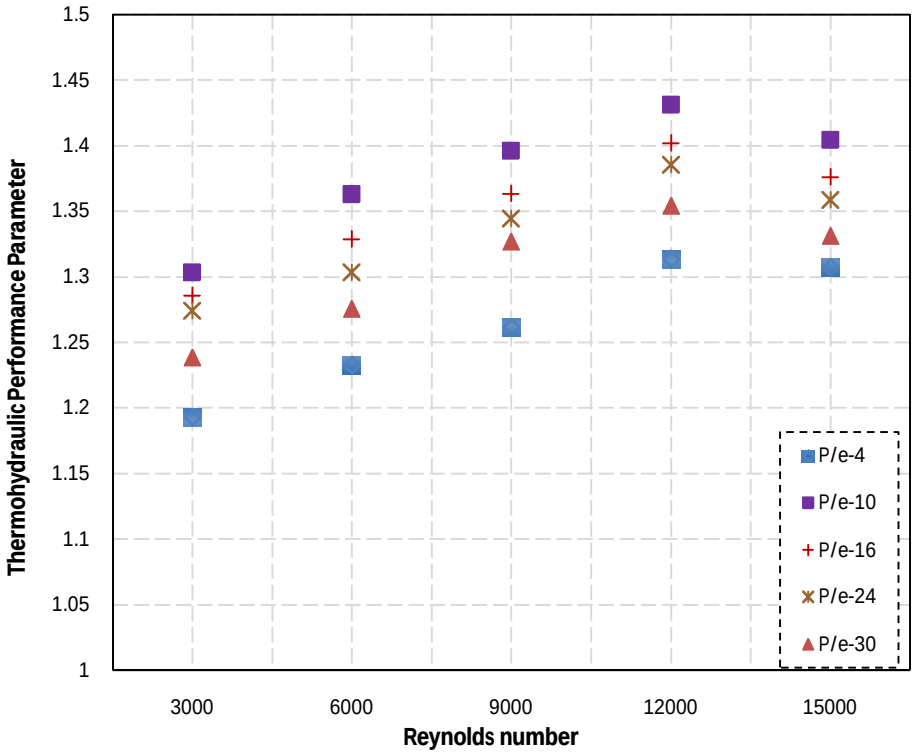

Fig. 4.32 Variation of thermo-hydraulic performance parameter with Reynolds number for different values of relative roughness pitch.

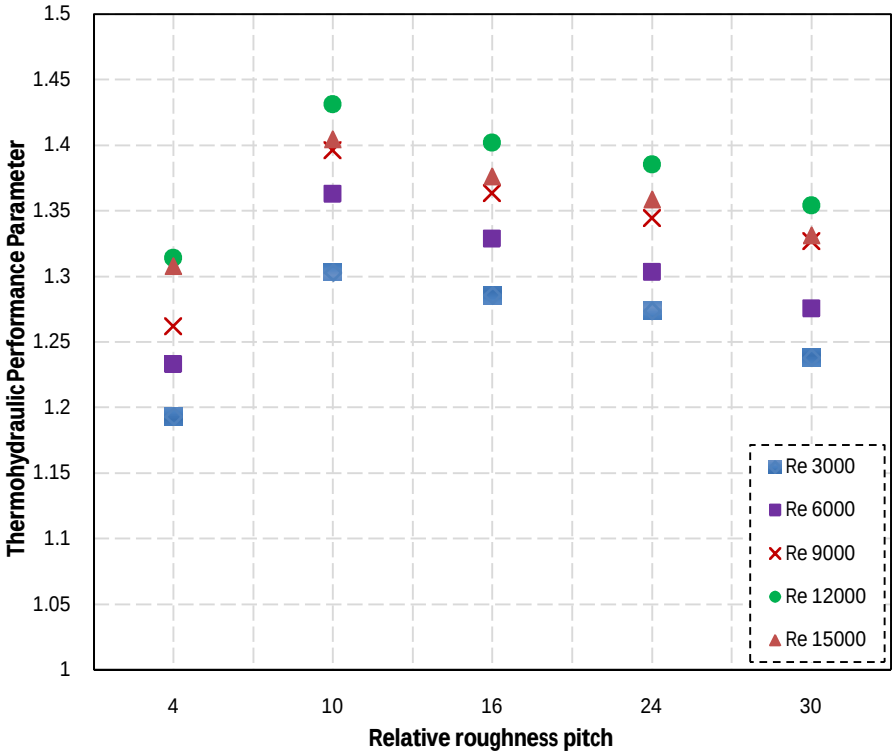

Fig. 4.33 Variation of thermo-hydraulic performance parameter with relative roughness pitch for different values of Reynolds number.

4.3.2. Effect of relative roughness width

Fig. 4.34 and Fig. 4.35 depicts the influence of relative roughness width on thermo-hydraulic performance. The thermo-hydraulic performance curve with respect to Reynolds number follows same trend and attains maximum value at Reynolds number of 12000 (Fig. 4.34). Initially thermo-hydraulic performance parameter increases as relative roughness width is increased from 10 to 85 and after that it declines and becomes lowest at relative rib width of 310 as the frictional losses are much higher at this value. Overall, thermo-hydraulic performance parameter varies from 1.16 to 1.49 for the investigated range. Maximum thermo-hydraulic performance of 1.49 is obtained at relative roughness width of 85 for Reynolds number of 12000.

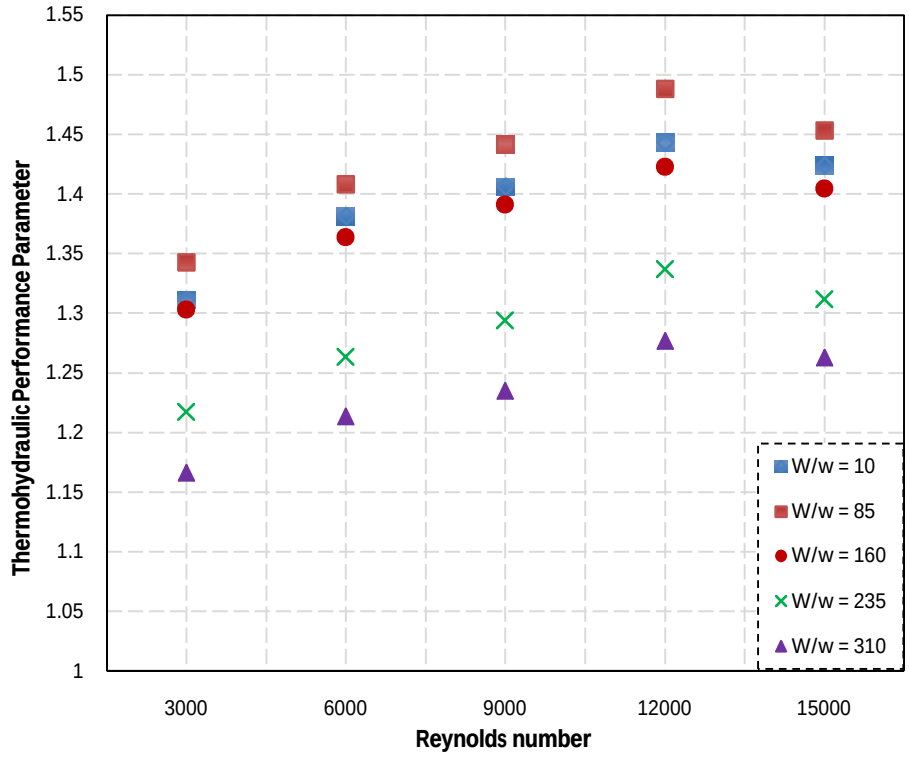

Fig. 4.34 Effect of Reynolds number on thermo-hydraulic performance parameter for different values of relative roughness width.

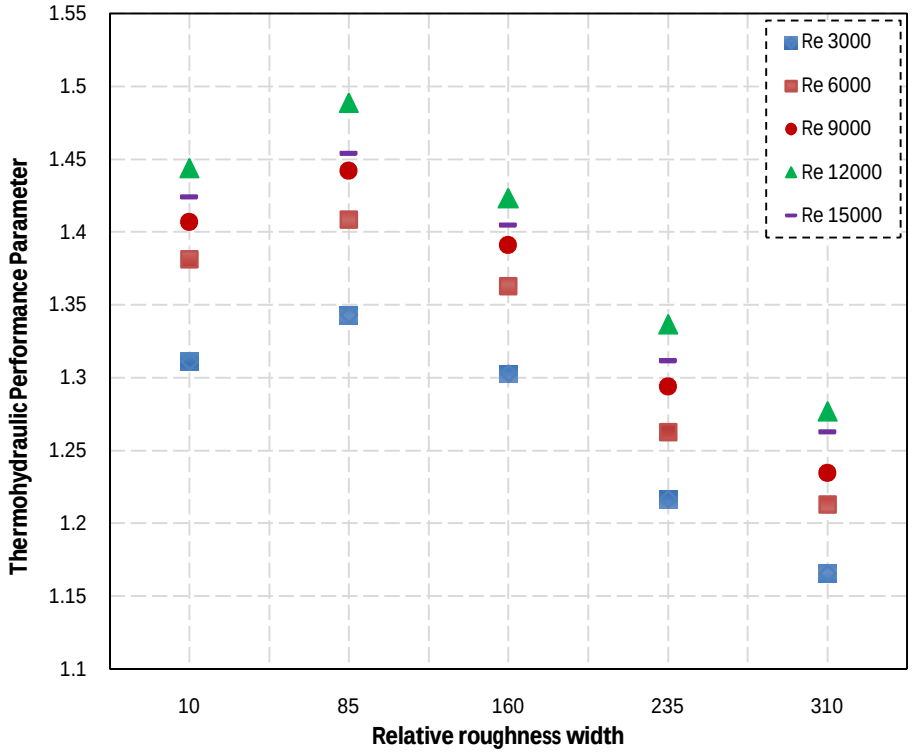

Fig. 4.35 Effect of relative roughness width on thermo-hydraulic performance parameter for different values of Reynolds number.

4.3.3 Effect of relative roughness height

Fig 4.36 and Fig. 4.37 has been plotted to demonstrate the effect of relative roughness height on thermo-hydraulic performance factor. Relative roughness pitch and relative roughness width has been fixed as 10 and 85 respectively corresponding to the maximum thermo-hydraulic performance obtained earlier. It can be clearly seen that thermo-hydraulic performance factor is a strong function of relative roughness height and Reynolds number. The thermo-hydraulic performance parameter increases up to its peak value at Reynolds number of 12000 and then it declines with further increment (Fig. 4.36). The parameter varies between 1.21 to 1.49 for the investigated range of relative roughness height. The parameter increases with increase in relative rib height (Fig. 4.37) and maximum value of 1.49 is obtained at relative roughness height of 0.043 and Reynolds number of 12000.

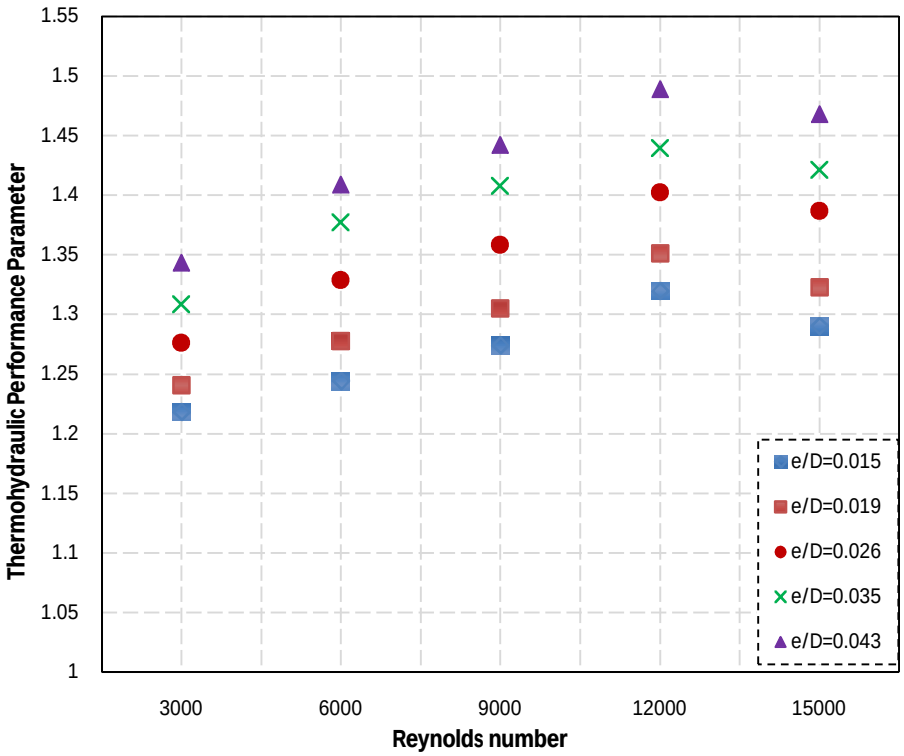

Fig. 4.36 Effect of Reynolds number on thermo-hydraulic performance parameter for different values of relative roughness height.

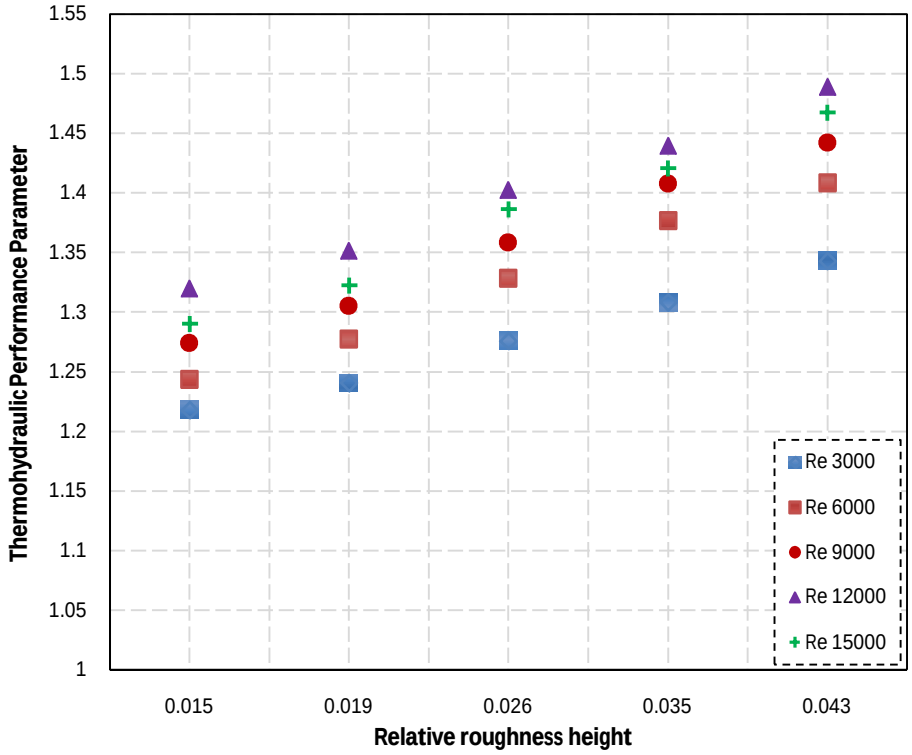

Fig. 4.37 Effect of relative roughness height on thermo-hydraulic performance parameter for different values of Reynolds number.

It has been found that solar air heater duct roughened with non-uniform cross-section square wave transverse rib with parameters combination as relative roughness pitch of 10, relative roughness width of 85 and relative roughness height of 0.043 provides maximum thermo-hydraulic performance parameter of 1.49 at Reynolds number of 12000 for the investigated range of parameters in this study.

CHAPTER-V

SUMMARY

The conventional solar air heaters are thermally inefficient attributable to the development of the laminar sub-layer adjacent to the absorber plate. The periodic rib roughness method is deemed to be the most effective and widely used technique for boosting the thermal performance as it creates turbulence in a flow only in the region close to the absorber plate surface where laminar sub-layer develops. Numerous shapes of artificial rib roughness have been reported in literature with the objective of heat transfer augmentation between air and absorber plate with least corresponding enhancement in friction factor. Earlier studies on rib roughened duct were carried out experimentally as well as using CFD for uniform cross-section rib roughness.

The present CFD based investigation on heat transfer and fluid flow analysis for non-uniform cross-section transverse rib of square wave profile has been done in 3-D using ANSYS Academic Research 15.0. The investigation covered the parameters range as relative roughness pitch from 4 to 30, relative roughness height from 0.015 to 0.043 and relative roughness width from 10-310 and Reynolds number from 3000-15000. For the validation of the CFD methodology, the CFD results are verified with the published experimental results. Based on the results of the present study, following noteworthy conclusions have been drawn:

1. With the increase in Reynolds number, the Nusselt number value augments while the friction factor declines for all values of investigated roughness parameters. This is due to the reduction in reattachment distance with increase in Reynolds number.
2. Both, the Nusselt number and friction factor increases with increase in relative roughness pitch up to 10 and then decrease with further raise for the range of Reynolds number investigated. This is because of optimal flow re-attachment phenomena in-between two consecutive ribs and more number of reattachment points per unit length at relative roughness pitch of 10 which results in maximum value of Nusselt number and friction factor.
3. Nusselt number attains maximum value at relative roughness width of 85 and lowers on both sides for all Reynolds number. On the other hand, friction factor continually increases with the increase in relative roughness width from 10-310.
4. Nusselt number and friction factor both increases with the increase in relative rib height for the considered range of Reynolds number. This increase is attributed to the reduction in reattachment distance and hence increase in reattachment length with increasing rib height.

5. The maximum augmentation in Nusselt number over that of smooth duct have been found to be 2.22 times for relative roughness pitch of 10, relative roughness height of 0.043, relative roughness width of 85 and Reynolds number of 15000 with corresponding enhancement in friction factor of 3.40 times. Whereas maximum enhancement in friction factor of 3.75 times is obtained at parameters combination of relative roughness pitch of 10, relative roughness height of 0.043, relative roughness width of 310 and Reynolds number of 15000.
6. The value of thermo-hydraulic performance parameter for the duct varies from 1.16 to 1.49 for the range of parameters covered in the investigation. It has been found that parameters combination as relative roughness pitch of 10, relative roughness height of 0.043 and relative roughness width of 85 offers maximum thermo-hydraulic performance parameter of 1.49 at Reynolds number of 12000.

Future Scope of the study

This investigation has shown significant improvement in thermal and hydraulic performance of transverse rib roughened duct. So, other rib arrangements such as inclined ribs, v-ribs, multiple v ribs, etc. should be investigated using non-uniform cross-section rib.

REFERENCES

Aharwal K R, Gandhi B K and Saini J S (2008) Experimental investigation on heat-transfer enhancement due to a gap in an inclined continuous rib arrangement in a rectangular duct of solar air heater. *Renew Energy* **33**: 585-96.

Alam T and Kim M (2016) Numerical study on thermal hydraulic performance improvement in solar air heater duct with semi ellipse shaped obstacles. *Energy* **112**: 588-98.

Alam T and Kim M (2017) A critical review on artificial roughness provided in rectangular solar air heater duct. *Renew and Sustain Energy Rev* **69**: 387-400.

Bhagoria J L, Saini J S and Solanki S C (2002) Heat transfer coefficient and friction factor correlations for rectangular solar air heater duct having transverse wedge shaped rib roughness on the absorber plate. *Renew Energy* **25**: 341-69.

Bhushan B and Singh R (2010) A review on methodology of artificial roughness used in duct of solar air heaters. *Energy* **35**: 202-12.

Boukadoum A B and Benzaoui A (2014) CFD based analysis of heat transfer enhancement in solar air heater provided with transverse rectangular ribs. *Energy Proc* **50**: 761-72.

Bopche S and Tandale M S (2009) Experimental investigations on heat transfer and frictional characteristics of a turbulator roughened solar air heater duct. *International J Heat Mass Trans* **52**: 2834-48.

Deo N S, Chander S and Saini J S (2016) Performance analysis of solar air heater duct roughened with multigap V-down ribs combined with staggered ribs. *Renew Energy* **91**: 484-500.

Gawande V B, Dhoble A S, Zodpe D B and Chamoli S (2015) Experimental and CFD-based thermal performance prediction of solar air heater provided with right-angled triangular rib as artificial roughness. *J Braz Soc Mech Sci Eng* **38**: 551-79.

Gawande V B, Dhoble A S, Zopde D B and Chamoli S (2016) Experimental and CFD investigation of convection heat transfer in solar air heater with L-shaped ribs. *Sol Energy* **131**: 275-95.

Gupta D, Solanki J S and Saini J S (1997) Thermohydraulic performance of solar air heaters with roughened absorber plates. *Sol Energy* **61**:33-42.

Gupta D, Solanki JS and Saini J S (1993) Heat and fluid flow in rectangular solar air heater ducts having transverse rib roughness on absorber plates. *Sol Energy* **51**:31-37.

Han J C and Zhang Y M (1992) High performance heat transfer ducts with parallel, broken v-shaped broken ribs. *Int J Heat Mass Trans* **35:** 513-23.

Hans, V S, Gill R S, and Singh S (2017) Heat transfer and friction factor correlations for a solar air heater duct roughened artificially with broken arc ribs. *Exp Therm and Fluid Sci* **80**: 77-89.

Hans V S, Saini J S and Saini R P (2009) Performance of artificially roughened solar air heaters- A review. *Renew and Sustain Energy Reviews* **13**: 1854-69.

Hans V S, Saini R P and Saini J S (2010) Heat transfer and friction factor correlations for a solar air heater duct roughened artificially with multiple v-ribs. *Sol Energy* **84**: 898-911.

Hwang S D, Jang I H and Cho H H (2006) Experimental study on flow and local heat/mass transfer characteristics inside corrugated duct. *Int J Heat Fluid Flow* **27**: 21-32.

Jaurker A R, Saini J S and Gandhi B K (2006) Heat transfer and friction characteristics of rectangular solar air heater duct using rib-grooved artificial roughness. *Solar Energy* **80**: 895-7.

Jin D, Zhang M, Wang Z and Xu S (2015) Numerical investigation of heat transfer and fluid flow in a solar air heater duct with multi V-shaped ribs on the absorber plate. *Energy* **89**:178-90.

Karmare S V and Tikekar A N (2007) Heat transfer and friction factor correlation for artificially roughened duct with metal grit ribs. *Int J Heat Mass Trans* **50**: 4342-51.

Karmare S V and Tikekar A N (2010) Analysis of fluid flow and heat transfer in a rib grit roughened surface solar air heater using CFD. *Sol Energy* **84**: 409-17.

Karwa R (2003) Experimental studies of augmented heat transfer and friction in asymetrically heated rectangular ducts with ribs on heated wall in transverse, inclined, v-continuous and v-discrete pattern. *Int Comm Heat Mass Trans* **30**: 241-50.

Karwa R, Maheshwari B K and Karwa N (2005) Experimental study of heat transfer enhancement in an asymmetrically heated rectangular duct with perforated baffles, *Int. Commun. Heat Mass Transf* **32**: 275-84.

Karwa R, Solanki J S and Saini J S (1999) Heat transfer coefficient and friction factor correlations for the Transitional flow regime in rib roughened rectangular ducts. *Int J Heat Mass Trans* **42**: 1597-1615.

Kumar A (2014) Analysis of heat transfer and fluid flow in different shaped roughness elements on the absorber plate solar air heater duct. *Energy Proc* **57**: 2102-11.

Kumar A and Kim M (2015) Convective heat transfer enhancement in solar air channels. *Applied Therm Eng* **89**: 239-61.

Kumar A and Kim M (2016) Heat transfer and fluid flow characteristics in air duct with various V-pattern rib roughness on the heated plate: A comparative study. *Energy* **103**: 75-85.

Kumar A and Kim M (2016) Thermohydraulic performance of rectangular ducts with different multiple V-rib roughness shapes: A comprehensive review and comparative study. *Renew and Sustain Energy Rev* **54**: 635-52.

Kumar A, Bhagoria J L and Sarviya R M (2009) Heat Transfer and friction factor correlations for artificially roughened solar air heater duct with discrete W-shaped ribs. *Energy Conv and Mang* **50**: 2106-17.

Kumar A, Saini R P and Saini J S (2012) Experimental investigation on heat transfer and fluid flow characteristics of air flow in a rectangular duct with Multi v-shaped rib with gap roughness on the heated plate. *Sol Energy* **86**: 1733-49.

Kumar A, Saini R P and Saini J S (2013) Development of correlations for Nu and f for SAH with roughened duct having multi v-shaped with gap rib as artificial roughness. *Renew Energy* **58**: 151-63.

Kumar A, Saini R P and Saini J S (2014) A review of thermohydraulic performance of artificially roughened solar air heaters. *Renew and Sustain Energy Rev* **37**: 100-22.

Kumar A and Kim M (2017) Solar air-heating system with packed-bed energy-storage systems. *Renew and Sustain Energy Rev* **72**: 215-27.

Kumar K, Prajapati and Samir S (2017) Heat transfer and friction factor correlations development for solar air heater duct artificially roughened with 'S' shape ribs. *Exp Therm and Fluid Sci* **82**: 249-61.

Kumar S and Saini R P (2009) CFD based performance analysis of a solar air heater duct provided with artificial roughness. *Renew Energy* **34**: 1285-91.

Jaurker A R, Saini J S and Gandhi B K (2006) Heat transfer and friction characteristics of rectangular solar air heater duct using rib-grooved artificial roughness. *Sol Energy* **80**: 895-907.

Lanjewar A.M, Bhagoria J L and Aggrawal M K (2015) Review of development of artificial roughness in solar air heater and Performance evaluation of different orientations for double arc rib roughness. *Renew and Sust Energy Rev* **43**: 1214-23.

Lanjewar A, Bhagoria J L and Sarviya R M (2011) Heat transfer and friction in solar air heater duct with W-shaped rib roughness on absorber plate. *Energy* **36**: 4531-41.

Layek A, Saini J S and Solanki S C (2007) Heat transfer coefficient and friction characteristics of rectangular solar air heater duct using rib-grooved artificial roughness. *Int J Heat Mass Trans* **50**: 4845-54.

Momin AME, Saini J S and Solanki S C (2002) Heat transfer and friction in solar air heater duct with v-shaped rib roughness on absorber plate. *Int J Heat Mass Trans* **45**: 3383-96.

Prasad B N and Saini J S (1988) Effect of artificial roughness on heat transfer and friction factor in a solar air heater. *Sol Energy* **41**: 555-60.

Prasad BN and Saini J S (1991) Optimal thermohydraulic performance of artificially roughened solar air heaters. *Sol Energy* **47**: 91-96.

Prasad K and Mullick S C (1983) Heat transfer characteristics of a solar air heater used for drying purposes. *Applied Energy* **13**: 83-93.

Ravi K R and Saini R P (2016) A review on different techniques used for performance enhancement of double pass solar air heaters. *Renew and Sustain Energy Rev* **56**: 941-52.

Sahu M M and Bhagoria J L (2005) Augmentation of heat transfer coefficient by using 908 broken transverse ribs on absorber plate of solar air heater. *Renew Energy* **30**: 2057-63.

Saini R P and Saini J S (1997) Heat transfer and friction factor correlations for artificially roughened ducts with expanded metal mesh as roughened element. *Int J Heat Mass Trans* **40**: 973-86.

Saini R P and Verma J (2008) Heat transfer and friction factor correlations for a duct having dimple-shaped artificial roughness for solar air heaters. *Energy* **133**: 1277-87.

Saini S K and Saini R P (2008) Development of correlations for Nusselt number and friction factor for solar air heater with roughened duct having arc-shaped wire as artificial roughness. *Sol Energy* **82**: 1118-30.

Singh S, Chander S and Saini J S (2011) Heat transfer and friction factor correlations of solar air heater ducts artificially roughened with discrete V-down ribs. *Energy* **36**: 5053-64.

Singh S, Singh B, Hans V S and Gill R S (2015) CFD (computational fluid dynamics) investigation on Nusselt number and friction factor of solar air heater duct roughened with non-uniform cross-section transverse rib. *Energy* **85**: 509-17.

Sukhatme S P and Nayak J P (2011) Solar Energy. 3rd ed. New Delhi *Tata Mc Graw-Hill.*

Tiwary G N (2013) Solar Energy: Fundamentals, Design, Modelling and Applications. *Alpha Science International, Limited.*

Varun, Saini R P and Singal S K (2007) A review on roughness geometry used in solar air heaters. *Sol Energy* **81**: 1340-50.

Varun, Saini R P and Singal S K (2008) Investigation of thermal performance of solar air heater having roughness elements as a combination of inclined and transverse ribs on absorber plate. *Renew Energy* **l33**: 1398-405.

Verma S K and Prasad B N (2000) Investigation for the optimal thermo-hydraulic performance of artificially roughened solar air heaters. *Renew Energy* **20**: 19-36.

Webb R L and Eckert E R G (1972) Application of rough surfaces to heat exchanger design. *Int J Heat Mass Transf* **15**: 1647-58.

Yadav A and Bhagoria J L (2013) A CFD (computational fluid dynamics) based heat transfer and fluid flow analysis of a solar air heater provided with circular transverse wire rib roughness on the absorber plate. *Energy* **55**: 1127-42.

Yadav A and Bhagoria J L (2013) Heat transfer and fluid flow analysis of solar air heater: A review of CFD approach. *Renew and Sustain Energy Rev* **23**: 60-79.

Yadav A and Bhagoria J L (2014b) A CFD based thermo-hydraulic performance analysis of an artificially roughened solar air heater having equilateral triangular sectioned rib roughness on the absorber plate. *Int J Heat Mass Trans* **70**: 1016-39.

Yadav A and Bhagoria J L (2014a) A numerical investigation of square sectioned transverse rib roughened solar air heater. *Int J Thermal Sci* **79**: 111-31.

Yadav S, Kaushal M, Varun and Sidhhartha (2013) Nusselt number and friction factor correlations for solar air heater duct having protrusions as roughness elements on absorber plate. *Exp Therm Fluid Sci* **44**: 34-41.

Yadav A and Thapak M K (2014) Artificially roughened solar air heater: Experimental investigations. *Renew and Sustain Energy Rev* **36**: 370-411.

VITA

Name of the student	**:**	Inderjeet Singh
Father's name	**:**	Jaswinder Singh
Mother's name	**:**	Mandeep Kaur
Nationality	**:**	Indian
Date of birth	**:**	13.07.1993
Permanent home address	**:**	House no. 115, I-Block, Bhai Randhir Singh Nagar, District – Ludhiana 141012

EDUCATIONAL QUALIFICATION

Bachelor degree	**:**	B. Tech (Mechanical Engineering)
University and year of award	**:**	Punjab Technical University, Jalandhar (2015)
OGPA/OCPA/% marks	**:**	64.5%
Master's degree	**:**	M.Tech (Mechanical Engineering)
Year of award	**:**	2017
OCPA	**:**	7.57
Title of Master's Thesis	**:**	Computational Fluid Dynamics Analysis on Heat and Fluid Flow of Square Wave Profile Transverse Rib Roughened Solar Air Heater Duct
Awards/Distinctions/ Fellowships/ Scholarships	**:**	2 times University Merit Scholarship during M.Tech